3-2022

Potential Solution to Meet Growing Demands of Refractory Metal: Selective Laser Melting of Molybdenum-Tungsten Alloy

Jae Yu

Potential Solution to Meet Growing Demands of Refractory Metal:
Selective Laser Melting of Molybdenum-Tungsten Alloy.

THESIS

Jae H. Yu, Captain, USAF

AFIT-ENY-MS-22-M-319

DEPARTMENT OF THE AIR FORCE
AIR UNIVERSITY

AIR FORCE INSTITUTE OF TECHNOLOGY

Wright-Patterson Air Force Base, Ohio

AFIT-ENY-MS-22-M-319

Potential Solution to Meet Growing Demands of Refractory Metal: Selective Laser Melting of Molybdenum-Tungsten Alloy.

THESIS

Presented to the Faculty

Department of Aeronautics and Astronautical Engineering

Graduate School of Engineering and Management

Air Force Institute of Technology

Air University

Air Education and Training Command

In Partial Fulfillment of the Requirements for the

Degree of Master of Science in Astronautical Engineering

Jae H. Yu, B.S.A.E.

Captain, USAF

March 2022

AFIT-ENY-MS-22-M-319

Potential Solution to Meet Growing Demands of Refractory Metal: Selective Laser Melting of Molybdenum-Tungsten Alloy.

THESIS

Jae H. Yu, B.S.A.E.

Captain, USAF

Committee Membership:

Ryan A. Kemnitz, PhD
Chair

Carl R. Hartsfield, PhD
Member

John S. Brewer, PhD
Member

Abstract

Selective laser melting (SLM) of refractory metals has been of high interest in research due to the metals' potential desirable characteristics in aeronautical and space applications. In particular, molybdenum and tungsten have been the focus of several studies in the search for high temperature and high strength purposes. However, there is still a significant knowledge gap to process defect-free alloys and make use of them in practical engineering functions. The aim of this study is to characterize the relationship between the microstructure and mechanical properties of the additive manufacturing (AM) of molybdenum and 30% tungsten system (Mo-30W) specimens and interpret how unique microstructural characteristics and defects relating to AM of Mo-30W alloy influence the fracture behavior. This study provides qualitative and quantitative approaches to characterize microstructure and mechanical properties of the various AM Mo-30W specimen by evaluating the effects of print build chamber gas, print speeds, build orientations, and post processing heat treatments through means of mechanical tests, chemical composition analysis, porosity identification, and fracture surface assessments. The principal findings of this research are that the addition of 3% hydrogen to the AM shielding atmosphere resulted in an 105% increase in bending strength in Mo-30W alloys. The hydrogen lessened coarse columnar grain, cracks, and pores which led to higher strength transgranular failure. Additionally, the optimal laser scan speed to print as-built Mo-30W was the lowest at 100 mm/s which showed the least microcracking and the highest bending strength of 615 MPa and highest hardness of 260 HV. Furthermore,

the vertically printed species had higher mechanical properties compared to alloys printed diagonally. Lastly, the results showed that the post-processing heat treatment at 1600°C significantly softened the material which reduced the uniform hardness and strain to failure. The thermal envelope underheated the alloy likely caused recrystallization inducing equiaxed microstructure to fracture easier. However, heat-treating diagonal Mo-30W at 2000°C significantly improved the average yield strength by 75% and average flexural strain by 59% from its as-built counterpart. This heat treatment technique provided internal stress relief to the alloy by reducing internal grain discontinuities and created cleavage fractures more difficult. These findings contribute to a better understanding of the effect of print shielding gas, print speed, build orientation, and the heat treatment on mechanical and microstructure properties of additive manufactured Mo-30W.

Acknowledgments

I would like to express my sincere appreciation to my faculty advisor for his guidance, mentorship, and flexibility throughout the course of this thesis effort. His insight and vision were greatly valued. Next, I would like to express my gratitude to my loved ones, friends, and family for their help and encouragement through this endeavor. I would also like to thank the Materials and Manufacturing and Aerospace Systems directorate of the Air Force Research Laboratories for sponsorship of this research.

Table of Contents

Page

List of Figures

Page

List of Tables

Page

List of Symbols & Acronyms

ANOVA Analysis of Variance

AM Additive Manufacturing

ASTM American Society for Testing and Materials

BCC Body-Centered Cubic

BSD Energy Dispersive X-Ray Spectroscopy

CAD Computer-Aided Design

DBTT Ductile-Brittle Transition Temperature

EDS Energy Dispersive X-Ray Spectroscopy

HT Heat Treatment

PBF Powder Bed Fusion

ISO International Organization for Standards

SEM Scanning Electron Microscope

SLM Selective Laser Melting

TEM Transmission Electron Microscope

W Tungsten

XCT X-Ray Computed Tomography

XRM X-Ray Microscope

Potential Solution to Meet Growing Demands of Refractory Metal: Selective Laser Melting of Molybdenum-Tungsten Alloy

I. Introduction

This thesis is a study of additively manufactured molybdenum and tungsten alloy. The study was based predominantly upon the qualitative microstructure analysis and quantitative mechanical tests for material characterization. The following chapter of the thesis presents the context of the study, specifies the problem under investigation, defines research objectives, and describes the significance of the research. The chapter concludes by stating the overview of the research methodology.

Context

Molybdenum and tungsten have been established as refractory metals with their appealing inherent characteristics such as high melting point, good thermal conductivity, high strength, and high hardness. The materials are used in many critical components across a wide range of applications in commercial, electronics, medical, aeronautical, space, and military industries. For instance, refractory metals are used for reentry vehicle nose tips due to their high resistance to water droplet and ice particle erosion [1]. However, tungsten is one of the densest metals, lacks ductility, and is expensive. Also, all high temperature applications are limited to a protective atmosphere or a vacuum due to the susceptibility of tungsten to oxidization in air at high temperature [2]. As a result, molybdenum as a substitute was introduced in times of shortage of tungsten due to its

similar characteristics as well as lower density and stable price [1]. Overall, tungsten is a difficult material to manufacture traditionally and additively.

Several tungsten alloys and molybdenum alloys were studied in the past, and many attained scientific significance due to their unique chemical, physical, mechanical, and thermal properties. Above all, the objective of alloying tungsten and molybdenum was to expand their properties at both ambient conditions and high temperatures.

Problem Statement

Components with complex geometry and ability to tolerate high temperature, support large stresses, and endure vacuum pressures are needed to meet the increasing demand of reduced cost and time for manufacturing in the field in electronics, medicine, aeronautical, space, and military industries. The materials like tungsten, molybdenum, and their alloys are suitable for these applications. Selective laser melting (SLM) is one of the additive manufacturing (AM) technologies that allow metal components to be manufactured to meet these conditions [3].

However, microstructural defects and irregular fracture behavior have hindered the widespread use of additively manufactured alloys. Even though SLM can produce complex metal alloys, the AM technique is hindered by defects, such as porosity, lamination, cracks, and poorly melted volumes, which have an adverse impact on physical and mechanical properties of manufactured specimens [4]. Consequently, AM alters the mechanical behavior from conventionally produced material making the additively manufactured parts infeasible. In addition, the lack of sufficient data on

additively manufactured alloys accessible to engineers and scientists prevent AM techniques from being used to their full capability in the aerospace industry [5].

Previous studies of additively manufactured tungsten and molybdenum alloys have found built parts to be plagued by crack systems that cannot be eliminated by modifying the build parameters [6, 7, 8]. The presence of these cracks reduces the mechanical performance of metal alloys and eliminating them are imperative if additively manufactured tungsten and molybdenum are to become a useful material for future AM applications.

In this thesis, we expand upon the results in Kemnitz et al. (2021) to address possible limitation of AM alloys and help fill gaps in the literature that had not been previously adequately described. With this intention, molybdenum and 30 wt% tungsten (M-30W) system is investigated in terms of suitability and cost-efficiency. Directing manufacturing advances with AM of tungsten and molybdenum are essential to utilize the unique properties of refractory metals in demanding high temperature and high strength applications in aeronautical and space industries.

Research Objectives

The aim of this study is to describe the effect of the print speed, build orientation, atmosphere gas, and post processing heat treatment (HT) of Mo-30W specimens. Although there are several studies considering these parameters to enhance relative density, i.e., minimize the porosity of pure molybdenum and tungsten, the studies on the AM of Mo-30W system have yet to be published. Notably, the goal is to explain the relationship between the microstructure and mechanical properties of the Mo-30W

specimens and interpret how unique microstructural characteristics and defects relating to AM of Mo-30W alloys influence the fracture behavior. Specifically, the objectives are:

- To characterize the mechanical properties of Mo-30W alloy using three-point bend test, evaluate the effects of the printing parameters (laser speed, build orientation, and atmosphere gas) in addition to post-processing heat treatment, and compare measured properties to previous empirical studies.
- To characterize the microstructure of Mo-30W alloy, observe changes due to different print laser speed, build orientation, and build chamber gas as well as post-processing heat treatment, and determine distinctive features.
- To identify the relationship between AM defect and microstructural characteristics to mechanical properties of the Mo-30W specimen
- To quantify the cause of variability of AM of Mo-30W fracture properties

Research Focus

The growing importance of manufacturing materials for high temperature applications in supersonic aircraft, re-entry vehicles, nuclear fission, power generation, and other space systems, has resulted in extensive research and development programs involving molybdenum and tungsten refractory metals [9]. How might the future of additive manufacturing of tungsten and molybdenum alloys look like in the near future? The design flexibility of AM and increasing studies on the additively manufactured tungsten molybdenum alloys can provide insight into the mechanisms of cracks and porosity. Correspondingly, it may be possible to improve mechanical properties of the

molybdenum-tungsten system as a result of new findings in AM print parameters and post-processing heat treatment. Lastly, it may prove possible to create low-cost additively manufactured molybdenum-tungsten alloys demonstrating a high-performance in extreme environment conditions.

Methodology

Additive manufacturing of Mo-30W specimen printed in pure argon (Ar) and argon-3% hydrogen (Ar-3H_2) atmospheres were compared using mechanical characterization, microcracking analysis, and chemical composition analysis. Mechanical properties were calculated through three-point bend test and Vickers hardness test. AM features and defects, such as porosity, lamination, cracks, and inadequately melted volumes were observed qualitatively by Scanning Electron Microscope (SEM) imaging. Lastly, chemical composition analysis and material microstructure was investigated using the Energy Dispersive X-Ray Spectroscopy (EDS) analysis.

Summary

The preceding information in this chapter covers the fundamental points concerning the variability of properties in AM of tungsten and molybdenum including a brief review of the refractory metals and AM technique. Chapter 2 will cover in-depth information of AM methods, properties of refractory materials, and effects of post-processing heat treatment as well as data derived from previous studies in AM of pure tungsten and molybdenum. Chapter 3 focuses on the methodology followed in this study, including details of the experimental material, equipment, procedures, and laboratory

methods. Chapter 4 examines the mechanical properties of Mo-30W in ultimate yield strength and Vickers hardness combined with discussion on crack-defect interactions and microstructure characteristics using SEM and EDS analysis. To finish, chapter 5 provides summary of the thesis, its significance and suggests possible future work, including potential for achieving fracture toughness and reducing cracks.

II. Background

Chapter Overview

The chapter is an organized review of existing literature and all relevant published studies on the topics of molybdenum, tungsten, and additive manufacturing. One of the main purposes is to clarify and explain terminologies and key concepts used in the context of this study including what is currently understood about the research topics. Next is to identify relationships between concepts and their practical implications by means of finding and critically analyzing studies done by researchers as well as scholars that have shaped this field of study. Lastly, inconsistencies, limitations, or gaps in knowledge within studies are acknowledged. Summary of studies that are critical for this study and have a central role in planning this research are tabulated in Table 1.

Table 1. The effect of processing parameter on properties of AM of materials.

Materials	Processing parameter	Data collection equipment	Affected properties or findings	Source & Year
Pure Mo	Laser power, layer thickness	Optically determined density	Higher densities require higher laser power and lower layer thickness	**[7]**, 2015
Pure W	Print speed, hatch spacing	SEM, weight density	Print speed significantly contributed densification	**[6]**, 2017
Pure Mo	Scanning strategy	SEM & EBSD	Scan strategy with 67 ° layer rotation reduced cracks	**[10]**, 2017
Pure W & W + 10%Ta	Shielding gas	Archimedes Law, SEM, EBSD	Lower oxygen level in build chamber increase densification	**[11]**, 2017
Pure W	Laser energy input	SEM, EBSD, XCT	Higher energy input leads to less porosity	**[12]**, 2018
Pure W	Particle size	Simulation model & SEM	Powder-to-laser absorptivity reduced with bigger particle size	**[13]**, 2019
Mo + 0.45% Carbon	Alloying	SEM, EBSD, TEM	Addition of carbon increased density, hardness, and bending strength	**[14]**, 2019
Pure Mo & Pure W	Impurities	SEM, EDS, EBSD, XRM, TEM	Oxygen impurities caused defect and leading to hot and cold cracks	**[8]**, 2019
Pure Mo	Laser energy, laser speed	OM, EBSD, SEM	High energy input led to low porosity, high speed affect crystallographic texture	**[15]**, 2020
Pure W & W + 25%Re	Alloying, post heat treatment	SEM, EDS, EBSD,	Addition of rhenium and post heat treatment increased bending strength	**[16]**, 2021
Pure W	Shielding gas	SEM, EDS	Addition of hydrogen to shielding gas increased bending strength	**[17]**, 2021

Refractory Metals and Additive Manufacturing Historical Perspectives

Refractory metals have an ideal combination of valuable physical properties which makes these metals exceptional in the modern technology. The refractory metals belong to group of transition elements in the periodic table, which are grouped due to the high strength of the interatomic bonds. Accordingly, these metals have high melting point, mechanical strength, and electrical conductivity. As is well known in the literature, the interatomic bond is one of the main factors which determine the crystalline structure and physical properties of metals and alloys [18]. The metals with maximum strength of interatomic bond have a body-centered cubic lattice.

Out of 11 refractory metals that fall into category of high melting point, niobium (Nb), molybdenum (Mo), tantalum (Ta), and tungsten (W) have been substantially researched in recent years as bases for structural alloys [19]. However, refractory metals like molybdenum and tungsten exhibit poor oxidation resistance, low weldability, difficult fabrication, and high Ductile-to-Brittle Transition Temperature (DBTT) which has prevented their application in the past. Several research endeavors in traditional manufacturing and technological advancement such as additive manufacturing were borne out of motivation to resolve the issues.

Tungsten and Molybdenum

The chemical, physical, mechanical, thermal properties of tungsten (W) are summarized in Table 2; along with the respective properties of molybdenum (Mo). Tungsten holds the highest melting point at 3410°C, the highest tensile strength, the fourth highest Young's modulus, and the sixth highest thermal conductivity of all metals

[5]. Tungsten retains most of its mechanical strength and hardness at high temperatures, is highly dense, and is also corrosion resistant at low to moderate temperatures.

Table 2. Properties of Tungsten and Molybdenum [5, 18].

Property	W	Mo
Atomic Number	74	42
Atomic mass, M (g mol^{-1})	183.8	95.9
Oxidation states	2,3,4,5,6	2,3,4,5,6
Crystal structure	Body-centered cubic	Body-centered cubic
Atomic radius, r_{metal} (Å)	1.41	1.39
Density, ρ (g cm^{-3})	19.25 – 19.35	10.1 – 10.3
Melting temperature, T_m (°C)	3410 - 3420	2607 – 2622
Linear thermal expansion coefficient, α (°C^{-1})	4.2 - 4.6 ×10^{-6}	4.8 – 5.5 ×10^{-6}
Thermal conductivity,κ (W m^{-1}K^{-1})	170 – 175	129 – 147
Specific resistivity, ρ (Ω·m)	5.4 – 6 ×10^{-8}	4.6 – 5.2 ×10^{-8}
Tensile strength, σ_u (MPa)	785 – 1080	785 - 890
Young's modulus of elasticity,E (GPa)	340 – 405	315 – 343
Strain at fracture, ε_f (%)	0-15	10-15
Poisson's ratio, ν	0.27 – 0.29	0.29 – 0.295
Hardness (MPa, HV)	2800, 285	1470, 150

Molybdenum has the fifth highest melting point of all elements. Its electrical conductivity is the highest of all refractory metals. It has high-thermal conductivity approximately 50% higher than that of iron or steels and consequently finds wide usage

in heat sinks [4]. Its low linear thermal expansion coefficient over a broad temperature range, enables its use in bimetal thermocouples. It possesses high tensile toughness, while being softer and more ductile than W. Its high specific elastic modulus makes it desirable for products that require both high stiffness and low weight. Molybdenum's thermal properties such as high conductivity, low coefficient of thermal expansion, and low specific heat indicates high interest to the electronic industry. Molybdenum also displays good machinability and low vapor pressure at elevated temperatures, so it is an easier metal to fabricate than tungsten [5].

Historically, molybdenum is used extensively as an alloying component of steels, electrodes in resistors, conductor for heat sinks, solid lubricant in high-temperature applications, making electrode components in radar devices, filaments in lamps, chemical catalyst in refining petroleum, components in rocket engines, liquid metal heat exchangers, and electrical tubes [5]. High melting-point and excellent strength-to-density ratio account for the use of molybdenum in nozzle rockets, control surfaces, re-entry cones, rudders of missiles, radiation shields, power source, heat sink, and parts subject to high temperature [1]. However, wide variety purposes in chemical environment and high-temperature applications are limited by the metal's low oxidization resistance at elevated temperature. Although recent work has shown that this can be overcome by the provision of a protective refractory outer coating that is impermeable to oxygen to a degree. [20]. Therefore, molybdenum performs best in inert or vacuum environments. Molybdenum started to develop into commercially significant metal when Coolidge and Fink (General Electric Company) first made the metal in ductile form around 1910. [22]. A substantial

amount of work on molybdenum compounds was achieved in the nineteenth century and the early part of the twentieth century; although much of this has not been replicated and validated by modern methods of manufacturing.

In 2019, the United States along with three other countries in the world provided more than 90% of total global production of molybdenum: the estimated production of 88,000,000 lb. [21]. Identified resources of molybdenum in the US are above five million tons, and the trend indicates that it is expected to supply world's needs for the anticipated future.

The history of tungsten resembles that of molybdenum in that the literature of tungsten grew very rapidly following its discovery [2]. It is used as a filament in incandescent lamps and alloying constituent in high-speed cutting tools [22]. Additionally, tungsten is used in springs, valves, magnetos, contact points, balance weights, anti-vibration tooling, bearings, spark plugs, radiation shields, and abundant other parts where strength, hardness, resistance to corrosion, and a high melting point are essential [5]. X-ray tubes anodes and electrodes are used in inert-gas or hydrogen-arc welding; and lastly, cutters and drills for wire drawing are also made up of tungsten [20].

US industrial product of tungsten ores and concentrates have ended since 2015, and the world production of tungsten, 85,000 metric ton, is led predominately by China in 2020 [23]. As the largest producer in the world, it accounts for approximately 82% of global supply. This trend indicates tungsten is likely to increase in price as demands goes up or during supply shortages.

Agte et al., in their book Tungsten and Molybdenum, found that molybdenum and tungsten have little resistance to reaction with air and water vapor at elevated temperature [24]. Tungsten begins to oxidize at 400 to 500°C and then vaporizes at 850°C where the vapor reaches about 1630°C at a pressure of 760 mm Hg [24]. Molybdenum oxidizes more readily, beginning at 370°C and becoming increasingly active at 650°C [20]. The molybdenum oxide sublimes at 1155°C at a pressure of 760 mmHg [24]. This implies that the two refractory metals can be heat treated only in a vacuum, inert gas, or pure hydrogen.

Additive Manufacturing

Additive manufacturing is the formalized term for what is popularly called 3D Printing. The fundamental principle of this technology is that a model, created using a three-dimensional Computer-Aided Design (3D CAD) software, can be manufactured directly without the requirement for process planning. AM technology drastically streamlines the process of manufacturing complex 3D objects directly from CAD data. This is because most AM technologies use powder or filament, including plastics, metals, ceramics, and paper as feedstock which melts by a localized heat source. Other standard manufacturing processes of molding, machining, forming, and joining require more assessment to determine specific equipment and processes to be used, to control order of fabrication, and additional fixtures required [3]. On the other hand, AM needs only some basic dimensional specifics, a little amount of knowledge as to how the AM machine works, and the materials that are used to manufacture the part.

The key to how AM works is that parts are made by adding material in layers; each layer is a thin cross-section of the piece drawn from the initial CAD data. The thinner each layer is, the closer it will look to the original CAD data. All commercialized AM machines use a layer-based approach. The major ways that they differ are in the materials selection, layer creation, and layer bondage [25].

Per International Organization for Standards (ISO), AM separates the techniques used to build the layers into seven categories, of which the three are suitable for metals [26]. Based on the input feed system and energy source, the metal melting-based AM methods can be broadly classified into directed energy deposition (DED), powder bed fusion (PBF), and sheet lamination. DED melt materials as they are being deposited. Commercial DED processes include using a laser or electron beam to melt powders. PBF processes container filled with material powder processed using an energy source like laser or electron beam. Sheet laminations deposit a layer of sheet materials. Many organizations have developed DED and PBF machines and the AM techniques including their descriptions are summarized in Table 3.

Quite a few of the listed AM techniques described are fundamentally the same, recognized only in name by the company for which the process was invented. For the purposes of clarity pertinent to this study, LaserCUSING and SLM will be used interchangeably with AM.

Table 3. Various AM technologies [4].

AM category	Technology	Company	Description
Directed energy deposition (DED)	Direct metal deposition (DMD)	DM3D Technology LLC (formerly POM Group)	Uses laser and metal powder for melting and depositing using a patented close loop process
	Laser engineered net shaping (LENS)	Optomec, Inc.	Uses laser and metal powder for melting and depositing
	Direct manufacturing (DM)	Sciaky, Inc.	Uses electron beam and metal wire for melting and depositing
	Shaped metal deposition or wire and arc additive manufacturing (WAAM)	Not commercialized yet (patented by Rolls Royce Plc.)	Uses electric arc and metal wire for melting and depositing
Powder bed fusion (PBF)	Selective laser sintering (SLS)	3D Systems Corp. (acquired Phenix Systems)	Uses laser and metal powder for sintering and bonding
	Direct metal laser sintering (DMLS)	EOS GmbH	Uses laser and metal powder for sintering, melting, and bonding
	Laser melting (LM)	Renishaw Inc	Uses laser and metal powder for melting and bonding
	Selective laser melting (SLM)	SLM Solutions GmbH	Uses laser and metal powder for melting and bonding
	LaserCUSING	Concept Laser GmbH	Uses laser and metal powder for melting and bonding
	Electron beam melting (EBM)	Arcam AB	Uses electron beam and metal powder for melting and bonding
Sheet lamination	Ultrasonic consolidation	Fabrisonic	Uses ultrasonic energy to consolidate layers of sheet metal and make parts

There are several variables unique to various AM technologies that can be used to control the process of the build, which in turn, affect the resultant material properties. Some variables associated with SLM are scanning parameters such as laser power, scanning speed, spacing between laser hatches, environmental conditions, scanning strategy, powder size, and layer thickness [3]. These parameters will determine factors

like the accuracy of the specimen geometry as well as its mechanical and physical properties. To ensure complete fusion of powder particles, scanning parameters are usually selected based on the volumetric laser energy density (E_v) relationship defined as

$$E_v = \frac{\mathrm{P}}{vth} \tag{1}$$

where P is the laser power, v is the laser velocity, t is the powder layer thickness, and h is the hatch spacing or distance between parallel scan lines. Low energy input will result in unmelted material and thus reduced density by the formation of irregular-shaped voids, while too high energy input will lead to higher melt pool dynamics and reduced density originating from pores formed due to entrapped gas [27]. In general, the porosity induced during SLM can be somewhat controlled by optimizing processing parameters which will be discussed in upcoming sections.

Several groups have labeled this technology as revolutionizing in terms of development and manufacturing. While additive manufacturing will not completely replace traditional manufacturing in the future, AM's tangible strengths become effective when it is combined with those conventional methods. The advantages of AM are customization, rapid prototyping, design of highly complex geometries, and reduction in cost and material [3]. As a result of designing 3D CAD data as the starting point, the product can be customized and promptly realized by printing the model. In addition, the layer-by-layer approach gives freedom to create complicated geometries and shapes. For example, NASA redesigned the rocket engine's injector to be consist of two parts instead of the 115 individual parts using AM. [28] As a result, it reduced the cost of making the rockets without changing the performance of the rocket engine.

Limitations of Additive Manufacturing

Despite these promising advantages, key problems directly related to the potential of AM prevent broader success. These shortcomings are the technological challenges in terms of powder property, build procedure, availability of standards, and post-processing [29]. The properties of the powder, namely material type, size, shape, purity, and packing density influence the mechanical properties of AM components. There is a growing body of literature that recognizes it is difficult to characterize powder properties and predicting final part performance is highly complex.

Next, wide-ranging build parameters and procedures limit producing optimal AM components. Microstructure, solidification texture, and defects such as porosity, cracks, and poor melting fusion are inevitable in AM processes. There is not a full literature knowledge of relationships between processing parameters and final component properties that have unique features and material properties [30]. Under those circumstances, research and development of worldwide standard databases with information on the mechanical and thermal properties of AM materials must be defined. It is critical to establish science-based standards to support design and validate mechanical performance with increased reliability. Lastly, all AM material require post-processing which can be significantly expensive and time consuming. A few of the post-processing techniques can include surface preparation to smooth out roughness, heat treatment to reduce all types of AM defects, and non-thermal techniques to increase specific properties of final AM component. A more detailed account of these effects specific to AM Mo-W system is given in the following section.

Factors Influencing Additive Manufactured Mo-W System

For the wider application of molybdenum and tungsten alloys in modern additive manufacturing, prior studies noted the importance of multiple factors impacting material properties of final parts. These are as follows:

Powder Properties - Size, Shape, and Packing Density

The SLM process uses metal powder as its feedstock material, intrinsically the properties of the starting powders and methods of preparation used to build AM material will have a critical impact on the alloy's properties and performances. Due to the complex nature of powders, characterizing their performance is not a small task. However, there are many empirical studies published to learn the influence of powder properties. Notably, spherical particles are likely to arrange and pack more efficiently than irregular particles which consequently influence the final component density significantly [29]. Dawes et al., have a thorough review of powder properties and assessment techniques provided in Table 4. The characteristics of the molybdenum and tungsten powder, prepared for this investigation, require these assessment techniques considerations.

Table 4. Powder properties and assessment techinque [31].

Particulate properties		Bulk properties	
Powder property	Assessment technique	Powder property	Assessment technique
Particle shape	SEM Optical microscopy	Apparent density	Hall flow, Freeman FT4
		Tap density	Tapped density tester
Particle size and particle size distribution	Sieve Laser diffraction Optical microscopy	Flowability	Hall flow, Freeman FT4, dynamic flow test
		Cohesiveness	Freeman FT4
Particle Porosity	Particle polishing and optical microscope	Surface area	BET surface area analysis
		Chemical composition	Inert gas fusion

Previous research by Vock et al., have established that powder properties can affect the density, surface roughness, internal build flaws, mechanical properties, and accuracy of the component [32]. In his study, flowability and particle size distribution played a key role influencing the final part quality but failed to quantify the powder-to-part correlation.

To determine effect of powder size, Zhang et al. performed experimental studies of SLM tungsten material using surface analysis [13]. The study revealed absorptivity of the power layer increased as particle size decreased. The laser energy absorptivity of the powder material is defined as the ratio of the powder material absorbed radiation to the laser energy incident radiation [13]. The particle diameter greater or equal to 35 μm experienced poor melting and resulted in the AM defect of splashing, which occurs from eruption of gas bubbles within the molten metal. The study only produced a small dataset,

one sample test for each particle size, which suggests limitations in that it likely did not test reliability of the results. However, these results are in agreement with those obtained by Vock et al. where smaller average particle size increased flowability.

Build Chamber Atmosphere and Oxygen Content

One of the major setbacks in AM of refractory metals such as molybdenum and tungsten is due to their high melting points and high DBTT. Their low oxidization resistance at elevated temperature result in parts with AM defects. The oxidation process comprises of two phases: 1) metal directly reacting with oxygen which causes a film of metal oxide to form, 2) oxygen reacting with the oxide film which separates the metal from direct reaction with the oxygen. The oxygen dispersed in the refractory metal substantially increases the hardness, while the brittle oxides scattered along the grain boundaries reduce the strength and deformability of the metals [18].

Ivekovic et al. demonstrated high densification of AM pure tungsten from 94.4% to 97.1% by lowering the oxygen content in the AM building chamber from 150-200 ppm to less than 50 ppm [11]. The density measured using Archimedes principle for AM tungsten and tungsten-5%tantalum increased 1.2% from 97.5% to 98.7%. However, their approach failed to address the oxygen impurities in their powder. Braun et al noted that oxygen impurities in the metal powder caused AM defects and increased DBTT [8]. On the other hand, their analysis did not take account of material hardness, nor did the study investigate other mechanical behavior due to increased oxides distributed in the metal.

Kemnitz et al. approached this problem by adding 3% hydrogen gas to the build chamber's shielding argon gas [17]. In their study, an inert gas fusion technique

determined that the oxygen content in the materials printed in pure argon was between 89-172 ppm while materials printed in Ar-3H_2 were 619-1027 ppm. According to Kemnitz et al., the bending strength of the final AM part produced in Ar-3H_2 gas increased between 90.58% to 121.62% compared to parts produced in pure argon gas. They concluded that it is due to ribbon-like microstructure as a result of greater presence of oxides which made cleavage fracture more difficult. This research shed new light on producing AM material with unique features and material properties by adding small amounts of hydrogen gas to the build chamber atmosphere to increase metal oxides within grain boundaries.

Print Parameters Studies

Another main roadblock in SLM of refractory metals such as molybdenum and tungsten is the occurrence of residual stresses in printed material. Mugwagwa et al., explained residual stress occur in AM of metallic material as melting of the powder reach equilibrium after rapid heating (melting) and cooling (solidifying) cycles [33]. Residual stress in return compromise the mechanical properties of printed parts. The following studies have attempted to remedy problems finding optimal build parameters in SLM to reduce residual stresses in molybdenum and tungsten.

Faidel et al. investigated the factors of laser power and layer thickness in SLM processing parameters that determined the affected properties of molybdenum. Accordingly, their study revealed that higher densification of the printed material correlated to higher laser power [7]. This study suffered from a design flaw in density measurement of the AM material where the densities were measured using optically

determined software. In a study where accuracies of three density measurement principles; Archimedes method, microscopic analysis, and X-ray scanning; were cross examined in metals, the Archimedes method showed the highest accuracy and reliability out of the three [34]. Therefore, the study would have been more useful if the method of density measurement differed in the Faidel et al., study.

In the following year, Enneti et al. showed lower printing speed and lower hatch spacing led to higher densification in SLM of tungsten. The majority of the contribution in density variation was due to printing speeds, impacting 75.7% of the differences [6]. One of the limitations in this study was working with 90 Watts laser power, which perhaps caused its low densification (59 – 75% of theoretical density) of SLM tungsten. The low laser power results in lower temperature and lower size of the molten pool of SLM. Although smaller molten pool can lead to smaller columnar grains than larger equiaxial grain which supports higher tensile strength, the prerequisite of high laser power is necessary for the high melting temperature requirements of molybdenum or tungsten [35].

Wang et al. was able to achieve 99.1% densities in SLM of pure molybdenum using laser power of 400 W. In that study, scanning rotation of 67° formed interlocking grain boundaries which prevented crack growth comparatively to scanning rotations of 0° and 90° [10]. However, these results were limited to microstructure analysis and are therefore not a representative of mechanical property characterization of pure molybdenum. The study acknowledged SLM molybdenum was characterized by columnar grains along the grain boundary but overlooked the possible explanation which

could be due to using higher laser power. Additional similar studies based on laser powers from 150 to 300 W can be beneficial to better understand its effect on microstructural and material properties.

Consistent with the preceding hypothesis, Sidambe et al. showed using laser power of 200W combined with 67° scanning rotation and higher laser energy density, up to 348 J/mm^3, led to stronger crystalline texture and lower porosity of SLM pure tungsten [12]. Despite these promising results, questions remained regarding mechanical properties of the fabricated parts. To develop a full picture of mechanical characterization of refractory metals, additional studies will be needed like fatigue tests or hardness tests.

Higashi et al. study confirmed previous findings and contributed additional empirical evidence that suggested that higher laser energy input and higher speeds led to lower porosities and superior directional crystallographic textures which affect material properties of molybdenum [15]. However, much of the research up to now have been qualitative in nature, quantitative tests of molybdenum and tungsten to measure mechanical properties would be valuable in the AM field of study. Collectively, these studies outlined numerous build parameters of SLM which play critical roles to reduce residual stress in molybdenum and tungsten. Figure 1. summarizes the results which corroborate the findings of various research to improve porosity and to improve mechanical properties of AM material.

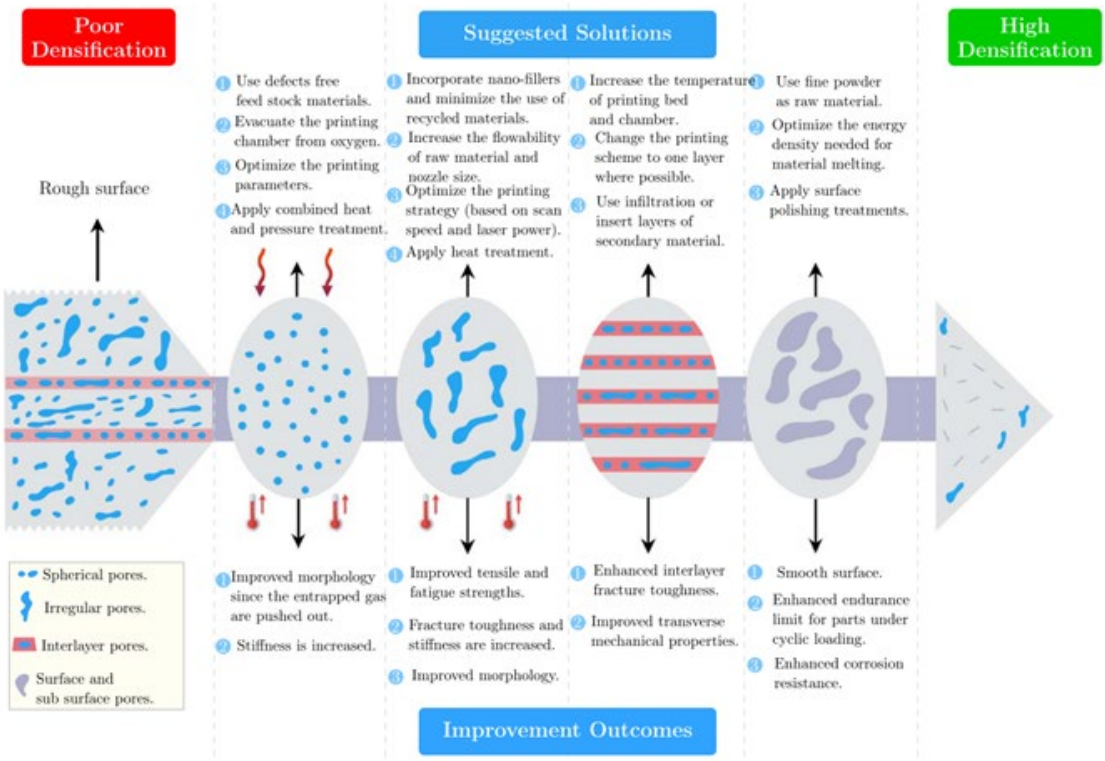

Figure 1. Factors influencing AM of material and how to improve [36].

Heat Treatment Effects

The heat treatment of metals and alloys consist in imparting a change in structures and properties of alloys without changing its composition. The structural changes varies based on the chemical composition of the alloy and temperature conditions. For example, the temperature conditions can happen in wide range of hot and cold temperatures, fixed durations, and number of frequencies. Heat treatments are used for AM parts to form desired microstructures and/or to relieve residual stresses and enhance ductility [3].

DebRoy et al., claimed that refractory metals such as molybdenum and tungsten cannot be heat treated to achieve higher mechanical properties because these materials

cannot undergo phase transformations upon heating and cooling. He stated that these alloys attain their properties through solid solution strengthening [37]. In contrast, Savitskii et al. determined that refractory metals like molybdenum and tungsten alloys can be strengthened through recovery and recrystallization processes which remove fibrous structure and form equiaxial structure, providing eliminations of lattice distortions and internal stress relief to the metals. This is evident in the case of molybdenum and tungsten alloy recrystallization without interstitial impurities which results in increased ductility. Furthermore, they stated the structure and properties of the molybdenum and tungsten after heat treatment are determined by "the rate of cooling from the region of single-phase solid solution and the rate of heating to the impurity solution temperature. The latter circumstance is due to the fact that the heating process is not only accompanied by the solution of fine precipitates but by the coagulation of coarser precipitates [18]." Nevertheless, such expositions are unsatisfactory because Savitzskii et al. investigated numerous heat treatment conditions for various molybdenum and tungsten alloys then revealed that optimum heat treatment conditions have not been discovered yet.

Low-temperature brittleness is an unfavorable attribute in pure tungsten. Therefore, previous studies have been aimed at lowering the ductile-to-brittle transition temperature (DBTT) and subsequently increasing the ductility of the tungsten [2]. According to Eckley et al., hot isostatic pressed (HIP) and annealed AM tungsten rhenium (W-Re) alloy increased the tensile strength of W-Re system, demonstrating tensile strength of 505.4 MPa (71.6% increase) and 659.8 MPa (124% increase) respectively [16]. Although the evidence presented supported the notion that post heat

treatment of refractory metals can be valuable in increasing mechanical properties, further uncertainty arises from the addition of rhenium which has the known effect of lowering the DBTT of the metal and reducing stress in the metal to be more ductile [38]. It is subjective to correlate the increase in tensile strength to post heat treatment conditions because the bending strength increased 340% in AM molybdenum carbon alloy in a similar study by Kaserer et al. [14] The alloying concepts were similar between the two studies which attempted to mitigate cracks of AM material and understand the effects of alloying. The discussion will next examine the experimental data results of mechanical properties of AM molybdenum, tungsten, and their alloys.

Mechanical Property Data of AM Molybdenum, Tungsten, and Their Alloy

Throughout this thesis, the term molybdenum and tungsten alloy will refer to Mo-30W which implies the alloy is made up 70% molybdenum and 30% tungsten by weight. The next sections will detail the experimental data available on AM of molybdenum and tungsten and their alloy. Furthermore, extensive research has shown that there is a lack of sufficient information or accessible data on AM of the Mo-30W system. As a result, theoretical alloy development of the Mo-30W system and its past empirical mechanical along with physical data on vacuum melted Mo-30W system will be detailed.

AM of Molybdenum

To investigate the mechanical properties of AM Mo-30W alloys, data from previous preliminary three-point bend experiments were collected to establish the baseline of mechanical property data of SLM pure molybdenum. The study was conducted to establish possible cause-and-effect relationship by isolating the effect of build chamber gas and print speeds on mechanical properties. The samples were printed using constant laser power of 200 W, hatch distance of 50 μm, and layer thickness of 20 μm. The scan speed was varied from 100 to 1000 mm/s and the build chamber gas varied between pure argon and argon + 3% hydrogen. All parts were printed with a typical AM meandering laser scanning strategy with 90° rotations between layers. Three point bending tests of all additively manufactured pure molybdenum specimens were performed using a servo-hydraulic machine. Table 5 presents mechanical property data results of the average flexural stress and a sample deviation on the samples of three AM molybdenum for specified print speeds and build chamber gases. What stands out in this table is the general pattern of increased bending strength with lower print speed and addition of 3% hydrogen to build chamber atmosphere. This finding broadly supports the work of other studies in this area linking laser speed and shielding gas to densification. The experimental bending strengths data specifically 100 mm/s printed in Ar/3%H2 were in agreement with the property data of molybdenum, 785 – 890 MPa, from previous cited literature in Table 2.

Table 5. Flexural stress and strains of molybdenum in pure Ar and Ar-3H_2.

Mo in Ar			Mo in Ar-3H_2		
Print speed (mm/s)	Average flexural stress (MPa)	Average flexural strain	Print speed (mm/s)	Average flexural stress (MPa)	Average flexural strain
100	673.39 ± 48.01	0.02237 ± 0.01263	100	875.92 ± 1.31	0.01279 ± 0.00128
200	593.77 ± 15.06	0.01925 ± 0.00442	200	744.38 ± 73.75	0.01207 ± 0.00066
300	561.1 ± 24.73	0.0163 ± 0.0016	300	700.9 ± 23.23	0.01111 ± 0.00036
400	521.9 ± 47.19	0.01706 ± 0.00156	400	681.58 ± 54.83	0.01167 ± 0.00067
500	463.72 ± 26.67	0.01548 ± 0.00327	500	651.66 ± 24.19	0.01322 ± 0.00203
600	457.18 ± 13.99	0.01442 ± 0.00043	600	674.1 ± 28.15	0.01197 ± 0.001
800	381.91 ± 2.6	0.01668 ± 0.00232	800	562.84 ± 51	0.01125 ± 0.00193
1000	336.7 ± 30.8	0.01264 ± 0.00122	1000	413.71 ± 47.45	0.00982 ± 0.00086

AM of Tungsten

Similarly, the experimental study was repeated for SLM of pure tungsten and gathered for this thesis. All parameters were kept the same as the molybdenum empirical study to determine the reference on the mechanical property data of SLM pure tungsten.

Table 6 displays the results of average flexural stresses and average flexural strains of AM pure tungsten varying print speeds and shielding gases obtained from this study. From the data below, it was apparent that pure tungsten with low-density microstructures and with significant porosity and cracks was produced in Ar gas atmosphere. These AM defects contributed to low flexural strengths and elongations of the materials. By contrast, the flexural strength data for samples produced in Ar-3H_2 gas atmosphere was comparable to that produced by the conventional fabrication methods, 785 – 1080 MPa, as listed in Table 2.

Table 6. Flexural stress and strains of tungsten in pure Ar and Ar-3H_2.

W in Ar			W in Ar-3H_2		
Print speed (mm/s)	Average flexural stress (MPa)	Average flexural Strain	Print speed (mm/s)	Average flexural stress (MPa)	Average flexural strain
100	336.22 ± 38.36	0.00581 ± 0.00088	100	985.56 ± 56.92	0.0086 ± 0.00029
200	419.61 ± 17.09	0.00682 ± 0.00164	200	933.26 ± 62.03	0.00923 ± 0.00044
300	447.18 ± 73.73	0.00647 ± 0.0016	300	870.60 ± 63.02	0.01028 ± 0.00077
400	458.10 ± 31.29	0.00601 ± 0.00098	400	875.02 ± 29.24	0.00972 ± 0.00051
500	504.02 ± 13.97	0.00649 ± 0.00072	500	783.56 ± 79.80	0.00807 ± 0.00121
600	507.10 ± 48.40	0.00785 ± 0.00097	600	911.91 ± 32.24	0.00975 ± 0.00065
800	517.12 ± 27.51	0.00688 ± 0.00085	800	857.00 ± 72.43	0.00885 ± 0.00102
1000	506.69 ± 35.43	0.00744 ± 0.00182	1000	785.24 ± 14.64	0.00822 ± 0.00046

AM of Tungsten and Molybdenum Alloys

Earlier studies of Mo-W alloys recognized molybdenum and tungsten form a continuous series that do not contain a miscibility gap [39]. A miscibility gap is a state in a phase diagram for a mixture of elements where the mixture exists as multiple states. In the same manner, Agte and Vacek in their book noted that forming continuous series depend on two conditions lattice constants and similar type of crystal lattice [24]. These two metals are isomorphic, and they are both crystalline in cubic body centered lattices with similar lattice constant parameters of 3.158 Å for tungsten and 3.140 Å for molybdenum [40]. In Physical Metallurgy of Refractory Metals and Alloys literature, the arrangement of continuous solubility for a broad range of solid metals requires similar structure of the outer electron shells of the atoms of the interacting components, isomorphism of their crystal lattices, and minor difference in their atomic diameters not

more than 8-15% [18]. Tungsten and molybdenum meet these criteria and the metals should dissolve well in one another.

Previous studies examined the properties of vacuum melted Mo-W alloys with 0-100% tungsten. In their work, Ababhkov et al concluded that the DBTT increased most when over 80% W is added. The strength of the alloy with 32% W was similar to unalloyed tungsten at all test temperatures [41, 42]. This finding suggests that alloying higher than 32% of tungsten is not recommended and the effect of alloying molybdenum and the presence of tungsten improves molybdenum's mechanical properties.

Most early studies as well as current work focus on physical, mechanical, and metallurgical properties of Mo-30W alloys demonstrated that melting point is 2843 °C, density of 11.902 g/cm^{-3}, tensile strength between 606.74 and 837.7 MPa, yield strength between 503.31 and 737 MPa, strain at fracture between 12 and 26%, average hardness of 256 DPH at room temperature, and average hardness of 70 and 27 DPH at 1093°C and 1650°C respectively [43]. Similarly, Batienkov et al demonstrated that Mo-30W alloys prepared by vacuum-arc melting exhibited yield strength between 773 and 960 MPa at room temperature [44]. Their work revealed that mechanical properties of the Mo-W alloy improved with an increase in tungsten content, but tungsten content over 30% worsens alloy deformability unless heating temperature is increased to over 1900 °C [44]. In agreement with these empirical studies, Savitskii et al. concluded that the tensile strength of vacuum arc melted Mo-30W alloy was approximately 84 kg/mm^2, 823.76 MPa, at 20 °C [18]. Additionally, the tensile strength of Mo-30W system decreased 16.7% from 823.76 MPa to 686.46 MPa after recrystallization. Interestingly, this

observation was also observed by Schmidt et al whom found the tensile strength of Mo-30W system declined 31% from 837.7 to 646.7 MPa.

Knowledge Gaps

The evidence suggests that studies on AM pure W and AM pure Mo are associated with Mo-W alloy system are weak and inconclusive. Research on the AM Mo-30W has been mostly restricted to limited comparisons of vacuum melted Mo-30W studies done between the 1950s to 1970s. Additionally, there is no published research on the effects of heat treatment on molybdenum-tungsten system and those that are not published have insufficient accessible data. Little is known about mechanical and microstructural characterization of AM Mo-30W, but the above reviews of AM pure molybdenum and pure tungsten highlight shortcomings that may help avoid similar flaws in this study.

Summary

In the past five years, a number of researchers have sought to determine higher densification, lower porosity, increased mechanical properties in AM of pure tungsten and pure molybdenum. This systematic understanding of AM processing parameters raises questions about mechanical properties and microstructural of AM molybdenum and tungsten alloy characterization. While molybdenum and tungsten and their alloy metallurgies are well understood, AM of molybdenum tungsten alloys have yet to be published nor there have been attempts to examine heat treatment on AM of any molybdenum-tungsten alloys. This proposed study will revise, extend, or refine the understanding and knowledge of the AM Mo-30W in addition to addressing the

limitations of the literature by means of combining qualitative, quantitative, and mixed research methods to answer the following questions:

- How do the printing parameters (laser speed, build orientation, and atmosphere gas) and post-processing heat treatment effect the mechanical and microstructural properties of the tungsten molybdenum alloys?
- What are the mechanical and microstructure characteristics of Mo-30W?
- What is the relationship between AM defects and microstructural characteristics and mechanical properties of Mo-30W?
- What is the variability of AM of Mo-30W fracture properties?

The next chapter provides an introduction to research methodologies and describes the study approach as well as methods, equipment, and software used in this study.

III. Methodology

Chapter Overview

The purpose of this chapter is to present a combination of qualitative, quantitative, and mixed research design methods that were adopted to provide data collection, data analysis, and to determine relationships between AM defects, mechanical properties, and microstructural characteristics of additively manufactured Mo-30W material. A summary of the methods used for Mo-30W characterization in this study is presented in Table 7. American Society for Testing and Materials (ASTM) has created six types of standards that relate to manufacturing processes such as testing, materials, classification, and operation. These six types are test method, specification, classification, practice, guide, and terminology standards [45]. For research purposes, the applicable methodologies were followed according to ASTM, ISO, and AFIT standard laboratory procedures established for safety and consistency.

Table 7. Summary of methods for Mo-30W characterization.

Characterization	Method	Equipment or software
Strength test	Three-point bend test	MTS Model 810
Fracture surface analysis	Electron microscopy	TESCAN MAIA3 SEM
Chemistry analysis	Energy dispersive spectroscopy	EDAX's OIM™
Porosity analysis	Optical microscopy	Zeiss Observer
Hardness test	Vickers micro hardness testing	Qness 60 A+ EVO
Statistical test	Analysis of variance	MATLAB r2021a

Particle Characterization and 3D Printer

The material manufactured in this study was plasma spheroidized tungsten powder and molybdenum powder provided by Tekna Advanced Materials (Sherbrooke, QC, Canada). The scanning electron microscope images of the materials are depicted in Figure 2 and the maximum particle sizes were 25 μm and 45 μm obtained by sieve, respectively. Previous research has established that the smaller the particle size, the better it melted for the powder layer [13]. Specific tungsten particle size distribution data is provided in [16]. Inert gas fusion technique in a LECO Oxygen/Nitrogen/Hydrogen 836 Elemental Analyzer machine determined the oxygen concentrations of the Mo powder and W powder to be 235 ppm and 219 ppm, respectively [46].

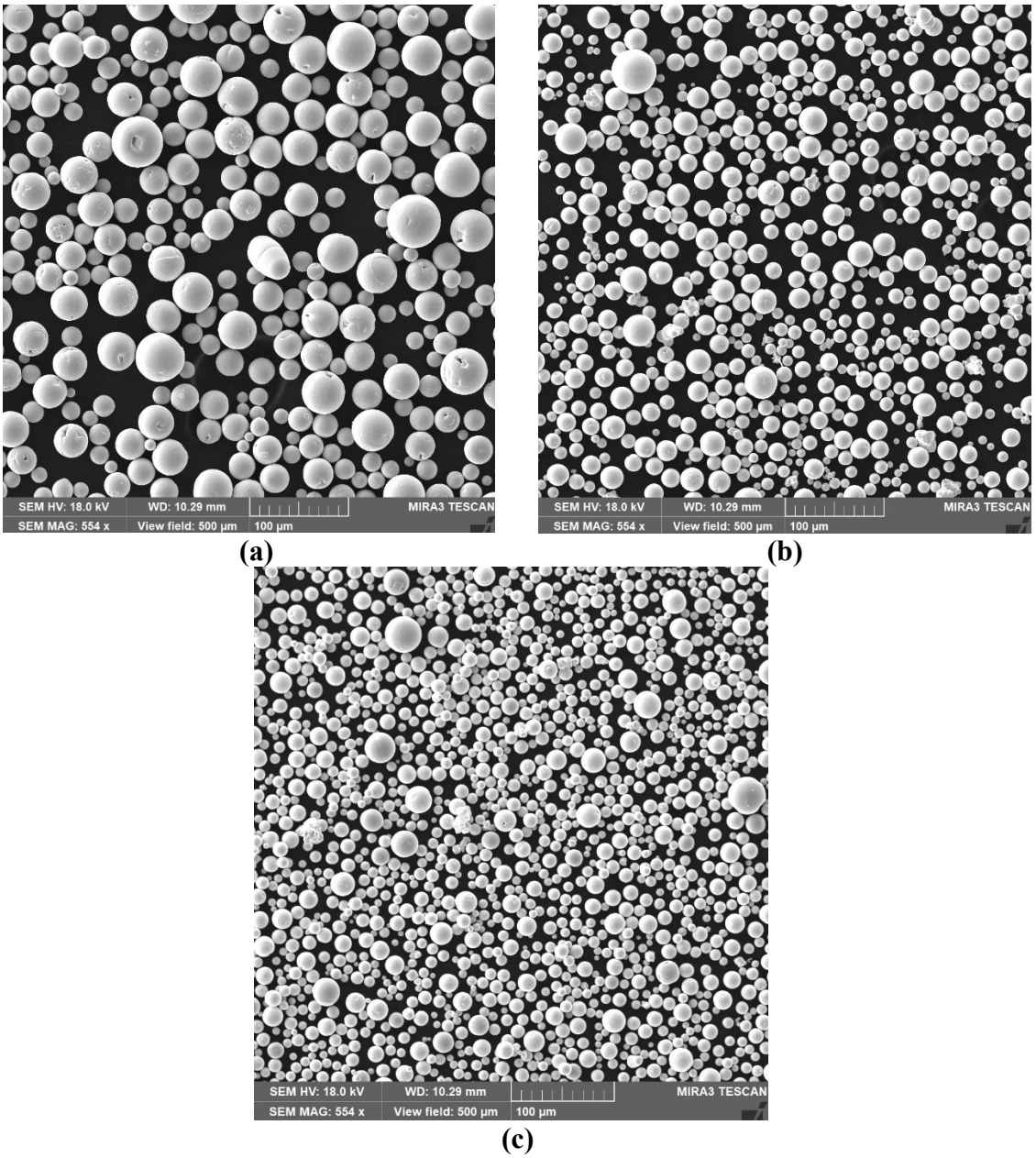

Figure 2. SEM images of size and spherical morphology of a) molybdenum (top left), b) tungsten (top right), c) mixed Mo and W (bottom) powders.

All AM test specimens were manufactured using a Concept Laser Mlab Cusing 200R 3D metal printer (Cincinnati, OH, USA) equipped with a 200-Watt fiber laser in continuous-wave mode to deliver maximum productivity. The laser emits a wavelength

of 1080 nm with a focus diameter of approximately 50 µm. In addition, the max scanning speed is 7 m/s and can create layer thickness 15 – 30 µm to boost flexibility and accuracy of the production [47]. All procedure steps take place under inert gas, shielded from external influences. Pure argon (Ar) gas and argon with 3% hydrogen (Ar-3H_2) were used as two shield gas atmospheres in this study. The machine settings were adjusted to maintain the oxygen at the lowest level possible (< 1000 ppm) [16]. The printer is displayed in Figure 3.

Figure 3. Concept Laser Mlab Cusing 200R 3D metal printer.

Printing Parameters and Experiment Materials

Previous studies on AM of pure tungsten and tungsten-rhenium alloy by Kemnitz et al. and Eckly et al. were used to design optimal print processing parameters based on densification, SEM images, and Electron Backscatter Diffraction (EBSD) maps. [16, 17]. The samples were printed using a laser power of 200 W, laser scanning speed of 100 mm/s to 400 mm/s, hatch spacing of 50 μm, and layer thickness of 20 μm. All parts were printed with a laser scanning strategy, 90° rotations between layers. Two different print orientations of vertical (90° or V) and diagonal (45°) were printed. Altogether, the molybdenum and tungsten were consolidated into three cuboids with dimensions 2 mm x 4 mm x18 mm applying each SLM build processing settings for a total of 180 Mo-30W specimens for testing. Table 8 displays the summary of printed Mo-30W specimens divided to as-built with various print parameters and designated for future heat treatment conditions. The density of the printed specimens was measured using Archimedes' principle. The differences observed in the density of the printed specimen were small when compared with theoretical density of the metals.

Table 8. Summary of Mo-30W specimen printed.

Specimen (#)	Shielding gas	Print speed (mm/s)	Print orientation (°)	HT temperature (°C)	HT duration (hours)
1-12	Ar	100-400	90	0	0
13-24	Ar	100-400	45	0	0
25-36	Ar-3H_2	100-400	90	0	0
37-48	Ar-3H_2	100-400	45	0	0
49-60	Ar	100-400	90	1600	4
61-72	Ar	100-400	45	1600	4
73-84	Ar	100-400	90	1600	8
85-96	Ar	100-400	45	1600	8
97-108	Ar	100-400	90	1600	12
109-120	Ar	100-400	45	1600	12
121-132	Ar	100-400	90	1600	24
133-144	Ar	100-400	45	1600	24
145-156	Ar	100,400	90	2000	12
157-168	Ar	100,400	45	2000	12
169-180	Ar	100,400	90	2200	6

Procedure and Equipment Used in Data Collection

In achieving the research design, several specific procedures and equipment were used in data collection and analysis. The following sections give full details of the equipment, techniques and procedures used for the thesis.

Post-Processing

All additively manufactured Mo-30W specimen sides were carefully cut off from the build plate by wire electrical discharge machining (EDM) by the AFIT machine shop. The specimens were then cleaned in isopropyl alcohol then ground to prepare their surfaces for mechanical testing. The specimens were ground using Buehler EcoMet 300 Pro Grinder Polisher (Lake Bluff, IL, USA) with 320 grit Mager Scientific silicon carbide (SiC) grinding disc papers. This process removes powder particles on both sides of the cuboid. These stuck powder particles may affect the accuracy of the density measurement, the deformation process, and the hardness of the surface layer [48]. The Mo-30W samples were then baked to eliminate trapped moisture at 100 °C for one hour using an Omegalux LMF-3550 furnace (Stamford, CT, USA) prior to mechanical testing. The grinder polisher and the furnace are depicted in Figure 4.

(a)

(b)

Figure 4. (a) Buehler Grinder Polisher and (b) Omegalux Furnace.

After the sample's fracture surface examination, the samples were prepared and mounted in conductive phenolic resin using a MetLab MetPress A automatic mounting press (MetLab Corporation, Niagara Falls, NY, USA) seen in Figure 5. The parameters for the press machine as follows: heating temperature at 180 °C, heating pressure at 4800 psi, heating time set to 25 minutes, cooling time set to 15 minutes, and cooling rate set to high.

Figure 5. MetLab MetPress Automatic Mounting Press.

All Mo-30W specimen pucks were accurately ground and polished for surface preparation. The grinding and polishing steps along with the settings used for the grind and polish machine are listed in Table 9. Grinding and polishing procedure for Mo-30W

specimen. After a minute in each step of the procedure, the samples were cleaned with isopropyl alcohol to remove any grinding media residues. Along with cleaning the components, personal protective equipment (PPE) were worn when handling specimen to minimize the risk of contamination.

Table 9. Grinding and polishing procedure for Mo-30W specimen.

1	Type	Surface	Grit size	Time	Base speed	Lubricant
1	Grind	SiC Grind Paper	240	5 min	200 rpm	Water
2	Grind	SiC Grind Paper	320	4 min	200 rpm	Water
3	Grind	SiC Grind Paper	400	4 min	200 rpm	Water
4	Grind	SiC Grind Paper	600	4 min	200 rpm	Water
5	Grind	SiC Grind Paper	800	4 min	200 rpm	Water
6	Polish	Mo Polish Paper	6 μm	3 min	150 rpm	Buehler MetaDi Supreme
7	Polish	Mo Polish Paper	3 μm	3 min	150 rpm	Buehler MetaDi Supreme
8	Polish	Mo Polish Paper	1 μm	3 min	150 rpm	Bulher MetaDi Supreme

The divided samples subjected to heat treatments were sent to American Isostatic Presses Inc. (Columbus, OH, USA). The samples were heat treated in a pure argon atmosphere at a temperature of 1600 °C for 4, 8, 12, 24 hours. Initial observations of relatively unmixed tungsten particles in the target alloy matrix suggested that the specified temperature was not sufficient. Thermo-Calc 2022a Software simulated the effects of heat treatment process to predict the states and microstructure that form. Two set of temperature and time span conditions were identified using 30% tungsten boundary

conditions defined in the target matrix. The Thermo-Calc heat treatment simulations are shown in Appendix B encapsulating the results. These results suggested a second batch of samples sent to be heat treated at 2000°C for 12 hours in the same location. In addition, the third batch of samples were sent to Rhenium Alloys Inc. (North Ridgeville, OH, USA) to heat treat the new samples at 2200°C for 6 hours.

Mechanical Testing

Tensile tests of all additively manufactured Mo-30W specimen, as built and heat treated, were performed using a servo-hydraulic MTS 810 load frame as seen in Figure 6. (MTS Systems Corporation, Eden Prairie, MN, USA). The three-point bend test operated by applying central force of the crosshead at a constant rate of displacement of 0.01 mm per second using 14 mm distance between end supports as depicted in Figure 6. Three-point bending test was chosen because it is less susceptible to errors due to material's geometry and ease of use for the experiment. On the contrary, one of its potential disadvantages is that the surface of the test material are likely act as fracture origin. The likely reason is the materials are prone to fracture under tensile stresses [49]. For example, the force bends material so that it is in tension on the convex side and experience compressive stresses on the concave side. Eventually, the convex side near the surface will fail first before the concave side breaks [50]. The specimen surfaces were prepared consistently, and the warped, twisted, and non-uniform specimen were omitted from analysis to keep the potential errors to a minimum.

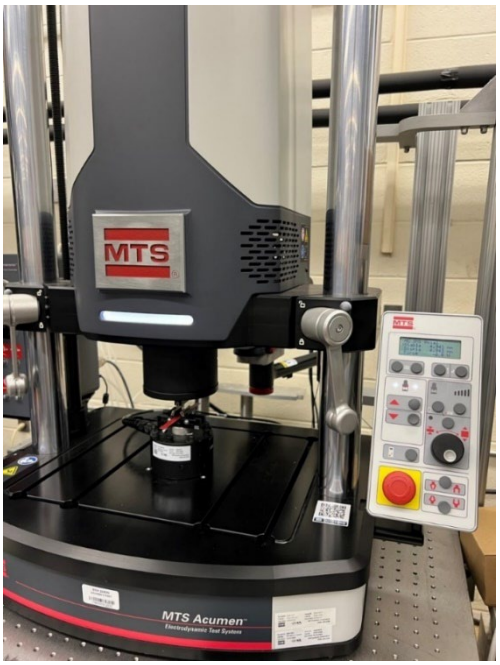

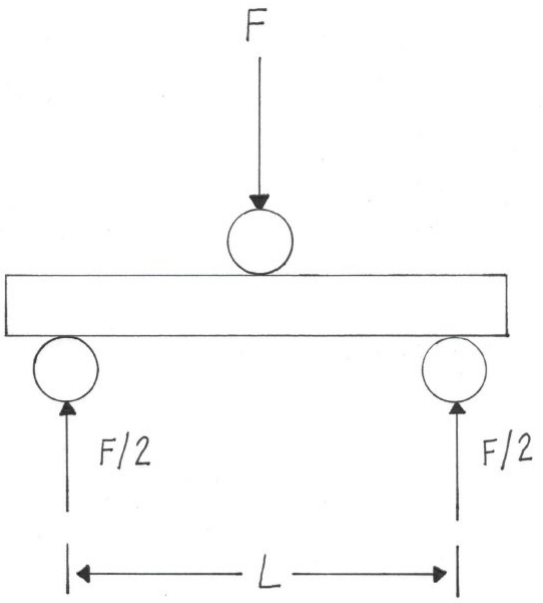

(a) **(b)**

Figure 6. (a) Material Testing System (MTS) Model 810 and (b) schematic of three-point bend fatigue test setup [49].

The axial load, time, displacement data were recorded for each Mo-30W specimen until failure. The flexural stress, σ_f, and flexural strain, ε_f, responses are calculated as seen equations below [49]:

$$\sigma_f = \frac{3FL}{2bd^2} \tag{2}$$

$$\varepsilon_f = \frac{6Dd}{L^2} \tag{3}$$

where F is the load at a given point, L is the support distance, b is the width of the specimen, d is the thickness of the specimen, and D is the maximum deformation from the center of the specimen.

Vickers hardness tests were carried out with Qness 60 A+ EVO and Qpix Control2 Software at room temperature in the Materials and Manufacturing directorate of the Air Force Research Laboratory (Dayton, OH, USA). The resistance of materials against surface indentation is termed as hardness. The Vickers hardness test uses a diamond indenter in a right pyramid shape with 136° between opposite faces at the top is forced into the surface of the sample as seen in Figure 7. The corresponding figure is an image of Vickers indentation where the mean indentation diagonals distances are used to calculate the Vickers hardness value by the following equations:

$$\text{Vickers hardness } (HV) = \frac{F}{SA} \tag{4}$$

$$SA = \frac{d^2}{2\sin\frac{136°}{2}} \tag{5}$$

where F is the measured force, SA is the surface area of indentation, and d is the mean indentation diagonal distance. A load of one kg and ten individual indentations were used to define the average hardness of the sample. All samples were fully polished using the procedure outlined in Table 9, and the hardness measurements were carried out by following the ASTM E92-17 [51].

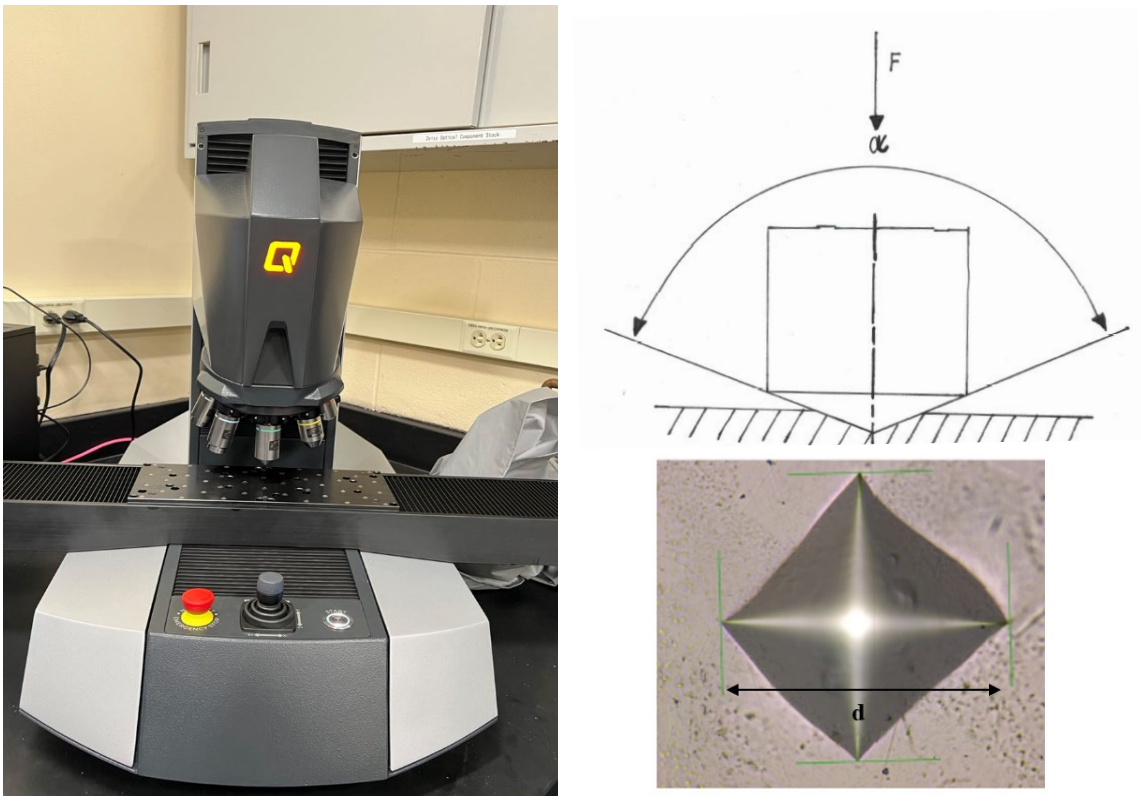

(a) (b)

Figure 7. (a) Qness 60 A+ EVO and (b) schematic of the test and Vickers indentation forced into sample.

Microstructure Analysis

After Mo-30W sample's bending strength tests were completed, all fracture surfaces were inspected by means of a TESCAN MAIA3 scanning electron microscope (TESCAN, Brno, Czech Republic) to evaluate the microstructure and fracture morphology. SEM can have a magnification range from 4x to 1,000,000x and field depth ranging from 0.7 μm to 4.3 mm [52]. The SEM microscope, shown in Figure 8, was used to visualize crack initiation points, microcracks, defects, and pores to characterize the microstructure then correlate to the findings from mechanical property tests.

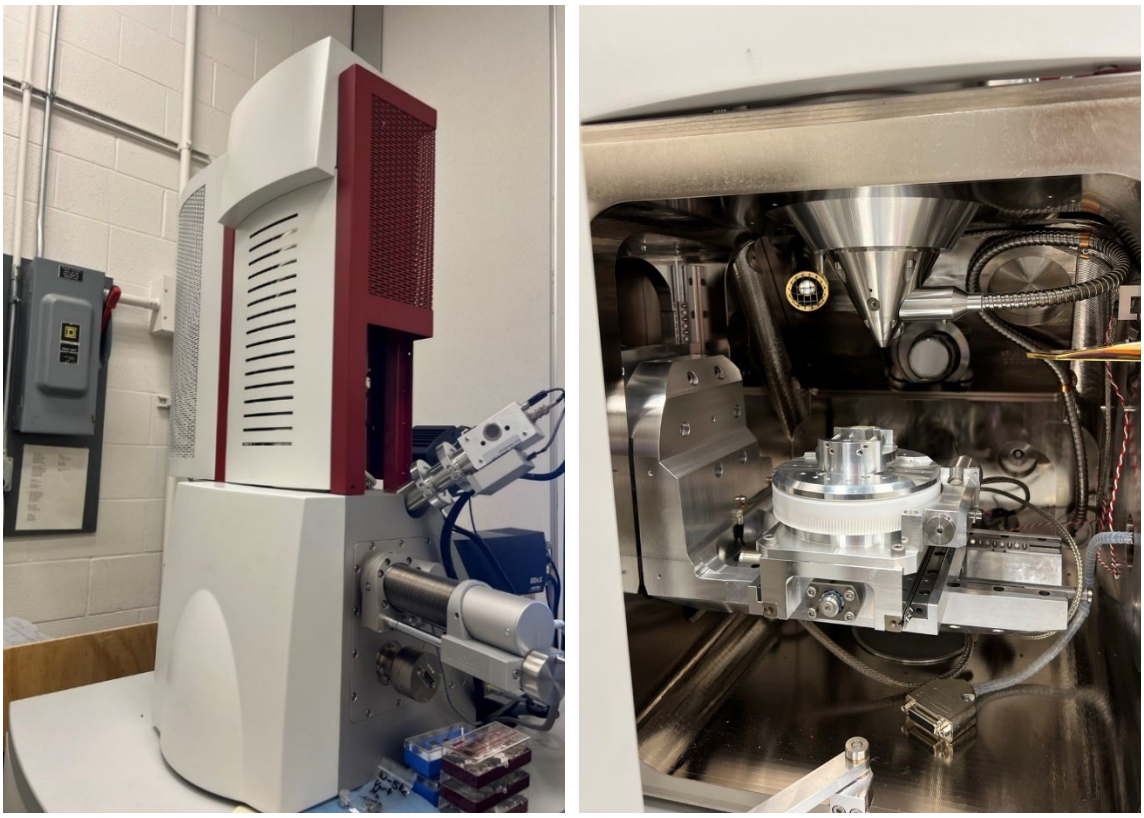

(a) **(b)**

Figure 8. a) Outside and b) inside view of TESCAN MAIA3 SEM.

Chemical Composition Analysis

In SEM, the chemical composition of the scanned areas was collected using an energy-dispersive X-ray spectroscopy (EDS) detector (Ametek Materials Analysis Division, Mahwah, NJ, USA) using working distance of 10 mm, magnification of 250x, 256x200 resolutions, and standard quality settings. EDAX's Orientation Imaging Microscopy (OIM) Analysis™ software (Ametek Materials Analysis Division, Mahwah, NJ, USA) was used to create element composition map of the material.

Porosity Analysis

After grinding and polishing, the metallographic specimen pucks were placed under a Zeiss Axio Observer Z1m optical microscope (Jena, Germany) and cross-sectional images were taken using 2.5x and 10x magnifications with resolutions of 5.55 µm and 1.33 µm to cover the specific area of interest. The ZEN microscope software performed quantitative porosity analysis by automatically counting and measuring porosity and defects [53]. The translation stages placed above the optical microscope allowed inverted cross-sectional images to be taken in a pattern of regularly spaced grids. Each cross-sectional image was taken with equivalent microscope settings such as light exposure. Figure 9 displays the optical microscope next to the software.

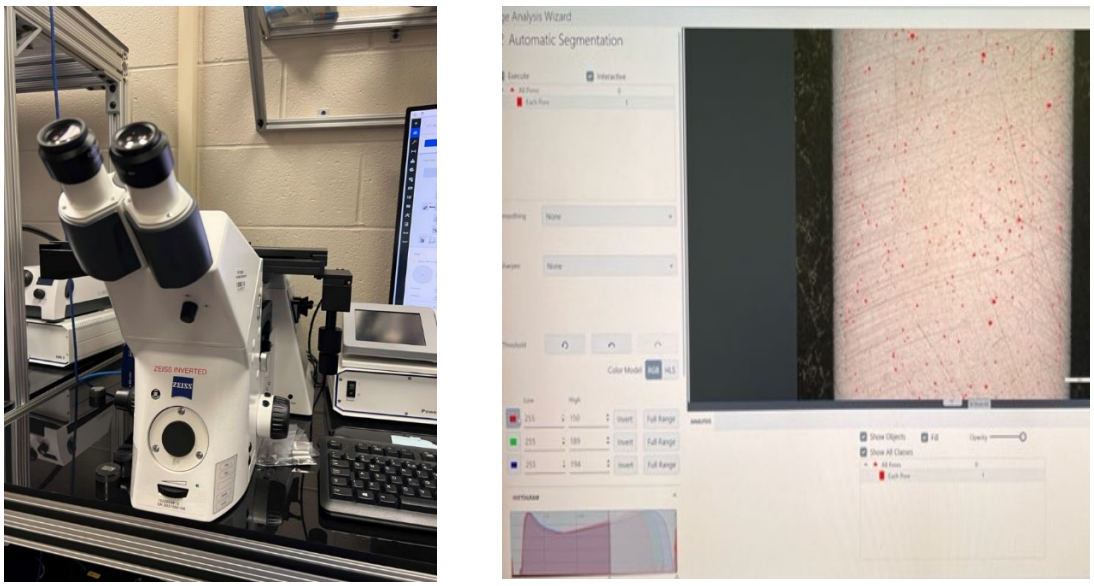

(a) **(b)**

Figure 9. (a) Zeiss Optical Microscope and (b) Zen Software.

The images captured with 2.5x magnification displayed the background outside of the specimen microstructure. Fortunately, the software used tolerance settings to identify pore shape in the region of interest, therefore the backdrop did not count in the porosity

analysis. An example of an image slice and its recognized pores with specified threshold setting is shown in Figure 10. The measurement results include every pore diameter, area, ellipse major, ellipse minor, and radius in pixel units. Since there was a level of subjectivity in configuring object detection manually, this was not as accurate as the other methods such as X-Ray CT discussed in previous chapter. Nevertheless, this porosity analysis was unbiased and simple to use for analysis and comparison.

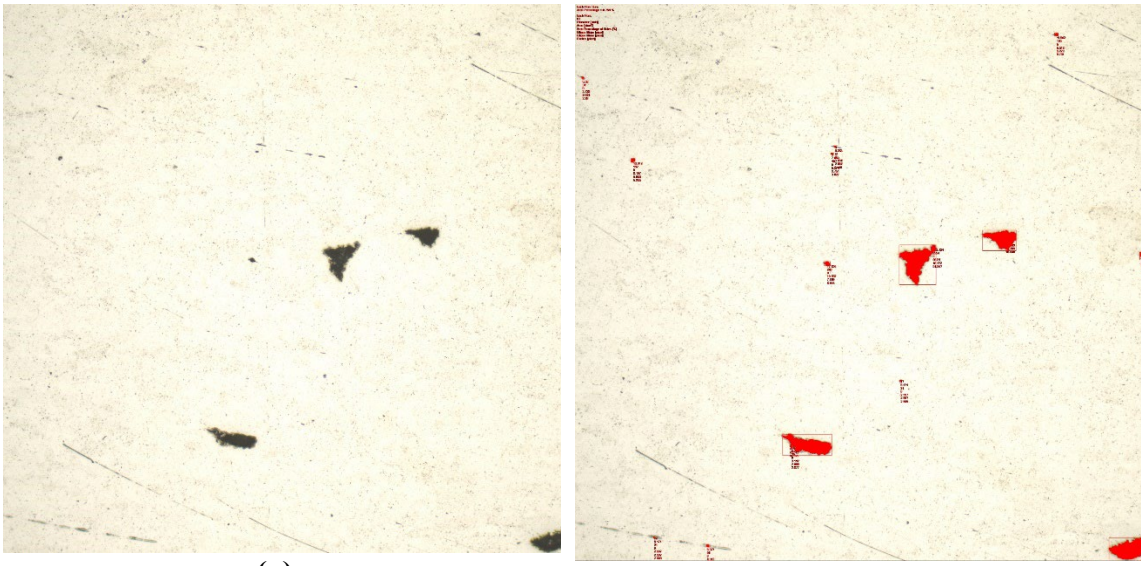

(a) **(b)**

Figure 10. Example in optical porosity analysis software, (a) image as captured (b) porosity measured in red.

Statistical Analysis

A statistical f-test and analysis of variance (ANOVA) determined the most important factor and the significance of the variabilities in mechanical properties. ANOVA is a statistical technique used for analyzing the difference between the means of

multiple samples. MATLAB ver. R2021a was used for statistical analysis for this study [54]. ANOVA can be illustrated as the hypothesis of interest as follows:

$$H_0: \mu_1 = \mu_2 = \mu_3 \ldots = \mu_k \quad (6)$$

$$H_a: \text{at least one difference among the means} \quad (7)$$

Where k = number of independent groups.

ANOVA was structured using the table below:

Table 10. Summary of ANOVA procedure [55].

Source	Sums of Square (SS)	Degrees of Freedom (df)	Mean Squares (MS)	F statistics	Probability > F
Groups	Regression Sums of Square (SSR)	k-1	Between Regression Mean Square (MSR) = SSR / (k-1)	MSR/MSE	P
Error (Residuals)	Error Sums of Square (SSE)	N-k	Error Mean Square (MSE) = SSE / (N-k)		
Total	Total Sums of Square (SST)	N-1			

$$\text{SSB} = \sum_{i=1}^{k} n_i(\bar{x}_i - \bar{x})^2 \quad (8)$$

$$\text{SSE} = \sum_{i=1}^{k} \sum_{j=1}^{n_i} n_i\left(x_{ij} - \bar{x}_i\right)^2 \quad (9)$$

$$\text{SST} = \sum_{i=1}^{k} \sum_{j=1}^{n_i} n_i\left(x_{ij} - \bar{x}\right)^2 \quad (10)$$

Where k = the number of groups, n_i = the sample size taken from respective group, x_{ij} = the j^{th} response sampled from the i^{th} group, $\bar{x}_i$ = sample mean from i^{th} group, N= total sample, $\bar{x}$ = mean of all responses.

Corresponding p-value for the F statistic can be found using a statistics textbook or a statistical toolset such as MATLAB. It is widely held view that p-values less than 0.05 mean it is statistically significant and indicate strong evidence for the alternative hypothesis.

Summary

This chapter explained the methods used in this qualitative, quantitative, and mixed study of Mo-30W mechanical and microstructural properties. The first section described the properties of molybdenum and tungsten powder used like spherical morphology, small particle size, and low oxygen content to meet the demand requirements to print satisfactory Mo-30W alloy. Next, the ideal build methods of the 3D printer were designed to print distinctive build processing settings of Mo-30W specimen. The analyses were accomplished using three-point bend test, electron microscopy, energy dispersive spectroscopy, optical microscopy, Vickers microhardness test, and analysis of variance. These methods were chosen to characterize the mechanical and microstructure properties of Mo-30W, determine the effects of the build parameters and post processing techniques, and identity unique characteristics of AM Mo-30W. The analytical procedures and a summary of the main findings obtained from them are described in the next chapter.

IV. Analysis and Results

Chapter Overview

The following chapter presents primary data analysis and results of the thesis. Mo-30W specimens were printed in Ar and Ar-3H_2 build chamber gases, 100 – 400 mm/s print speeds, vertical and diagonal build orientations, and post processed at temperatures of 1600 °C for 4, 8, 12, 24 hours, 2000 °C for 12 hours, and 2200 °C for 6 hours. The section is structured as follows: the chemical composition, fracture strengths, hardness, crack surfaces, porosity, and statistical significances of various printed Mo-30W specimen. Afterwards, the results are interpreted, evaluated, and explained to develop a better understanding for the effects of different printing parameters and post-processing heat treatments. Finally, the mechanical and microstructural properties of SLM Mo-30W alloys were characterized.

Chemical Composition Analysis

Investigation of the internal EDS maps taken of as-built samples revealed that molybdenum and tungsten particles in the alloys are not mixed well. The individual unmixed phases of Mo and W were more pronounced in the representative elemental maps of both molybdenum and tungsten in the specimen printed in Ar compared to specimen printed in Ar-3H_2 shown in Figure 11. However, the addition of hydrogen in the build chamber atmosphere had significant grain refinements to the Mo-30W. The hydrogen addition possibly induced higher melt pool temperature or heat flow of the laser which accordingly improved tungsten particle diffusivity and reduced pore density.

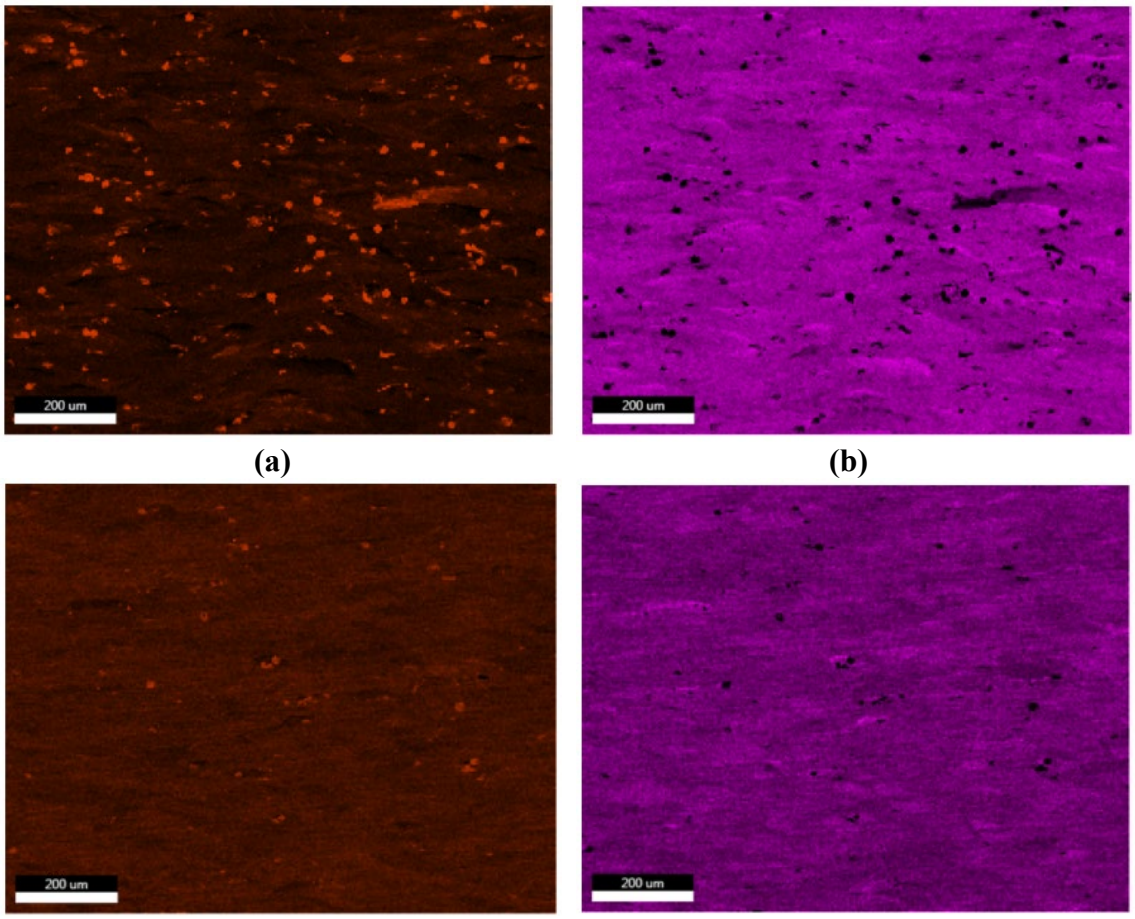

(a) **(b)**

(c) **(d)**

Figure 11. EDS map showing location of each particle of Mo-30W specimen printed (a, b) in Ar and (c, d) in Ar-3H_2, – W in orange and Mo in pink.

Figure 12. The heat treatment temperature at 1600°C reduced grain size substantially by relieving the processing stress originated during the printing, but the durations of this heat treatment condition appeared to have no significant effect on homogeneity of Mo-30W specimens.

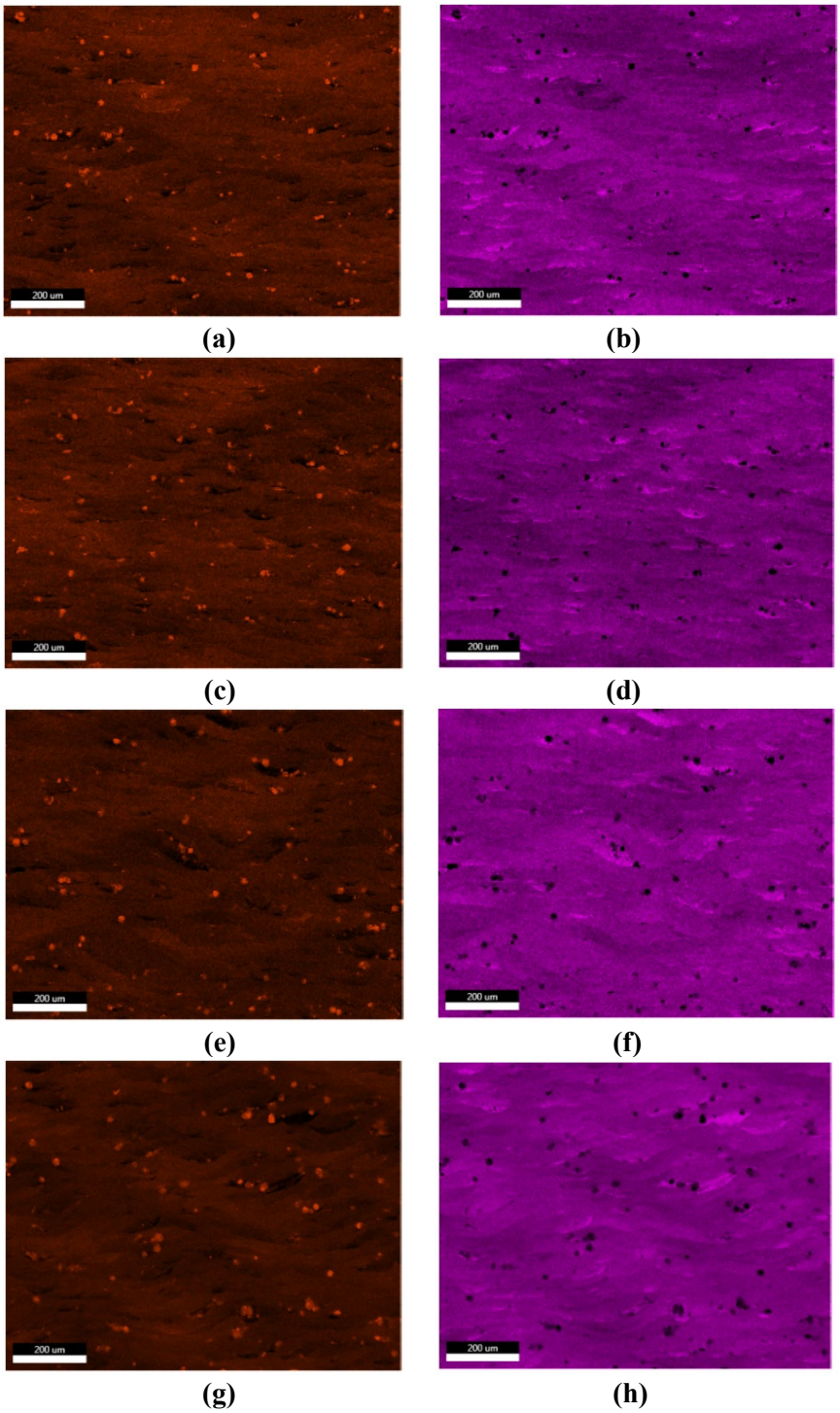

Figure 12. EDS map showing location of each particle of vertical heat-treated Mo-30W specimen at 1600 for (a, b) 4 hours, (c, d) 8 hours, (e, f) 12 hours, and (g, h) – W in orange and Mo in pink.

In contrast to early findings, specimen printed in pure argon and heat treated at 2000°C resulted in relatively higher homogeneous microstructure. Corresponding EDS maps of Mo-30W specimen printed in Ar with 100 mm/s and 400 mm/s print speed are depicted in Figure 13. According to this figure, a higher speed led to more well-mixed alloy and this observation may support the hypothesis that it lowered the E_v which subsequently reduced the vaporization of Mo during printing process.

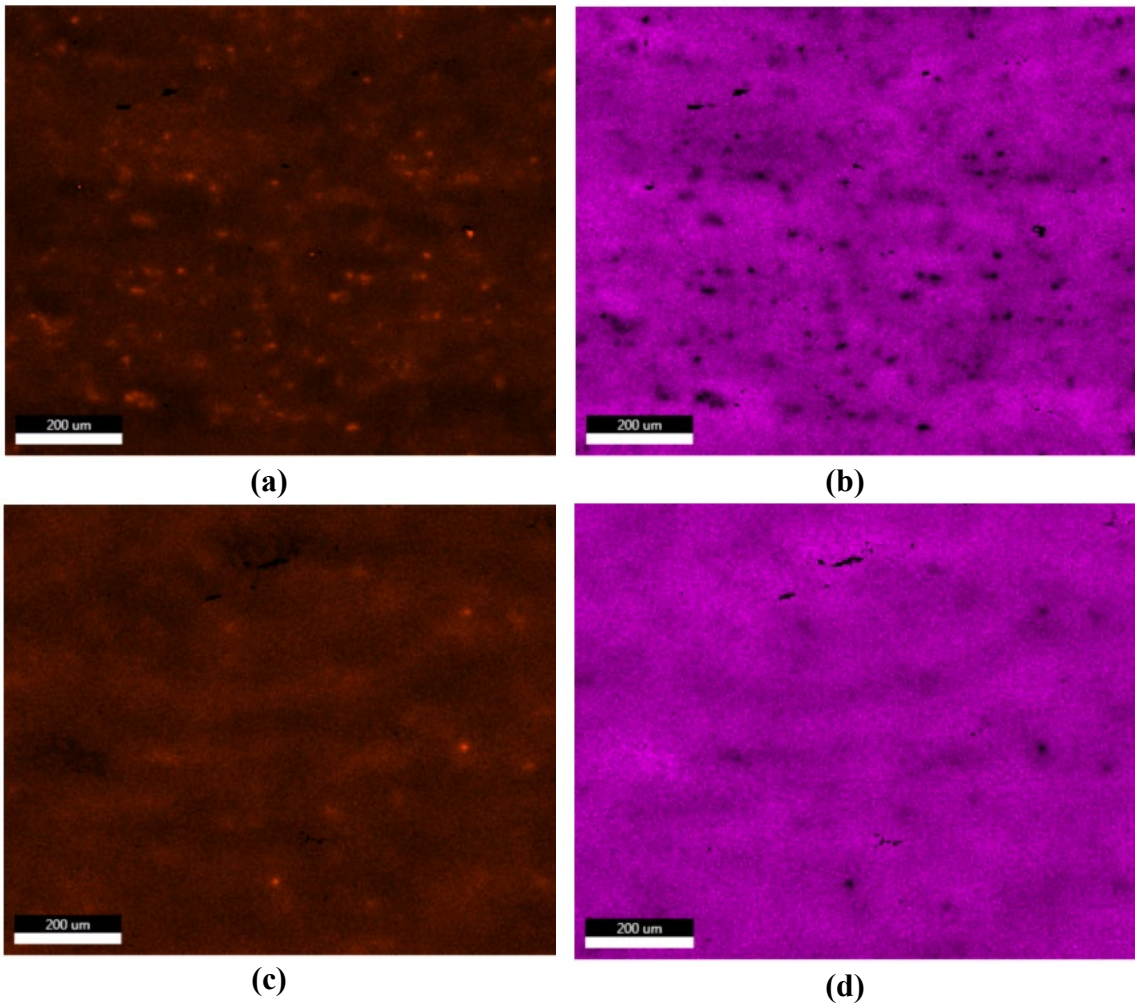

(a) **(b)**

(c) **(d)**

Figure 13. EDS map showing location of each particle of vertical heat-treated Mo-30W specimen at 2000 °C for 6 hours printed (a, b) in 100 mm/s and (c, d) in 400 mm/s – W in orange and Mo in pink.

To confirm the desired 70% molybdenum and 30% tungsten composition were achieved, the weight percentages (wt%) of the two elements were determined from the EDS maps and summarized in Table 11.

Table 11. EDS-EDAX results of Mo-30W alloys.

HT temperature (°C)	HT duration (hours)	Build chamber atmosphere	Print speed (mm/s)	Mo (wt%)	W (wt%)
N/A	N/A	Ar	100	60.02 ± 6.27	39.97 ± 6.27
N/A	N/A	Ar-3H_2	100	61.69	38.31
1600	4	Ar	100	66.51 ± 1.83	33.49 ± 1.83
1600	4	Ar	200	76.71 ± 6.88	23.29 ± 6.89
1600	4	Ar	300	71.59 ± 3.32	28.41 ± 3.33
1600	4	Ar	400	58.81 ± 1.02	41.19 ± 11.03
1600	8	Ar	100	67.48 ± 0.57	32.52 ± 0.57
1600	8	Ar	200	66.48 ± 7.83	33.51 ± 7.83
1600	8	Ar	300	72.22 ± 1.29	27.78 ± 1.29
1600	8	Ar	400	65.96 ± 6.31	34.03 ± 6.31
1600	12	Ar	100	70.35 ± 3.05	29.64 ± 3.05
1600	12	Ar	200	63.64 ± 3.34	36.35 ± 3.34
1600	12	Ar	300	68.99 ± 0.72	31.00 ± 0.72
1600	12	Ar	400	57.50 ± 6.02	42.50 ± 6.02
1600	24	Ar	100	72.13 ± 1.87	27.86 ± 1.87
1600	24	Ar	200	66.76 ± 3.37	33.23 ± 3.37
1600	24	Ar	300	68.70 ± 0.74	31.29 ± 0.74
1600	24	Ar	400	65.86 ± 0.69	34.14 ± 0.69
2000	12	Ar	100	67.54	32.46
2000	12	Ar	400	74.19	25.81

Approximately 60 wt% of molybdenum reported here suggested that molybdenum tends to evaporate in SLM of Mo-30W in pure Ar and Ar-3H_2. Also, the summary results indicated the hydrogen addition induced lower tungsten weight percentage. This suggest that the addition of hydrogen in the build chamber gas reduced tungsten oxides from forming in Mo-30W as compared to specimens printed in pure Ar.

In addition, SLM of Mo-30W with a higher weight percentage of tungsten was feasible using the lower print speed. The lower the printing speed, the higher the E_v, which subsequently might be responsible for the more rapid evaporation of Mo as discussed before. Furthermore, these findings provide a solid evidence base for the early weight gain of molybdenum and weight loss of tungsten during the heat treatment. The thermal effect possibly caused the formation of Mo oxides and increased formation of higher order volatile tungsten oxides. These unstable oxides dissipated, which consequently lowered the mass of tungsten. Although variation of chemical compositions were relatively low, multiple elemental maps of each sample may determine more well-defined trends. The following section discusses the results of mechanical testing of Mo-30W specimen.

Results of Mechanical Testing

Three-point Bend Tests

All Mo-30W specimen data obtained from the three-point bend tests are presented in Table 12. – Table 14., their corresponding stress-strain are plotted together in Figure 14. – Figure 17. All the tested samples in the tables and graphs were broken up by a specific build parameter giving more complete information on each of their effects on Mo-30W specimens. For instance, Table 12 and Figure 14 consist of the effects of SLM printer's build chamber gas types on Mo-30W while Table 13 and Figure 15 involve the effects of post-processing heat treatments. Full measured axial load (N) and vertical displacement (mm) of Mo-30W specimen used to calculate the flexural stresses and strains are shown in Appendix D.

The flexural stresses (MPa) and flexural strains (mm/mm) for Mo-30W specimen printed in Ar and Ar-3H_2 with various speeds reported in Table 12 were the average of three tests with standard deviations. The top half of the table shows specimen printed in a vertical orientation and the bottom half of the table displays specimen printed in a diagonal orientation.

Table 12. Flexural stress and strains of vertically and diagonally printed Mo-30W in pure Ar and Ar-3H_2.

Vertical Mo-30W in Ar			Vertical Mo-30W in Ar-3H_2		
Print speed (mm/s)	Average flexural stress (MPa)	Average flexural Strain	Print speed (mm/s)	Average flexural stress (MPa)	Average flexural strain
100	299.57 ± 59.50	0.00831 ± 0.00104	100	615.34 ± 36.18	0.0071 ± 0.0018
200	111.81 ± 23.67	0.00521 ± 0.00078	200	328.05 ± 26.15	0.00572 ± 0.00063
300	147.35 ± 6.59	0.00751 ± 0.0009	300	266.00 ± 22.37	0.00537 ± 0.00135
400	81.60 ± 3.71	0.00512 ± 0.00081	400	202.84 ± 14.03	0.00582 ± 0.00027
Diagonal Mo-30W in Ar			Diagonal Mo-30W in Ar-3H_2		
Print speed (mm/s)	Average flexural stress (MPa)	Average flexural Strain	Print speed (mm/s)	Average flexural stress (MPa)	Average flexural strain
100	222.33 ± 13.24	0.0093 ± 0.00119	100	421.81 ± 13.91	0.00654 ± 0.00063
200	137.96 ± 22.62	0.0058 ± 0.00175	200	392.20 ± 14.03	0.00756 ± 0.00022
300	229.55 ± 0	0.01018 ± 0	300	387.67 ± 44.66	0.00795 ± 0.00044
400	202.06 ± 13.61	0.01008 ± 0.00123	400	350.71 ± 10.42	0.00761 ± 0.00033

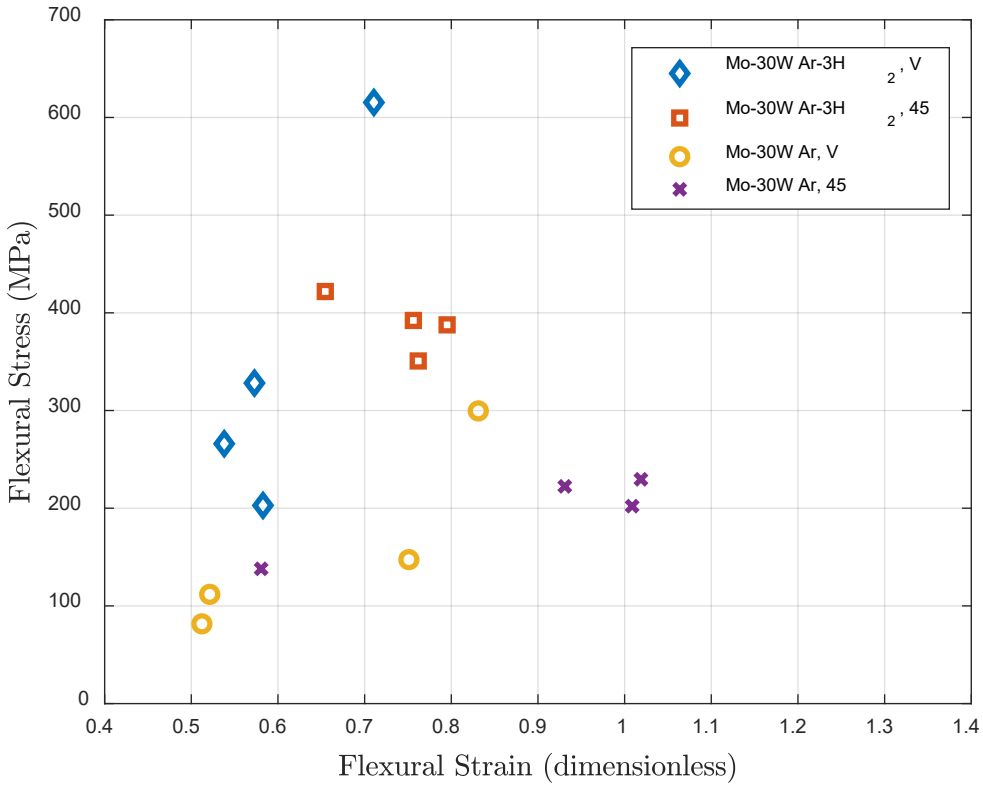

Figure 14. Stress and strain relationship of Mo-30W vertically and diagonally printed in Ar and Ar-3H$_2$.

What stands out in this table was the general pattern of significantly lower bending strength of Mo-30W specimen printed in pure argon than their similar build orientation counterparts printed in Ar-3H$_2$. Out of all tests of Mo-30W, specimens vertically printed in Ar-3H$_2$ had the highest average flexural strength of 615.34 MPa which was 105% greater than the specimens printed in Ar with the same printing orientation. Similarly, the highest average bending strength of Mo-30W specimens printed diagonally in Ar-3H$_2$ was 421.81 MPa, 89.8% larger than a sample produced in Ar with an identical orientation. Compared to averaged literature yield strength value of

773.14 MPa, the bending strength of SLM produced Mo-30W was comparable to conventional fabrication methods.

No significant differences were found between the effects of build chamber atmosphere, print orientation, and print speeds to the ductility of the Mo-30W specimen. All samples exhibited brittle fractures at a room temperature with flexural strains at failure less than 1% when compared to literature strain at fracture value of 12 to 26% for traditionally fabricated Mo-30W.

Diagonally built samples have relatively lower bending strengths compared to the vertically built samples. This meant the build orientation had a significant effect on the bending strength. Additionally, initial observations suggested that there may be combined effects of build orientations and print speeds on the variation of bending strengths. There seemed to be a sharp decrease of approximately 46 – 67 % in flexural strength of vertically printed specimen with increasing printing speeds, but the bending strengths of diagonally printed specimen stay consistently within 350 MPa to 421 MPa across all printing speeds. This observation may support the hypothesis that SLM defects such as pore and cracks were reduced using diagonal print orientations, but the grain microstructures were coarser than Mo-30W specimen printed vertically at a print speed of 100 mm/s. Therefore, the complement Mo-30W specimen printed diagonally had lowered the mechanical strengths. Further investigations in microstructure analysis are necessary to make a more complete conclusion.

To establish possible cause-and-effect relationship by isolating the effect of heat treatment methods on mechanical properties, the various heat treatment conditions were

applied to specimens printed only in pure Ar. The flexural strengths and flexural strains for Mo-30W specimens printed in pure Ar with various speeds and heat treatments reported in Table 13 were the average of three tests with standard deviations displayed as well. The top third of the table shows specimen heat treated at 1600°C for 4 and 8 hours, the center third displays Mo-30W heat treated at 1600°C for 12 and 24 hours, and the bottom third of the table shows samples heat treated at 2000 °C for 12 hours and 2200°C for 6 hours.

Two samples exposed to heat treatment at 2200°C showed signs of dimensional warping. There are many explanations as to why some samples distorted upon annealing. Some examples are impurities within material, anisotropy causing asymmetric distribution of heating and cooling, and excessive temperature exposure. These samples were excluded from mechanical tests to keep the potential errors to a minimum as discussed earlier.

Table 13. Flexural stresses and flexural strains of vertically printed Mo-30W in pure Ar with varying durations and temperatures of heat treatment.

Vertical Mo-30W in 4-hour HT 1600°C			Vertical Mo-30W in 8-hour HT 1600°C		
Print speed (mm/s)	Average flexural stress (MPa)	Average flexural Strain	Print speed (mm/s)	Average flexural stress (MPa)	Average flexural strain
100	390.51 ± 26.83	0.00655 ± 0.00073	100	372.03 ± 27.52	0.00546 ± 0.00025
200	297.01 ± 24.65	0.00441 ± 0.00027	200	299.53 ± 61.18	0.00485 ± 0.00131
300	228.66 ± 18.28	0.00389 ± 0.00025	300	255.18 ± 28.91	0.004 ± 0.00052
400	238.81 ± 00.13	0.00386 ± 0.00009	400	198.68 ± 26.41	0.00366 ± 0.00007
Vertical Mo-30W in 12-hour HT 1600°C			Vertical Mo-30W in 24-hour HT 1600°C		
Print speed (mm/s)	Average flexural stress (MPa)	Average flexural Strain	Print speed (mm/s)	Average flexural stress (MPa)	Average flexural strain
100	403.88 ± 26.82	0.0072 ± 0.00076	100	431.71 ± 16.25	0.00643 ± 0.00021
200	277.70 ± 46.09	0.00538 ± 0.00131	200	254.61 ± 28.8	0.00605 ± 0.00115
300	227.88 ± 31.39	0.0047 ± 0.00121	300	234.78 ± 8.98	0.00561 ± 0.00227
400	198.49 ± 20.34	0.00331 ± 0.00024	400	204.11 ± 33.54	0.00378 ± 0.00014
Vertical Mo-30W in 12-hour HT 2000°C			Vertical Mo-30W in 6-hour HT 2200°C		
Print speed (mm/s)	Average flexural stress (MPa)	Average flexural Strain	Print speed (mm/s)	Average flexural stress (MPa)	Average flexural strain
100	374.77 ± 37.68	0.00618 ± 0.00037	100	278.03 ± 46.55	0.00499 ± 0.00072
400	408.42 ± 80.82	0.00652 ± 0.00081	400	313.1 ± 43.89	0.00481 ± 0.00049

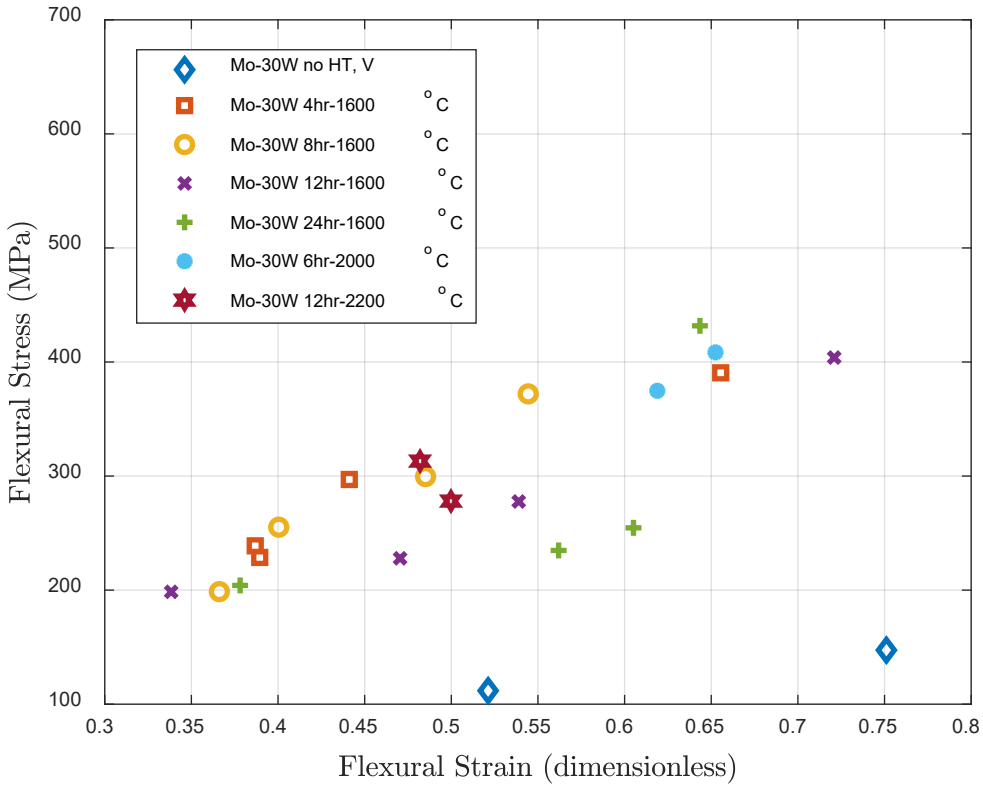

Figure 15. Stress and strain relationship of Mo-30W vertically printed in pure Ar with varying durations and temperatures of heat treatment.

Closer inspection of the table and the figure above shows all the heat treatment conditions slightly improved the bending strengths of Mo-30W specimen. For all heat-treated Mo-30W specimens at 1600°C printed in 100 mm/s, the bending strength increased an average of 25.23% compared to as-built Mo-30W. This finding is consistent with the chemical composition analysis in which the specimens were able to achieve relatively higher homogenous solid alloy compared to as-built Mo-30W without the heat treatment. The heat treatment at a temperature of 2000 °C and 2200 °C led to significant improvement in the bending strength of Mo-30W printed in speed of 400 mm/s. These

samples exhibited an average flexural stress of 408.42 MPa and 313.10 MPa respectively which were 408.42% and 283.70% increase compared to as-built Mo-30W equivalent. According to Ipsen USA, the eutectic chart of maximum temperature between molybdenum and tungsten in vacuum is 1927 °C, therefore the specimen heat treated above this temperature were comparatively homogenous alloy evident from the chemical composition analysis which caused an increase in mechanical strength [56]. These findings are consistent with that of Savitzskii et al. who stated the increase in mechanical strengths as a result of heat treatment can be attributed to several factors. For instance, residual strain elimination by recovery, recrystallization, and grain growth. Additional inspections in the microstructure evaluations are necessary to support this claim.

For easier visualization of the bending strength data included in Table 13, multiple plots showing the responses obtained by three-point bending test for each Mo-30W group types are shown in Figure 16. In this plot, the result of flexural stresses and flexural strains for all Mo-30W samples and their means were plotted. The graph shows that there is a slight decrease in ductility as print speeds increase across all heat-treated samples. However, all samples exhibited brittle fractures at a room temperature with flexural strains at failure less than 0.8%. The following part of this section moves on to describe the effects of heat treatment on diagonally printed Mo-30W samples.

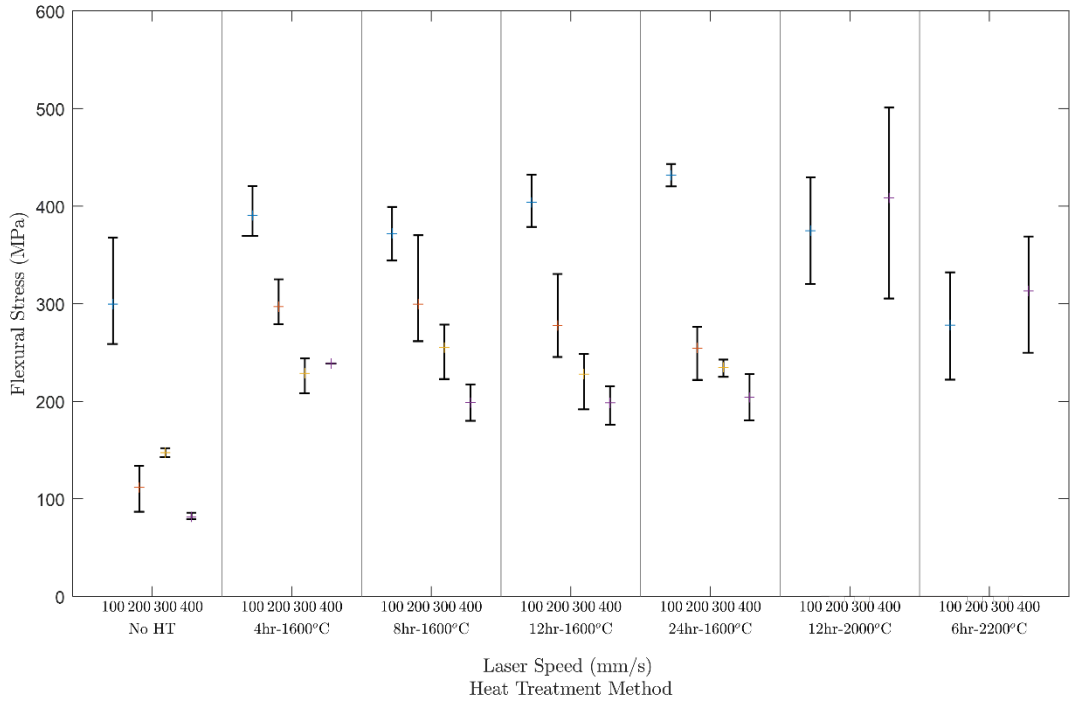

(a)

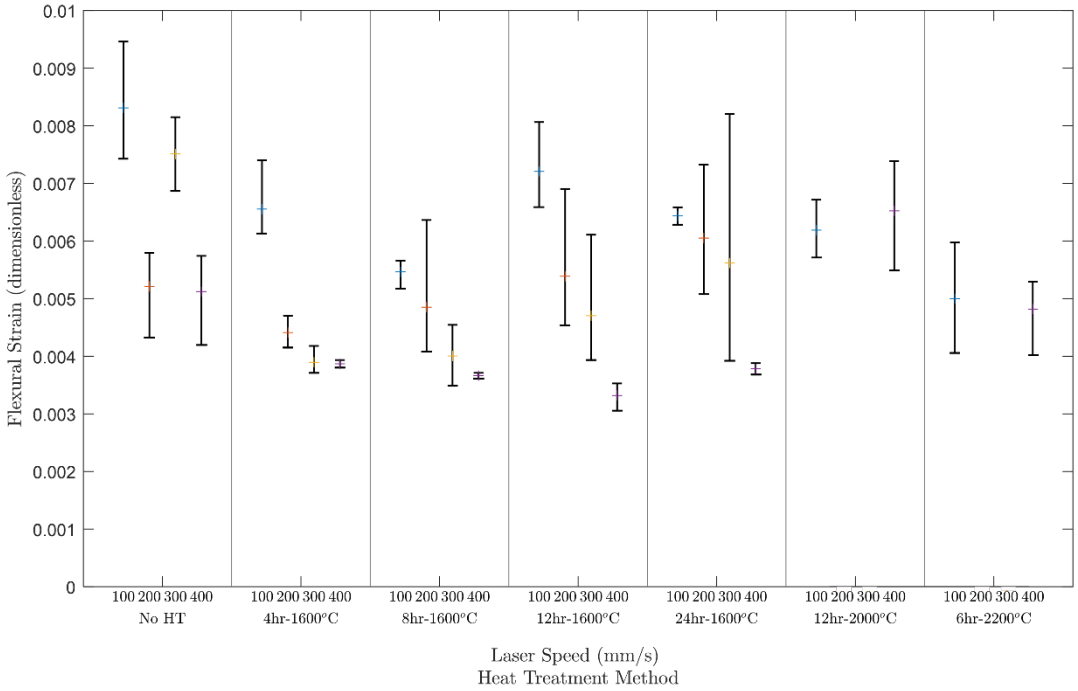

(b)

Figure 16. All vertical Mo-30W with varying heat treatment methods (a) flexural stress and (b) flexural strain responses obtained by three-point bending test.

Like the results of vertically printed Mo-30W, the average flexural stresses (MPa) and flexural strains (mm/mm) for Mo-30W specimens printed diagonally with various speeds and heat treatments are tabulated in Table 14. The top third of the table shows specimen heat treated at 1600°C for 4 and 8 hours, the center third displays Mo-30W heat treated at 1600°C for 12 and 24 hours, and the bottom third of the table shows samples heat treated at 2000°C for 12 hours.

Table 14. Flexural stress and flexural strains of diagonally printed Mo-30W in pure Ar with varying durations and temperatures of heat treatment.

Diagonal Mo-30W in 4-hour HT 1600°C			Diagonal Mo-30W in 8-hour HT 1600°C		
Print speed (mm/s)	Average flexural stress (MPa)	Average flexural Strain	Print speed (mm/s)	Average flexural stress (MPa)	Average flexural strain
100	287.93 ± 24.42	0.00609 ± 0.00038	100	262.71 ± 06.35	0.00596 ± 0.00105
200	331.48 ± 08.52	0.00519 ± 0.00059	200	363.45 ± 22.10	0.00553 ± 0.00049
300	357.71 ± 24.37	0.00566 ± 0.00123	300	311.37 ± 25.80	0.00472 ± 0.00035
400	351.32 ± 30.54	0.00558 ± 0.00081	400	331.85 ± 44.36	0.00517 ± 0.00023
Diagonal Mo-30W in 12-hour HT 1600°C			Diagonal Mo-30W in 24-hour HT 1600°C		
Print speed (mm/s)	Average flexural stress (MPa)	Average flexural Strain	Print speed (mm/s)	Average flexural stress (MPa)	Average flexural strain
100	288.10 ± 19.11	0.00564 ± 0.00038	100	339.62 ± 13.01	0.00589 ± 0.00034
200	318.61 ± 09.33	0.00529 ± 0.00027	200	297.60 ± 41.43	0.00521 ± 0.00067
300	311.49 ± 03.57	0.00534 ± 0.0004	300	319.98 ± 15.39	0.00489 ± 0.00044
400	283.05 ± 08.99	0.00509 ± 0.00011	400	308.13 ± 11.25	0.00541 ± 0.00072
Diagonal Mo-30W in 12-hour HT 2000°C					
Print speed (mm/s)	Average flexural stress (MPa)	Average flexural Strain			
100	512.56 ± 0.62	0.00792 ± 0.00032			
400	614.61 ± 8.33	0.01208 ± 0.00138			

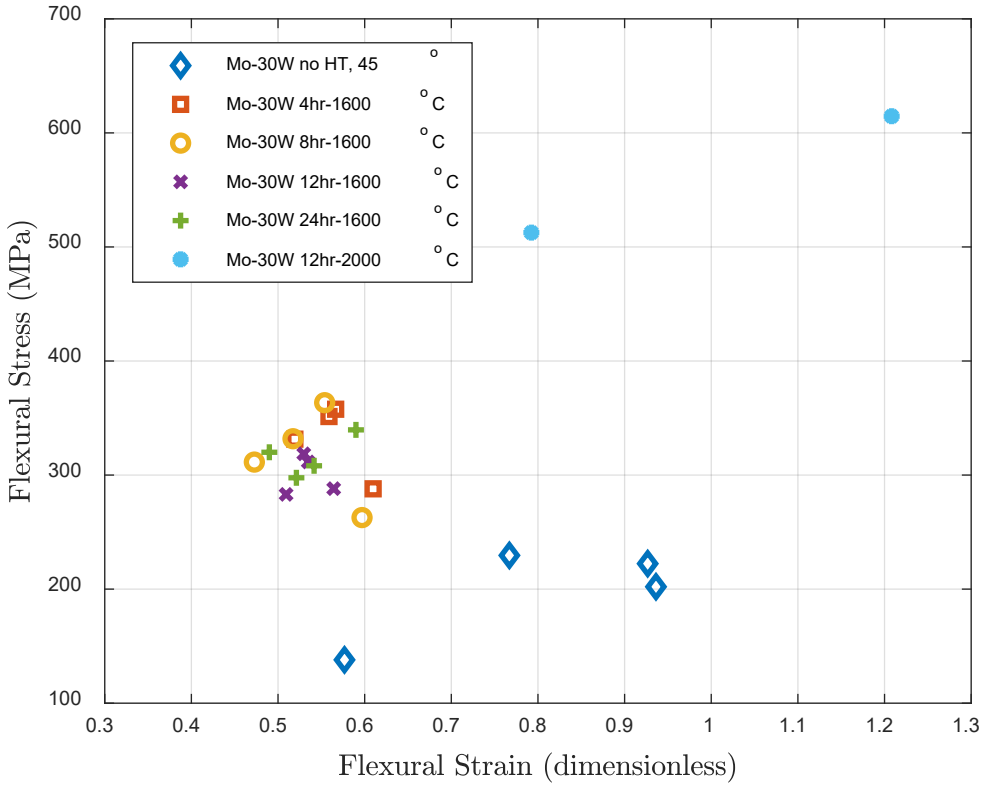

Figure 17. Stress and strain relationship of Mo-30W diagonally printed in pure Ar with varying heat treatment conditions.

These results are in accord with vertically printed Mo-30W with varying duration and temperature of heat treatment conditions. Likewise, these heat-treated Mo-30W specimen printed in 100 mm/s diagonally, the bending strength increased an average of 52.11% compared to as-built Mo-30W. By comparison, higher print speed with 400 mm/s increased the average bending strength of Mo-30W by 86.97%. There appears no clear generalization on the effect of 1600°C heat treatment duration and laser print speeds

to the flexural stress and strain. These results validated Thermo-Calc heat treatment simulations for a required higher temperature for Mo-30W alloy diffusion progression.

The results of Mo-30W heat treated at 2000°C for 6 hours are significant in at least two major respects. First, the average flexural stress of specimens printed at 400 mm/s achieved 614.1 MPa, an increase of 204.17% from their as-built counterpart. It was comparable to the highest average yield strength of 615.34 MPa attained by vertically printed in 100 mm/s Mo-30W. Additionally, the average flexural strain improved 19.84% from 0.01008 to 0.01208, and it was the highest flexural strain value as close as the strain value from SLM of pure Mo discussed previously. The ductility slightly improved which shows that it is a key indication of well-mixed SLM produced alloy.

As explained earlier, a similar observation was observed where diagonally printed specimens exhibited flexural strengths within a small range of 262 MPa to 363 MPa across all printing speeds and the heat treatment temperature of 1600°C between for all times. Applying heat treatment at 2000°C for 6 hours, resulted in a dramatic increase in the mechanical strength and elongation. This effect was recognized to correspond to the changes in the grain structure and phases present in the Mo-30W material when heat treatment occurred above the molybdenum-tungsten alloy's eutectic temperature of 1927°C. Similar to vertically printed Mo-30W, multiple plots showing the responses obtained by three-point bending test for each diagonal Mo-30W group types are shown in Figure 16. for simpler visualization of the bending strength data. In this plot, the result of flexural stresses and flexural strains for all diagonal Mo-30W samples and their means were plotted.

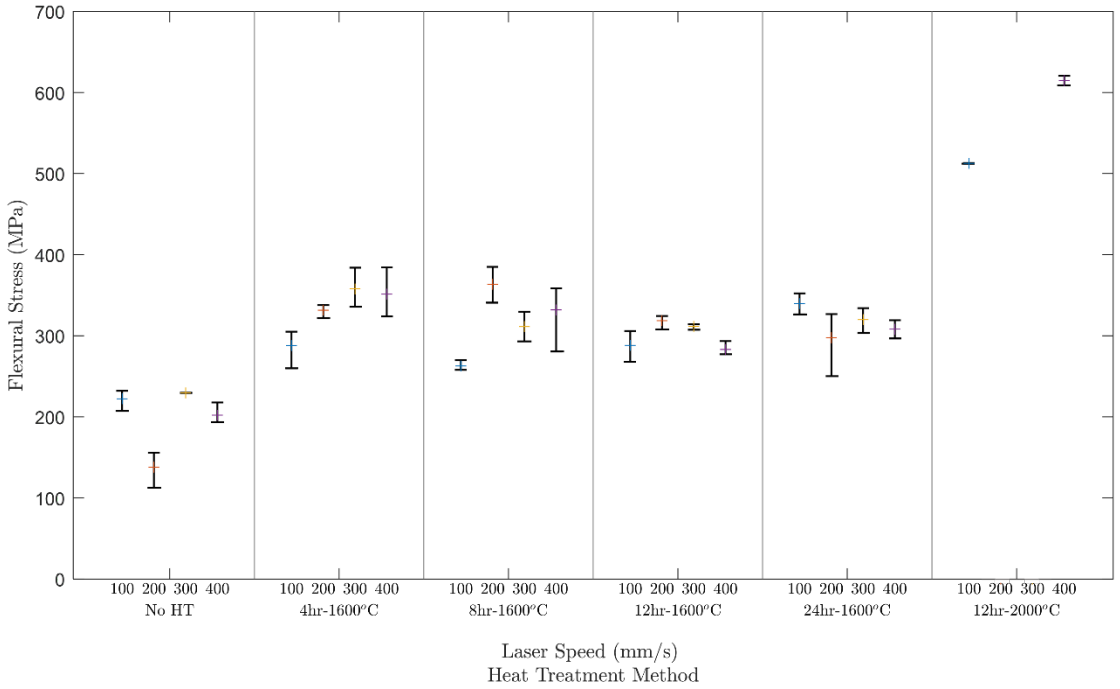
Flexural Stress (MPa)
700
600
500
400
300
200
100
0
100 200 300 400
No HT
4hr-1600°C
8hr-1600°C
12hr-1600°C
24hr-1600°C
12hr-2000°C
Laser Speed (mm/s)
Heat Treatment Method

(a)

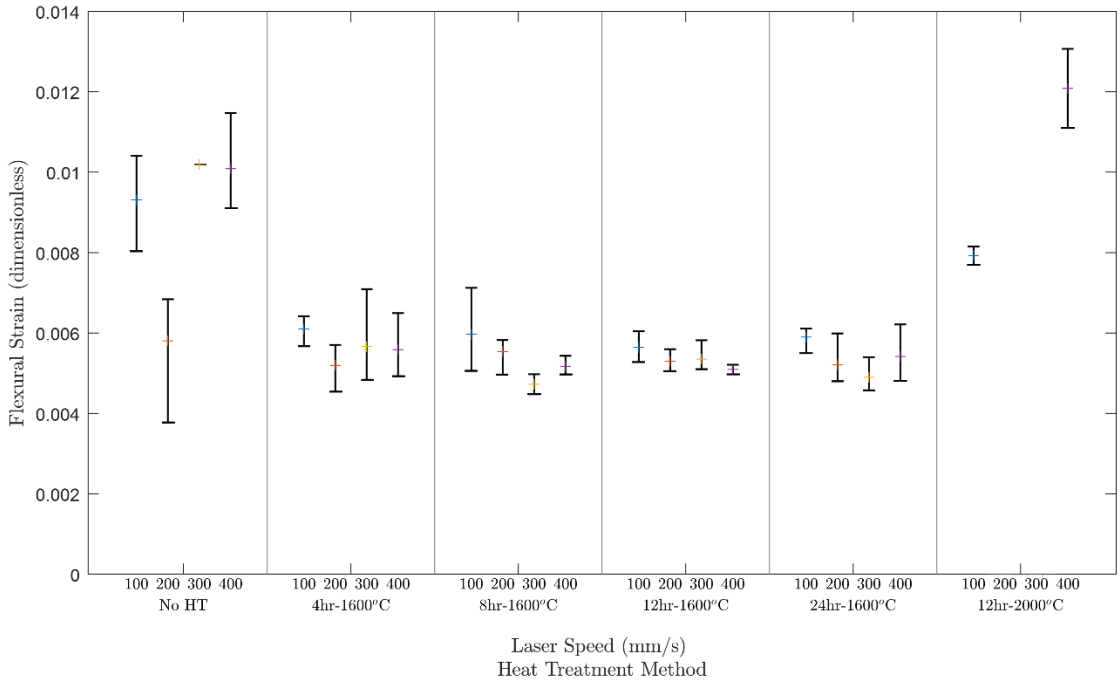
Flexural Strain (dimensionless)
0.014
0.012
0.01
0.008
0.006
0.004
0.002
0
100 200 300 400
No HT
4hr-1600°C
8hr-1600°C
12hr-1600°C
24hr-1600°C
12hr-2000°C
Laser Speed (mm/s)
Heat Treatment Method

(b)

Figure 18. All diagonal Mo-30W with varying heat treatment methods (a) flexural stress and (b) flexural strain responses obtained by three-point bending test.

Micro Hardness Tests

Preliminary Vickers micro hardness tests were conducted on Mo-30W specimens printed in pure Ar, tabulated in Table 15, to observe the effects of print speeds on the hardness of SLM produced Mo-30W. The table indicates that the print speed had no significant effects on the average Vickers hardness of the Mo-30W specimen.

Table 15. Vertical Mo-30W printed in pure Ar hardness obtained from Vicker micro harness test.

Print speed (mm/s)	Average Vickers hardness (HV)	Minimum Vickers hardness (HV)	Maximum Vickers hardness (HV)
100	204.30 ± 16.67	179	224
400	201.67 ± 17.56	173	225

Next, Vickers micro hardness were measured for all vertical heat-treated Mo-30W specimens printed in build chamber gas of pure Ar with laser speed of 100 mm/s. Additionally, Vickers hardness values were calculated for Mo-30W specimen printed vertically with laser scan speed of 100 mm/s and in atmosphere gas of Ar-3H_2 as the initial set of vertical specimens showed the highest bending strengths. Mo-30W samples which were heat-treated at 2000 °C for 12 hours and printed diagonally at a speed of 400 mm/s were also measured due to their high bending strength and ductility. The results of the microhardness tests arranged by various post-processing heat treatment, build chamber gas, and print orientation categories are shown in Table 16.

Table 16. Summary of Mo-30W hardness obtained from Vicker micro harness test.

HT method (°C-hours)	Build chamber gas	Print orientation (°)	Average Vickers hardness (HV)	Minimum Vickers hardness (HV)	Maximum Vickers hardness (HV)
None	Ar-3H_2	90	260.30 ± 13.73	243	291
1600-4	Ar	90	189.70 ± 16.02	164	214
1600-8	Ar	90	187.98 ± 42.35	72.80	215
1600-12	Ar	90	190.20 ± 16.25	174	221
1600-24	Ar	90	177.30 ± 22.06	144	213
2000-12	Ar	90	178.40 ± 14.98	160	194
2000-12	Ar	45	190.14 ± 04.88	185	198

This data readily shows that the heat treatments have the effect of softening the material, effectively reducing the hardness of the Mo-30W compared to the as-printed Mo-30W sample. For example, the vertical Mo-30W specimen in the current heat treatments had a decrease in hardness of approximately 9.59%, likely due to recovery and recrystallization of the material. The addition of hydrogen in the build chamber gas improved the Vickers hardness of Mo-30W by 27.41% in comparison to as-built specimen in pure Ar. The hardness can be sensitive to the pores and defects in the specimen; therefore, this provides indication that the 3% hydrogen minimized the definite pores and defects within the samples. The highest average Vickers hardness value of 260.30 HV presented in this table agree reasonably with the value, 256 DPH, seen in the studies by Schmidt et al., specifically the as-built non-heat-treated Mo-30W specimen [43].

The hardness were generally uniformly distributed along the middle indents with standard deviations around 20, and the small differences likely relate to distribution of residual stress where the fractured material were in state of mixed tensile and compressive stresses [57]. Surprisingly, the hardness data of Mo-30W specimen that underwent 8 hours of heat treatment was the most consistent, but one significantly low hardness test point (72.8 HV), likely near an AM void defect, caused the variation in the data. Appendix F displays the complete results of the microhardness distributions for all the samples. It may be the case that the micro hardness tests on as-built specimens may attain more evenly distributed hardness values compared to fractured specimens.

What stands out in the table is the Mo-30W printed diagonally at speed of 400 mm/s then heat-treated at 2000 °C for 12 hours had similar Vickers hardness as the other heat-treated samples. This observation may support the hypothesis that Mo-30W's hardness have little to no dependence on build orientation. The 2200 °C heat treated specimen were not included in the summary due to issues with metallographic preparation of the hardness test specimen.

Microstructure and Fracture Surface Analysis

As discussed in the background, features of microstructure, texture, and defects developed by SLM produced alloys can have unique effects on their mechanical properties. The fracture surface images taken by SEM for Mo-30W printed in pure Ar and Ar-3H_2 varying print speeds were examined next. Figure 19 shows fracture surfaces from each of these atmospheres in the unheated treated condition. Uneven micron sized oxide or carbide precipitates in various shapes appear in the fracture surfaces. The

arrangement of the precipitates are both within the grains and along the grain boundaries. The specimens printed in pure argon showed more extensive precipitation and poorly melted powder than the equivalent build parameters in Ar-3H_2. The large clumps of precipitates and unmelted powders weaken grain boundaries where cracks can easily propagate through during mechanical loading. The presence of these cracks lowered the bending strength of specimens printed in pure argon which resulted in the low strength values observed. The precipitates formed in the microstructure were the byproduct of the intrinsic impurities such as oxygen or carbon content of the molybdenum and tungsten powders as well as oxygen in the build environment. It is also possible the carbide and high oxide content contributed to the severely reduced ductility observed in the mechanical testing.

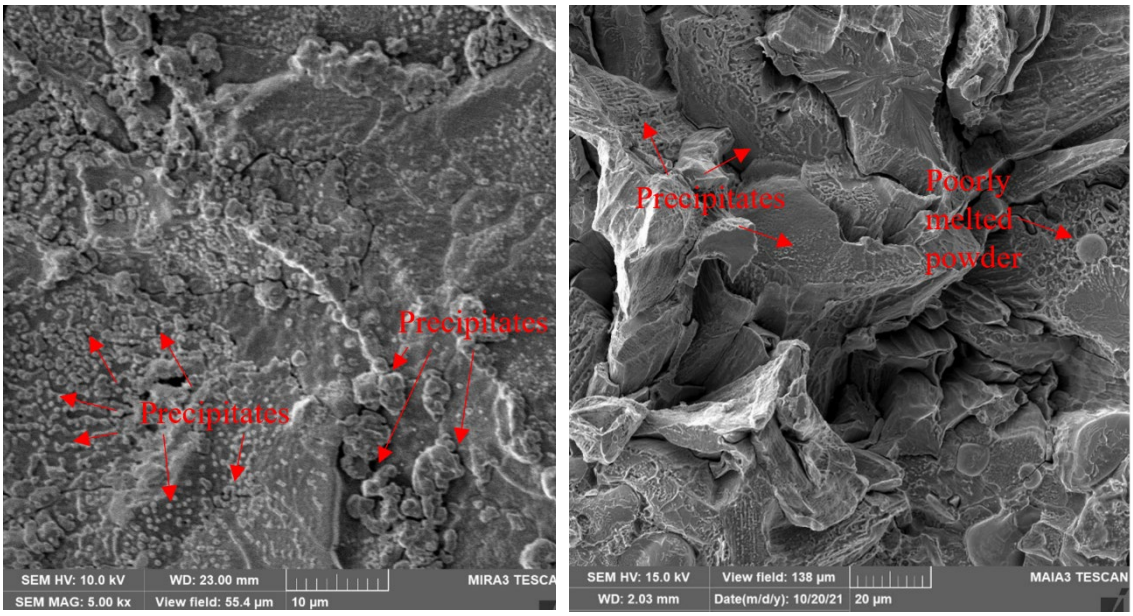

(a) **(b)**

Figure 19. SEM high magnification image of fracture surfaces of vertical Mo-30W printed in (a) pure Ar (b) Ar-3H_2 at laser speed of 100 mm/s.

The addition of hydrogen reduced the production of higher order tungsten oxides and more refined columnar microstructure can be seen for specimen printed in Ar-3H_2 [17]. As depicted in Figure 20, coarsely crystalline molybdenum and tungsten fractured by cleavage through the grains. The faint outline of striations were visible and a uniform distribution of finely disperse inclusions of precipitates can be observed for Mo-30W specimen printed with 100 mm/s.

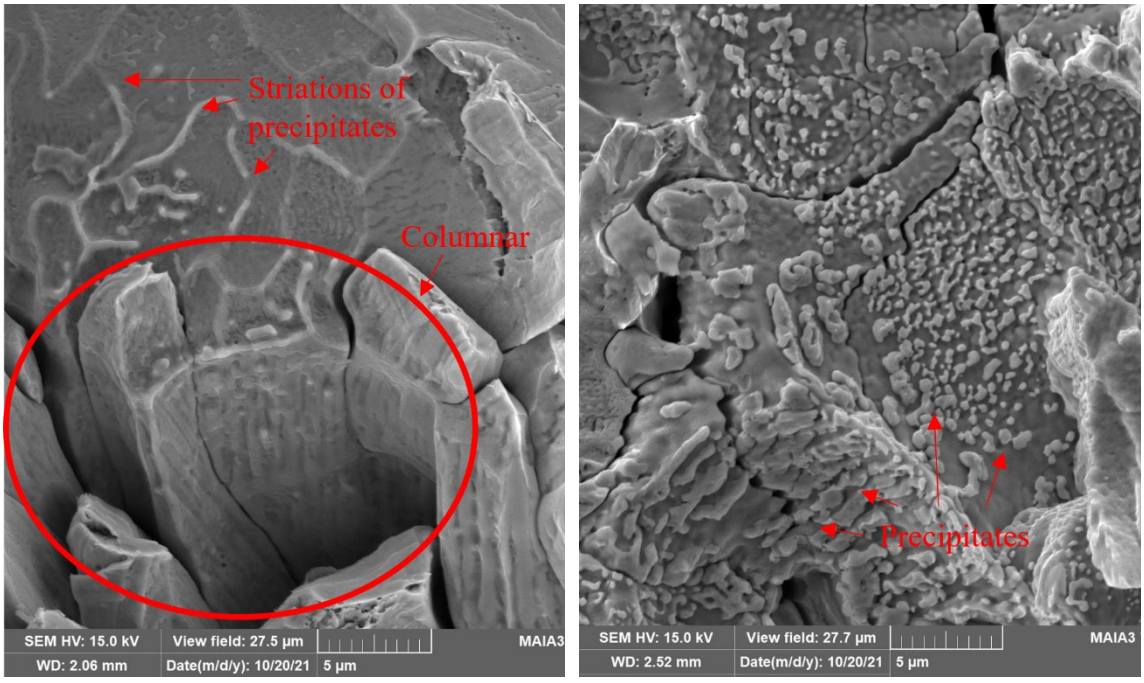

(a) **(b)**

Figure 20. SEM closeup image of fracture surfaces of vertical Mo-30W printed at laser speed of (a) 100 mm/s (b) 400 mm/s. In Ar-3H_2 and no HT.

Similar microstructural characteristics can be observed for specimen printed in speed of 400 mm/s in pure argon. In addition, more planar and flat brittle fractures can be observed at higher speeds as depicted in Figure 21. The weakness of brittle intergranular fractures contributed to reduced bending strength.

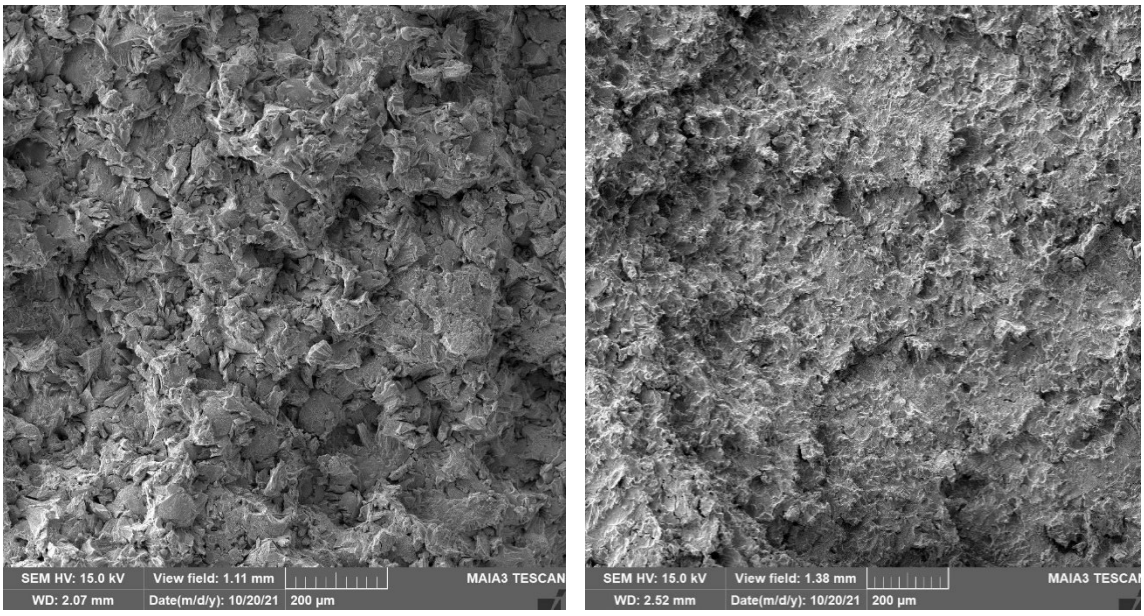

(a) **(b)**

Figure 21. SEM distant image of fracture surfaces of vertical Mo-30W printed at laser speed of (a) 100 mm/s (b) 400 mm/s. In Ar-3H_2 and no HT.

Mo-30W specimen printed at speed of 100 mm/s in Ar-3H_2 and no HT was observed to have the least amount of AM defects. Figure 22. below displays poorly melted powder possibly due to vaporization of molybdenum and microvoid that act as vulnerable locations for microcracks.

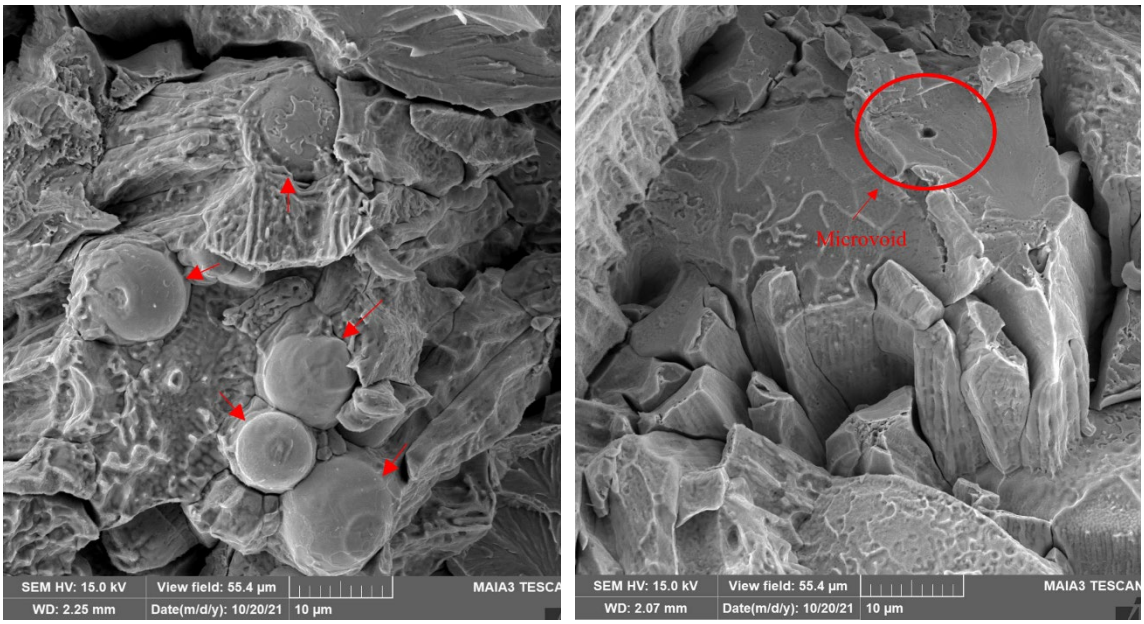

(a) **(b)**

Figure 22. SEM high magnification image of (a) poorly melted powders and (b) micropore where microcracks can propagate.

Irregular-shaped voids and defects were detected in both the as-built and heat-treated conditions; however, the imperfections occurred more overwhelmingly in heat-treated at 1600°C compared to the as-built specimens as depicted in Figure 23. Note the size of the pore or void is roughly equivalent to the size of 50 µm which is 50 times the size of the microvoid shown in previous Figure 22.

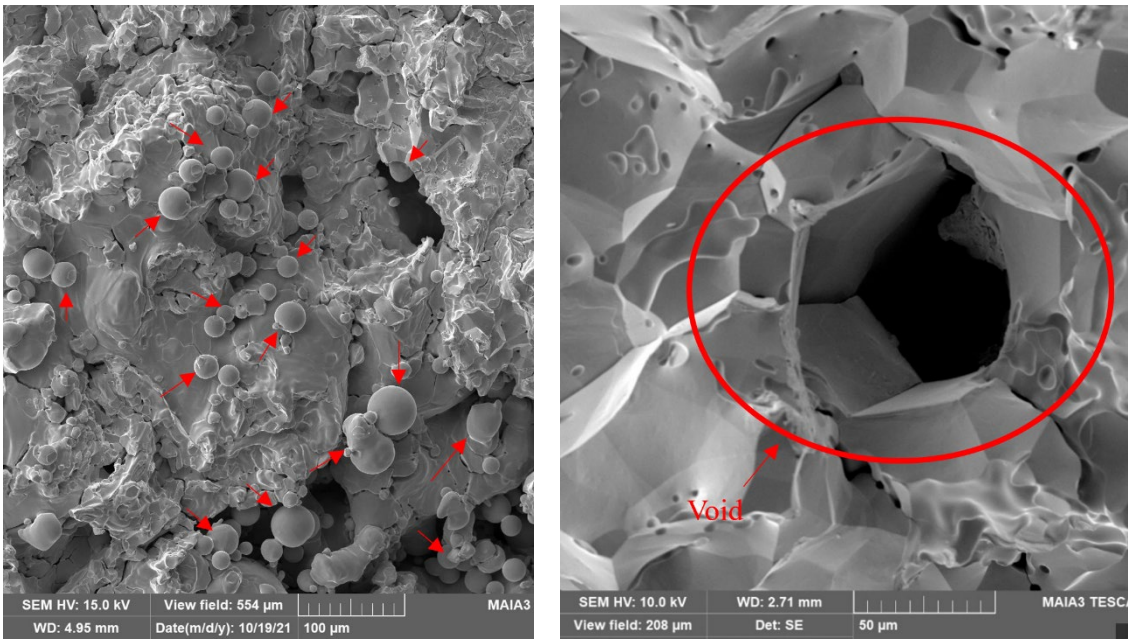

(a) **(b)**

Figure 23. SEM image of (a) poorly melted powder group and (b) large pore where crack can originate.

With the increase in heat treatment temperature, the growth of the precipitate films are faster, which would weaken the interatomic grain bond as seen in Figure 24. Therefore, these conditions likely caused recrystallization, inducing equiaxed microstructure to fracture easier as compared to specimen printed in Ar-3H_2. The equiaxed microstructure provided an easier means to traverse the fracture surface along the grain boundaries by intergranular fracture. However, the precipitates of carbide or oxides formed in the microstructure are dissipated as a result of the heat treatment. This strengthened grain boundaries and improved the bending strength of specimens printed in pure argon.

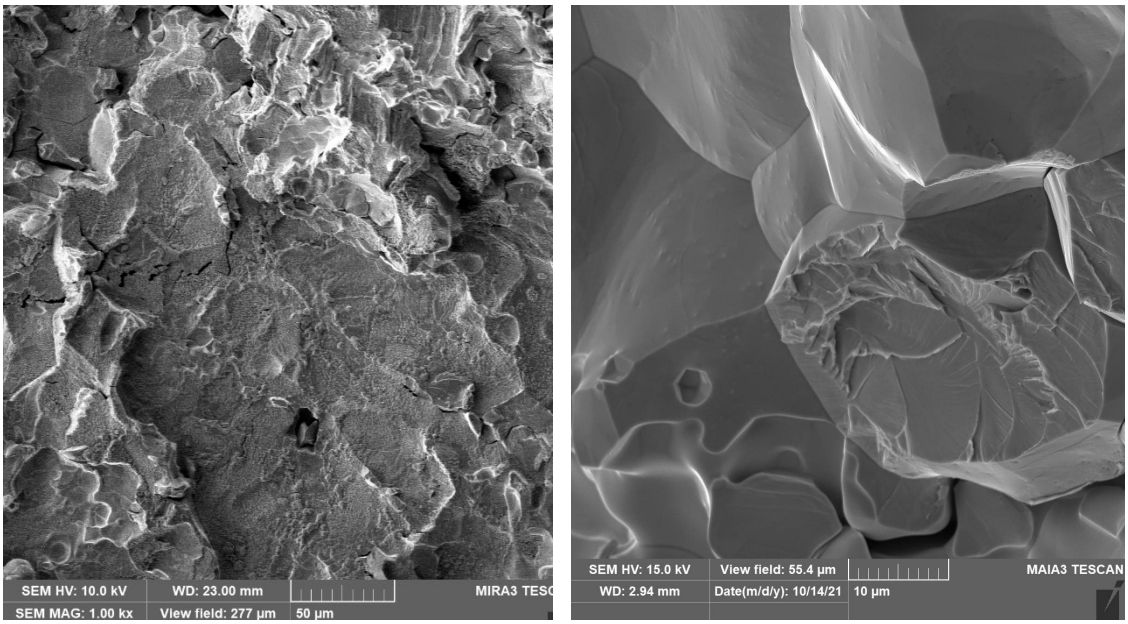

(a) **(b)**

Figure 24. SEM high magnification image of fracture surfaces of vertical Mo-30W with (a) no HT and (b) HT at 1600°C for 4 hours. In pure Ar and print speed of 100 mm/s.

Figure 25 below shows the Mo-30W specimen experiencing mostly intergranular fracture between grains, but a small presence of cleavage fracture can be spotted. This evidence connects with increased average flexural strength of 374 – 408 MPa for this heat-treated Mo-30W specimen at 2000°C.

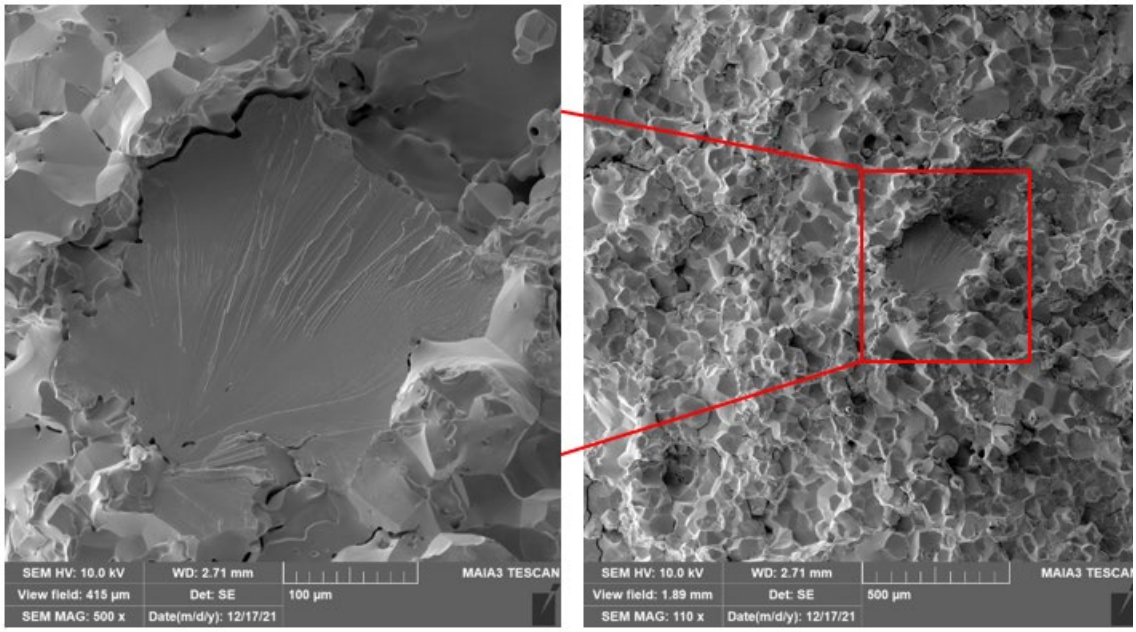

Figure 25. SEM image of fracture surface of vertical Mo-30W printed at laser speed of 100 mm/s. In pure Ar and HT at 2000°C for 6 hours.

In Figure 26, the fractures proceed along cleavage planes and along the grain boundaries more prominently observed which correlate to increased strength of 513 – 615 MPa and strain of 0.8% - 1.2% to Mo30W specimen printed with speed of 100 mm/s and 400 mm/s respectively. There appears to be no elastic fracture characteristics such as equiaxed or columnar dimples like microvoid coalescence observed through SEM images of the highest ductile (flexural strain of 1.21%) Mo-30W specimen.

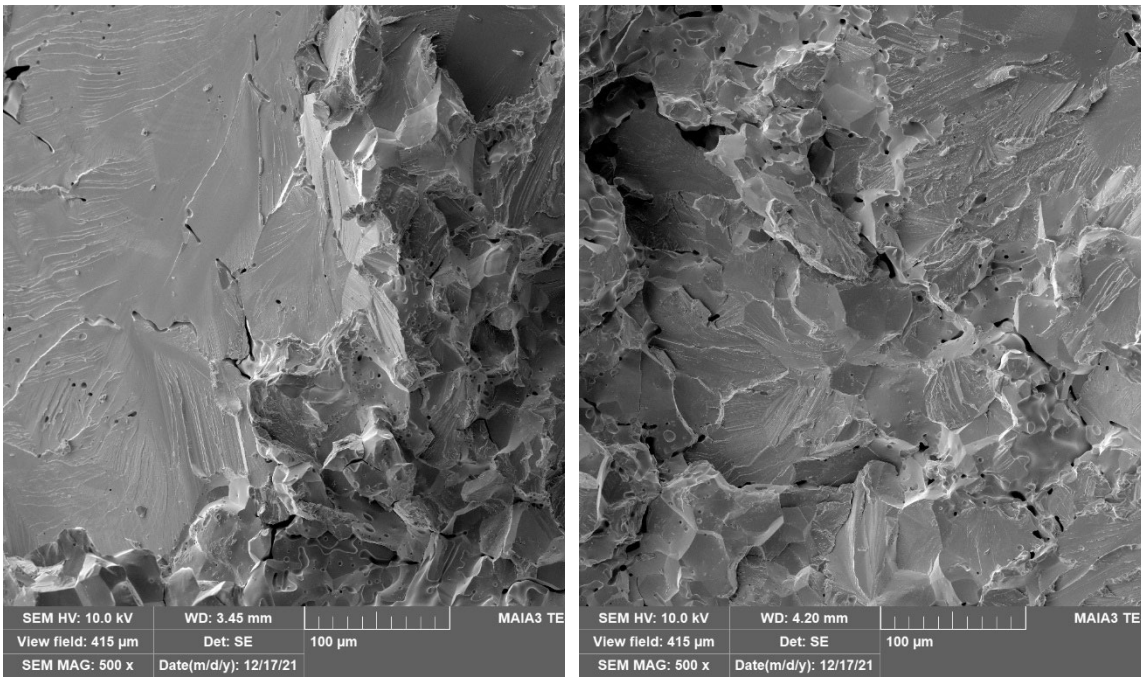

(a) **(b)**

Figure 26. SEM image of fracture surfaces of diagonal Mo-30W printed at laser speed of (a) 100 mm/s and (b) 400 mm/s. In pure Ar and HT at 2000C for 6 hours.

Figure 27. reveals there is an appearance of interesting ribbon-like grain structure. However, intergranular fractures are still the dominant forms for both speeds which results in poor bending strength and ductility.

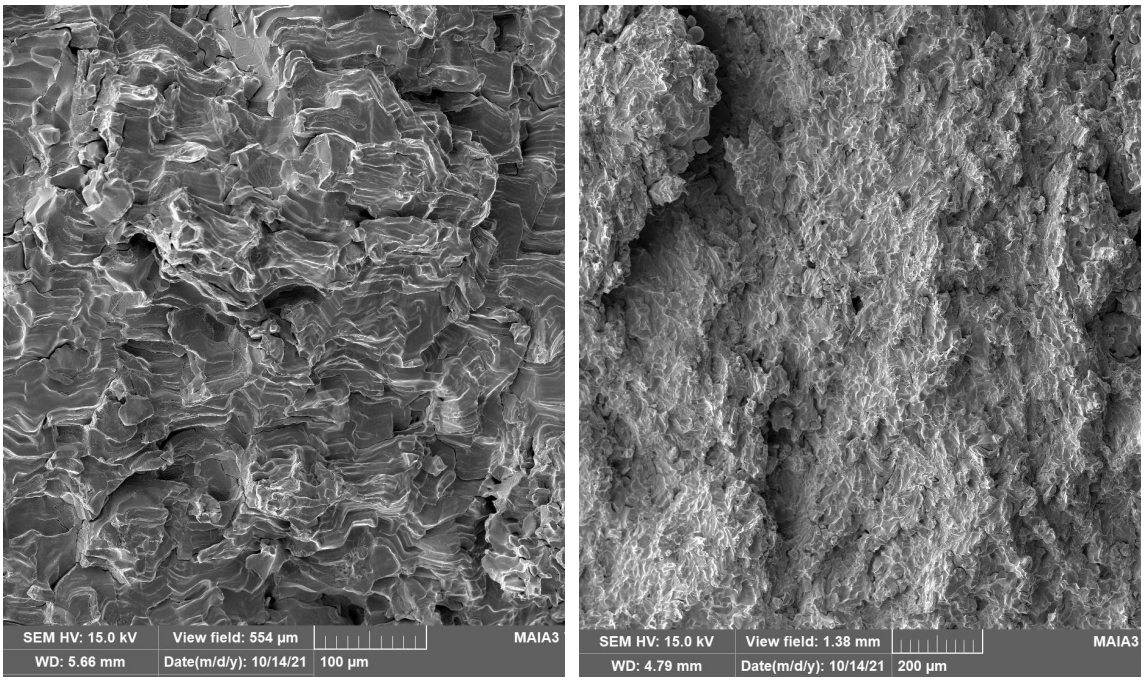

(a) **(b)**

Figure 27. SEM image of fracture surfaces of diagonal Mo-30W printed at laser speed of (a) 100 mm/s and (b) 400 mm/s. In pure Ar and HT at 1600C for 8 hours.

Porosity Analysis

The frequencies of void defects and porosity were counted, and the area percent of the pores were correlated to Mo-30W specimen post processed conditions at temperatures of 1600°C for 4, 8, 12, 24 hours, 2000°C for 12 hours, and 2200°C for 6 hours. This analysis aims to identify the relationship between AM defects and mechanical properties of Mo-30W. The result of the porosity analysis for all the cases are tabulated and depicted in Figure 28. The samples printed in 100 and 400 mm/s were used based on their widest range of measured mechanical properties. The print orientation stayed constant to be vertical throughout this study.

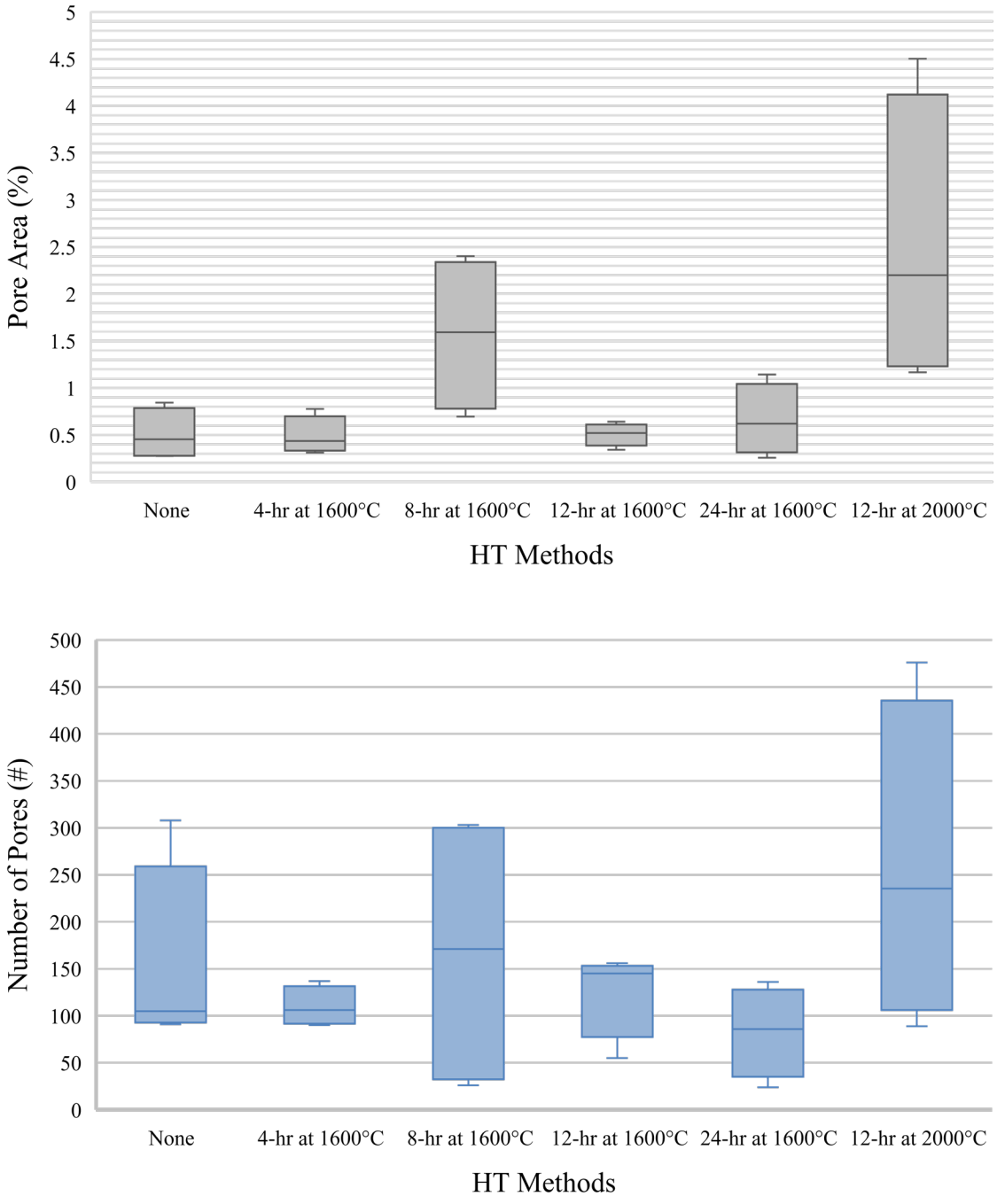

Figure 28. Porosity Area (%) and number of pores (#) for various HT methods.

The figure above suggests a weak link may exist between average bending strength and average porosity percentage. The average flexural stress of Mo-30W printed with 100 mm/s and 400 mm/s were 615 MPa and 203 MPa respectively while porosity area percentage were 0.84% and 0.62% respectively. This inconsistency may be due to small sample size since an examination of polished surface indicated that specimen printed in 100 mm/s had extensively fewer voids compared to 400 mm/s as shown Figure 29.

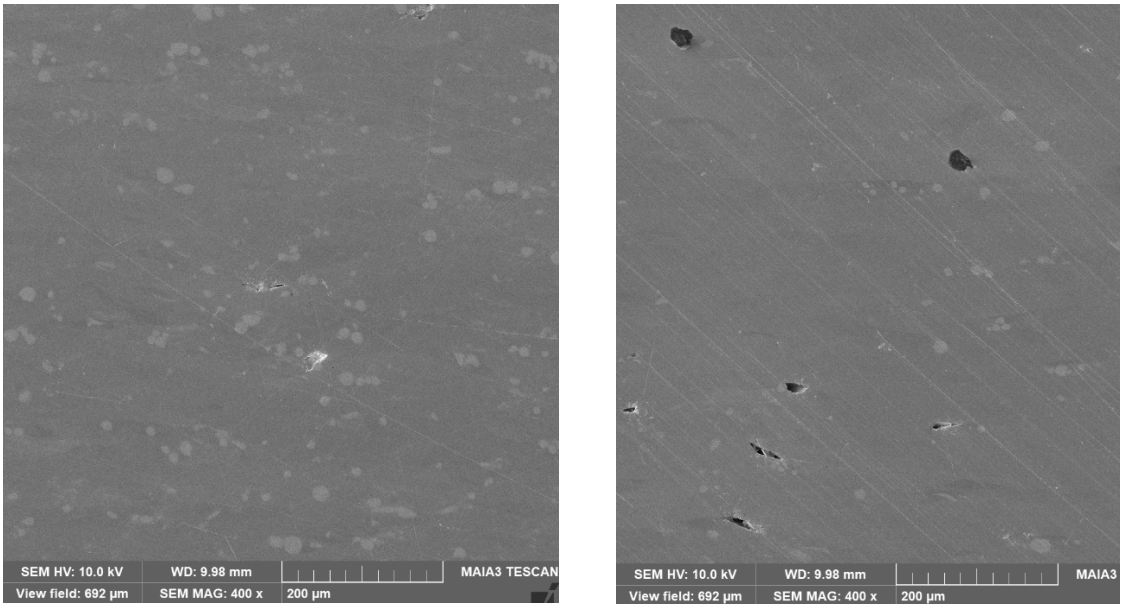

(a) **(b)**

Figure 29. SEM image of polished Mo-30W surface of print speed of (a) 100 mm/s (b) 400 mm/s printed in vertical orientation, in Ar-3H_2, and no HT.

Closer inspection of the porosity percentage variation from Mo-30W specimen heat-treated for 8 hours at 1600°C showed many irregular large defects in Figure 30. This is, in fact, supported by the micro hardness test where the seventh indent measured 76 DPH due to this defect in the middle. In comparing with Mo-30W printed with 100 mm/s

with no heat treatment, there appears lack of fusion defect, spherical porosity, surface defects that were automatically detected and measured.

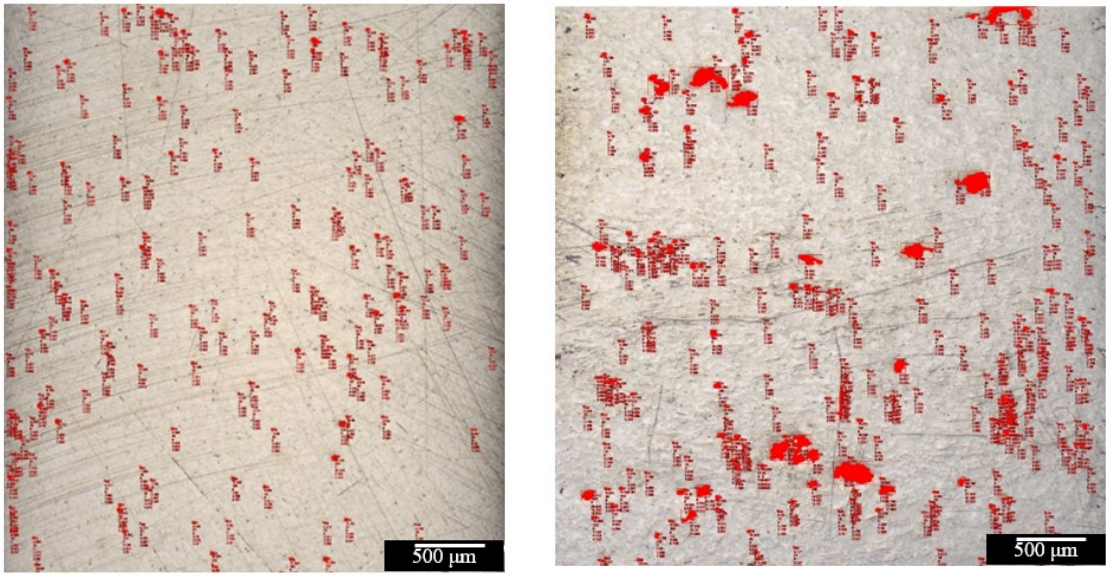

(a) **(b)**

Figure 30. Cross-sections of vertical Mo-30W printed in pure Ar seen from light optical microscopy 2.5x (a) as built 100 mm/s and no HT, (b) 400 mm/s and heat treated at 1600°C for 8 hours.

Interestingly, heat-treated Mo-30W at 2000°C for 12 hours had the most pore area when it had above average bending strength between 375 to 408 MPa. The Figure 31 gives a possible explanation because of problems encountered during the metallographic preparation. There appears to be controlled circular crack indents with respect to the grinding path and a long elliptical cutaway is found. During grinding, leftover tungsten residue particle perhaps scoured the molybdenum material of Mo-30W specimen.

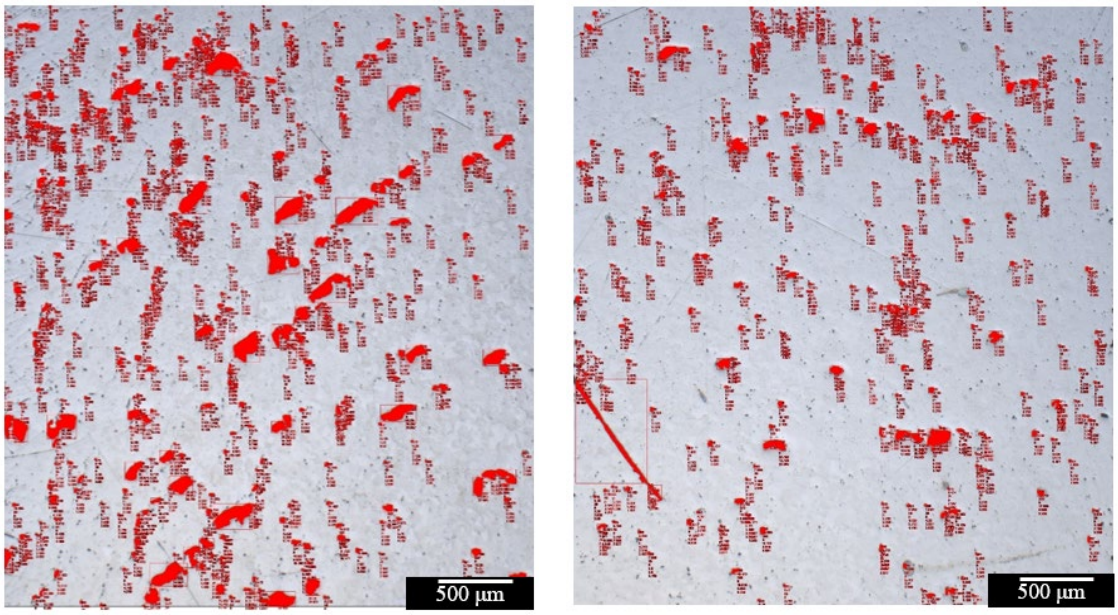

(a) **(b)**

Figure 31. Cross-sections of vertical Mo-30W printed in pure Ar heat treated at 2000°C for 12 hours - seen from light optical microscopy 2.5x (a) 100 mm/s (b) 400 mm/s.

Nevertheless, the general trend in the Figure 28 revealed that there are no clear relationship or significance between porosity percentage or number of pores with the mechanical strengths in contrary to expectations even excluding these data explained above. However, with a small sample size, caution must be applied, as these findings might not be transferable to a larger sample size of cross-sections measured.

ANOVA

To identify the existence of statistical significance between print speeds, print orientations, build chamber gases, and heat treatment conditions within the mechanical test results, an ANOVA was performed as shown in Table 17. The ANOVA found

statistically significant differences in all the parameters to the bending strength. Additionally, there were few significant interaction effects on the bending strength such as between print speed and print orientation. It is noted that if any of the parameters had an effect, reducing or improving bending strength, then the ANOVA will report a statistically significant result.

Table 17. 4-way ANOVA for the flexural stress.

Source	SS	df	MS	F	Prob>F
Print speed	$\mathbf{9.29 \times 10^4}$	1	$\mathbf{9.29 \times 10^4}$	24.17	$\mathbf{2.31 \times 10^{-6}}$
HT method	$\mathbf{8.42 \times 10^4}$	1	$\mathbf{8.42 \times 10^4}$	21.91	$\mathbf{6.39 \times 10^{-6}}$
Print orientation	$\mathbf{7.81 \times 10^4}$	1	$\mathbf{7.81 \times 10^4}$	20.32	$\mathbf{1.32 \times 10^{-5}}$
Build chamber gas	$\mathbf{4.23 \times 10^5}$	1	$\mathbf{4.23 \times 10^5}$	110.22	$\mathbf{1.29 \times 10^{-19}}$
Print speed and HT method	$\mathbf{8.15 \times 10^4}$	1	$\mathbf{8.15 \times 10^4}$	21.21	$\mathbf{8.79 \times 10^{-6}}$
Print speed *print orientation	$\mathbf{1.56 \times 10^5}$	1	$\mathbf{1.56 \times 10^5}$	40.69	$\mathbf{2.15 \times 10^{-9}}$
Print speed *build chamber gas	$\mathbf{6.46 \times 10^3}$	1	$\mathbf{6.46 \times 10^3}$	1.68	**0.20**
HT method* print orientation	$\mathbf{5.57 \times 10^3}$	1	$\mathbf{5.57 \times 10^3}$	1.45	**0.23**
Print orientation * build chamber gas	$\mathbf{2.57 \times 10^3}$	1	$\mathbf{2.57 \times 10^3}$	0.67	**0.42**
Print speed* HT method* print orientation	$\mathbf{2.74 \times 10^4}$	1	$\mathbf{2.74 \times 10^4}$	7.14	$\mathbf{8.40 \times 10^{-3}}$
Print speed*print orientation * build chamber gas	**888.67**	1	**888.67**	0.23	**0.63**
Error	$\mathbf{5.68 \times 10^5}$	148	$\mathbf{3.84 \times 10^3}$		
Total	$\mathbf{1.53 \times 10^6}$	159			

A low probability value implies a strong statistical significance. The most significant factors on the bending strength was the build chamber gas with the probability

value of 1.29×10^{-19}. This supports the observations that Mo-30W specimens printed in Ar-3H_2 build chamber gas exhibited higher bending strength as compared to the samples printed in pure Ar. The high probability values for the multiple interacting build parameters are not evidence of "no effect." If all the different main build parameters were statistically significant on the bending strengths, it would be contradictory to say that there were no effects of combinations of the build factors. This is easily seen in the bending strength data results where addition of hydrogen to the build chamber gas improved the bending strength but increasing the printing speed lowered the bending strength.

The same factors were used for ANOVA on the flexural strain as displayed in Table 17. The ANOVA found statistically significant differences in print speed, heat treatment methods, and print orientation to the ductility of Mo-30W. The most significant factors on the flexural strain was the heat treatment method with the probability value of 1.79×10^{-8}. This is verified in three-point bend test results where the majority heat treated Mo-30W demonstrated decreased in flexural strain as compared to the as-built specimens.

Table 18. 4-way ANOVA for the flexural strain.

Source	SS	df	MS	F	Prob>F
Print speed	$\mathbf{9.61 \times 10^{-6}}$	1	$\mathbf{9.61 \times 10^{-6}}$	4.85	**0.03**
HT method	$\mathbf{7.03 \times 10^{-5}}$	1	$\mathbf{7.03 \times 10^{-5}}$	35.49	$\mathbf{1.79 \times 10^{-8}}$
Print orientation	$\mathbf{2.90 \times 10^{-5}}$	1	$\mathbf{2.90 \times 10^{-5}}$	14.65	$\mathbf{1.90 \times 10^{-4}}$
Build chamber gas	$\mathbf{1.22 \times 10^{-6}}$	1	$\mathbf{1.22 \times 10^{-6}}$	0.62	**0.43**
Print speed and HT method	$\mathbf{2.02 \times 10^{-7}}$	1	$\mathbf{2.02 \times 10^{-7}}$	0.10	**0.75**
Print speed *print orientation	$\mathbf{2.37 \times 10^{-5}}$	1	$\mathbf{2.37 \times 10^{-5}}$	11.96	$\mathbf{7.09 \times 10^{-4}}$
Print speed *build chamber gas	$\mathbf{2.68 \times 10^{-6}}$	1	$\mathbf{2.68 \times 10^{-6}}$	1.35	**0.25**
HT method* print orientation	$\mathbf{9.84 \times 10^{-6}}$	1	$\mathbf{9.84 \times 10^{-6}}$	4.97	**0.03**
Print orientation * build chamber gas	$\mathbf{7.33 \times 10^{-7}}$	1	$\mathbf{7.33 \times 10^{-7}}$	0.37	**0.54**
Print speed* HT method* print orientation	$\mathbf{3.51 \times 10^{-6}}$	1	$\mathbf{3.51 \times 10^{-6}}$	1.77	**0.19**
Print speed*print orientation * build chamber gas	$\mathbf{1.86 \times 10^{-6}}$	1	$\mathbf{1.86 \times 10^{-6}}$	0.94	**0.33**
Error	$\mathbf{2.93 \times 10^{-4}}$	148	$\mathbf{1.98 \times 10^{-6}}$		
Total	$\mathbf{4.46 \times 10^{-4}}$	159			

Summary

Methods presented in this chapter focused on mechanical behavior and microstructures characteristics of Mo-30W. EDS results of as-built Mo-30-W samples showed unmixed phases of Mo and W, but the samples heat treated at 2000°C resulted in relatively higher homogeneous microstructure.

Several conclusions on the material behavior were drawn from the three point bending experiments. As-built AM Mo-30W specimens printed in the lowest speed and

in Ar-3H_2 build chamber gas exhibited a highest average bending strength, 23% lower bending strength compared to values provided in literature for both conventionally processed Mo-30W. Diagonally printed Mo-30W heat treated at 2000°C demonstrated highest ductility and outperformed their as-built counterparts in terms consistency and reliability. Vickers micro hardness showed a material softening of the heat-treated samples and no significant hardness change was seen due to build orientation.

As part of the microstructure and fracture surface analysis, the addition of hydrogen resulted in more refined columnar microstructure and improved bending strength as an outcome. Also, SEM images showed the fractures proceed along cleavage planes and along the grain boundaries more prominently observed in heat-treated Mo-30W specimen at 2000°C which correlate to increased strength. For heat treatment method at 1600°C, irregular-shaped voids and defects were more noticeable contributing to reduced bending strength. Non-heat-treated specimen printed at higher speeds exhibited decreased bending strength as a result of the brittle intergranular fractures weakness.

The porosity analysis revealed that the frequencies of void defects and porosity percentage have little significance with the mechanical strengths of Mo-30W in various build configurations. Last of all, the most important factors on the bending strength was build chamber gas using ANOVA. These factors are consistent with previous studies on AM pure molybdenum and tungsten. The last chapter provides summary of the thesis, its significance and recommendation for potential future work.

V. Conclusions and Recommendations

Chapter Overview

This thesis has investigated the material characterization of SLM Mo-30W. Particularly, the purpose was to determine mechanical and microstructure properties using three-point bend test, Vickers micro hardness test, electron microscopy, energy dispersive spectroscopy, and optical microscopy. This chapter concludes with the summary of the findings, key takeaways, and the significance of the research. Finally, recommendations for future research are provided.

Conclusions of Research

The primary objectives of the research were: 1) to characterize the mechanical properties of Mo-30W alloy using mechanical tests, evaluate the effects of the printing parameters and post-processing heat treatment, and compare measured properties to previous empirical studies; 2) to characterize the microstructure of the Mo-30W alloy, observe changes due to different print parameters and post-processing heat treatment, and determine distinctive features; 3) to identify the relationship between AM defects and microstructural characteristics to mechanical properties of the Mo-30W specimen; 4) to quantify the cause of variability of AM of Mo-30W fracture properties. The findings and discussion performed in this study provide important insights into the SLM of Mo-30W alloy. This study has shown that two types of print orientations, four different print speeds, two different build chamber gases, and four categories of heat treatment conditions were adopted to SLM of Mo-30W alloy. The effects of these build parameters

on the mechanical, microstructure properties of Mo-30W were investigated in detail. The following conclusions can be drawn from this study:

1. The significance of build chamber shielding gas atmosphere is clearly supported. In the vertical orientation under pure argon gas, Mo-30W demonstrated tensile strength of 300 MPa and Vickers hardness of 204 HV, while under Ar-3H_2 atmosphere, samples displayed the highest bending strength of 615 MPa and highest toughness of 260 HV. Hydrogen likely reduced higher order oxides of Mo and W which then inhibit grain growth and refined microstructure.
2. After heat treatment at 1600°C across 4 – 24 hours, the bending strength of the vertical Mo-30W increased by approximately 25.23%. The temperature likely induced equiaxed microstructure resulting in easier intergranular fracture, but the precipitates of carbide or oxides are dissipated resulting in increased bending strength. A heat treatment at 2000°C for 6 hours provided internal stress relief to the alloy by reducing internal grain discontinuities which made cleavage fracture more difficult. It improved the bending strength of diagonal Mo-30W to 615 MPa, 204.17% increase and strain at fraction to 1.2%, a 19.84% improvement. Vickers hardness decreased approximately 9.59% with all heat treatment conditions, and it reached a lowest value of Vickers hardness indicative of softening
3. The most statistically significant factors on the bending strength and strain to fracture were the build chamber gas and heat treatment method respectively as a result of ANOVA.

4. The optimal laser scan speed to print as-built Mo-30W was the lowest at 100 mm/s which showed the least microcracking and the highest bending strength of 615 MPa and highest hardness of 260 HV. Compared to averaged literature yield strength value of 773.14 MPa and hardness value of 256 DPH, the bending strength and hardness value of SLM produced Mo-30W was comparable to conventional fabrication methods.
5. One of the more significant findings to emerge from this study was that diagonal heat-treated at 2000°C Mo-30W samples outperformed their as-built counterparts in terms consistency and reliability.
6. The summation of AM defects such as frequencies and sizes of porosities emerged as unreliable predictor of the mechanical properties SLM produced Mo-30W.

Significance of Research

In order to develop high-temperature technology for applications in supersonic aircraft, nuclear fission, and space applications, it is essential to lead research aimed at finding and employing new high temperature and high strength material alloy compositions [58]. The empirical findings in this study demonstrated the possibility to increase the mechanical property of SLM produced molybdenum and tungsten alloy by optimizing print parameters and applying heat treatments. These results will serve as a baseline for forthcoming research papers in AM of Mo-30W system mechanical and microstructural characterization at elevated temperatures. Moreover, the understanding of the roles and the effects of the print parameters and post-processing methods are likely to

bring advances in the AM Mo-30W for practical uses in aerospace and military applications.

Recommendations for Action

The optimum heat-treatment methods for Mo-30W have not been fully worked out and the potentials applied to molybdenum and tungsten alloys are only starting to be used. The findings of this study have a number of important implications for future practices regarding Mo-30W, and it revealed the need for a new heat treatment technique to be designed and tailored specifically for Mo-30W materials. Additionally, the lack of ductility at room temperature is a critical bottleneck that limits SLM produced Mo-30W. Future heat treatment conditions need to primarily focus on increasing the ductility of Mo-30W.

Recommendations for Future Research

Based on the conclusions, there are some areas which have not been adequately looked at and analyzed to date. In the following areas, respective recommendations and need for possible future studies using the same experimental set up are presented. Implementation of the recommended studies would form a more complete understanding of the Mo-30W system. It would be interesting to consider:

- Elevated temperature tensile tests of Mo-30W
- Additional post processing techniques such as quenching, annealing, normalizing, stress relieving, and hot isotropic pressing on Mo-30W

- Additional mechanical and microstructural characterization on diagonally heat-treated Mo-30W
- Effects of various percentage of hydrogen in the build chamber gas mixture on the mechanical and microstructural properties of Mo-30W
- Addition of the popular strengthening agents (hafnium, titanium, or zirconium) to the Mo-30W alloy to reduce grain coarsening and increase strength [38]
- Alloying Mo-30W with 0.15% carbon for refining the microstructure without cracking [59]
- Alloying Mo-30W with rhenium to increase ductility, recrystallization temperature, and ultimate tensile strength [60]
- Strategically positioned AM voids to improve the fracture response [61]

Summary

The pursuit for structural materials that can operate at higher temperatures and higher strengths remains a continuing challenge in aeronautical, space and nuclear engineering. Two suitable materials which could be used at significantly higher temperatures are molybdenum and tungsten, due to appealing inherent characteristics such as high melting point, high strength, high conductivity, and high hardness. However, the structural use of the refractory metals are severely restricted by their low ductility and weak fracture toughness at ambient temperatures [5].

To expand upon current properties of refractory alloys and achieve new limits, the SLM parts may require use of thermal or non-thermal techniques to improve material

properties. Choosing and properly implementing the optimal SLM build parameters, powder purities, and post-processing techniques to eliminate of current shortcomings of AM are critical to succeed for the future application in aerospace innovations.

Appendix A

```
%%%%%%%%%%%%%%%%
% 70% Molybdenum 30% Tungsten manufactured by selective laser melting
% 4-8-12-24hr Vacuumed Heated at 1600C and 12-6hr at 2000C 2200C
% 100-200-300-400 Print Speeds
% Vertical-45deg Orientation
% Bend Test Data
%
% Author: Maj Ryan Kemnitz
% Revised: Capt Jae Yu - 11 October 2021
% Revised: 25 Feb 2022
%%%%%%%%%%%%%%%%
close all;clear all; clc
set(0,'defaulttextinterpreter','latex')

%% Mo-30W in Ar Vertical
cd 'C:\Users\Jay\Desktop\AFIT\AERO799\Yu and Abaya\Mo-30W\Ar\Vertical'
B = dir('**/*.txt');

for i = 1:length(B);
    file = [B(i).folder,'\',B(i).name];
    temp = importdata(file);

    A{i} = -temp.data;

    first_loc = find(A{i}(:,2)>2e-3,1);
    A{i}(:,1) = A{i}(:,1)-A{i}(first_loc,1);

    last_loc = find(A{i}(:,1)>0.5,1);
    if isempty(last_loc) == true
        last_loc = length(A{i}(:,1));
    end

    C{i} = A{i}(first_loc:last_loc-3,:);

     [val(i,1),loc] = max(C{i}(:,2));
    max_disp(i,1) = C{i}(loc,1);
end

speeds = [100;100;100;200;200;200;300;300;400;400;400];
unique_speeds = unique(speeds);
dims = importdata('MoMeasurement_V.xlsx');
widths = dims(:,1);
thicks = dims(:,2);

real_stress = 3*val*1000*14./(2*widths.*thicks.^2);
real_strain = 6*max_disp.*thicks/14^2;
MOWH90_all = [speeds real_strain real_stress];
```

```
for i = 1:length(unique_speeds)
    o = (i-1)*3+1;
    p = i*3;
    locs = find(speeds==unique_speeds(i));
    average_stress(i) = mean(real_stress(locs));
    average_strain(i,1) =100*mean(real_strain(locs));

end

EV = 200./(0.020*0.050*unique_speeds);

MOWH90 = [unique_speeds EV average_stress' average_strain];
hold on
plot(real_strain*100,real_stress,'s','LineWidth',2)

%% Mo-30W in Ar 45 deg
clearvars -except MOWH90 MOWH90_all

cd 'C:\Users\Jay\Desktop\AFIT\AERO799\Yu and Abaya\Mo-30W\Ar\45'
B = dir('**/*.txt');

for i = 1:length(B);
    file = [B(i).folder,'\',B(i).name];
    temp = importdata(file);

    A{i} = -temp.data;

    first_loc = find(A{i}(:,2)>2e-3,1);
    A{i}(:,1) = A{i}(:,1)-A{i}(first_loc,1);

    last_loc = find(A{i}(:,1)>0.5,1);
    if isempty(last_loc) == true
        last_loc = length(A{i}(:,1));
    end

    C{i} = A{i}(first_loc:last_loc-3,:);

     [val(i,1),loc] = max(C{i}(:,2));
    max_disp(i,1) = C{i}(loc,1);
end

speeds = [100;100;100;200;200;200;300;400;400;400];
unique_speeds = unique(speeds);

dims = importdata('MoMeasurement_45.xlsx');
widths = dims(:,1);
thicks = dims(:,2);

real_stress = 3*val*1000*14./(2*widths.*thicks.^2);
real_strain = 6*max_disp.*thicks/14^2;
MOWH45_all = [speeds real_strain real_stress];
```

```
for i = 1:length(unique_speeds)
    o = (i-1)*3+1;
    p = i*3;
    locs = find(speeds==unique_speeds(i));
    average_stress(i) = mean(real_stress(locs));
    average_strain(i,1) =100*mean(real_strain(locs));

end

EV = 200./(0.020*0.050*unique_speeds);

MOWH45 = [unique_speeds EV average_stress' average_strain];
hold on
plot(real_strain*100,real_stress,'o','LineWidth',2)

%% 4hr Heat Vertical
clearvars -except MOWH90 MOWH90_all MOWH45 MOWH45_all

cd 'C:\Users\Jay\Desktop\AFIT\AERO799\Yu Data\Mo-30W\4hr Heat\Vertical'
B = dir('**/*.txt');

for i = 1:length(B)
    file = [B(i).folder,'\',B(i).name];
    temp = importdata(file);

    A{i} = -temp.data;

    first_loc = find(A{i}(:,2)>2e-3,1);
    A{i}(:,1) = A{i}(:,1)-A{i}(first_loc,1);

    last_loc = find(A{i}(:,1)>0.5,1);
    if isempty(last_loc) == true
        last_loc = length(A{i}(:,1));
    end

    C{i} = A{i}(first_loc:last_loc-3,:);

     [val(i,1),loc] = max(C{i}(:,2));
    max_disp(i,1) = C{i}(loc,1);
end

speeds = [100;100;100;200;200;200;300;300;300;400;400];
unique_speeds = unique(speeds);
dims = importdata('MoMeasurement_4hrV.xlsx');
widths = dims(:,1);
thicks = dims(:,2);

real_stress = 3*val*1000*14./(2*widths.*thicks.^2);
real_strain = 6*max_disp.*thicks/14^2;
```

```
MOW4hrV_all = [speeds real_strain real_stress];
for i = 1:length(unique_speeds)
    o = (i-1)*3+1;
    p = i*3;
    locs = find(speeds==unique_speeds(i));
    average_stress(i) = mean(real_stress(locs));
    average_strain(i,1) =100*mean(real_strain(locs));

end

EV = 200./(0.020*0.050*unique_speeds);

 MOW4hrV = [unique_speeds EV average_stress' average_strain];
hold on
plot(real_strain*100,real_stress,'s','LineWidth',2); grid on

%% 4hr Heat 45 deg
clearvars -except MOWH90 MOWH90_all MOWH45 MOWH45_all...
    MOW4hrV MOW4hrV_all

cd 'C:\Users\Jay\Desktop\AFIT\AERO799\Yu Data\Mo-30W\4hr Heat\45'
B = dir('**/*.txt');

for i = 1:length(B)
    file = [B(i).folder,'\',B(i).name];
    temp = importdata(file);

    A{i} = -temp.data;

    first_loc = find(A{i}(:,2)>2e-3,1);
    A{i}(:,1) = A{i}(:,1)-A{i}(first_loc,1);

    last_loc = find(A{i}(:,1)>0.5,1);
    if isempty(last_loc) == true
        last_loc = length(A{i}(:,1));
    end

    C{i} = A{i}(first_loc:last_loc-3,:);

     [val(i,1),loc] = max(C{i}(:,2));
    max_disp(i,1) = C{i}(loc,1);
end

speeds = [100;100;100;200;200;200;300;300;300;400;400;400];
unique_speeds = unique(speeds);

dims = importdata('MoMeasurement_4hr45.xlsx');
widths = dims(:,1);
thicks = dims(:,2);
```

```
real_stress = 3*val*1000*14./(2*widths.*thicks.^2);
real_strain = 6*max_disp.*thicks/14^2;

MOW4hr45_all = [speeds real_strain real_stress];

for i = 1:length(unique_speeds)
    o = (i-1)*3+1;
    p = i*3;
    locs = find(speeds==unique_speeds(i));
    average_stress(i) = mean(real_stress(locs));
    average_strain(i,1) =100*mean(real_strain(locs));

end

EV = 200./(0.020*0.050*unique_speeds);

MOW4hr45 = [unique_speeds EV average_stress' average_strain];
hold on
plot(real_strain*100,real_stress,'o','LineWidth',2)

%% 8hr Heat Vertical
clearvars -except MOWH90 MOWH90_all MOWH45 MOWH45_all...
    MOW4hrV MOW4hrV_all MOW4hr45 MOW4hr45_all
cd 'C:\Users\Jay\Desktop\AFIT\AERO799\Yu Data\Mo-30W\8hr Heat\Vertical'
B = dir('**/*.txt');

for i = 1:length(B)
    file = [B(i).folder,'\',B(i).name];
    temp = importdata(file);

    A{i} = -temp.data;

    first_loc = find(A{i}(:,2)>2e-3,1);
    A{i}(:,1) = A{i}(:,1)-A{i}(first_loc,1);

    last_loc = find(A{i}(:,1)>0.5,1);
    if isempty(last_loc) == true
        last_loc = length(A{i}(:,1));
    end

    C{i} = A{i}(first_loc:last_loc-3,:);

     [val(i,1),loc] = max(C{i}(:,2));
    max_disp(i,1) = C{i}(loc,1);
end

speeds = [100;100;100;200;200;200;300;300;300;400;400];
unique_speeds = unique(speeds);
dims = importdata('MoMeasurement_8hrV.xlsx');
widths = dims(:,1);
```

```
thicks = dims(:,2);

real_stress = 3*val*1000*14./(2*widths.*thicks.^2);
real_strain = 6*max_disp.*thicks/14^2;

MOW8hrV_all = [speeds real_strain real_stress];

for i = 1:length(unique_speeds)
    o = (i-1)*3+1;
    p = i*3;
    locs = find(speeds==unique_speeds(i));
    average_stress(i) = mean(real_stress(locs));
    average_strain(i,1) =100*mean(real_strain(locs));

end

EV = 200./(0.020*0.050*unique_speeds);

MOW8hrV = [unique_speeds EV average_stress' average_strain];
hold on
plot(real_strain*100,real_stress,'s','LineWidth',2)

%% 8hr Heat 45 deg
clearvars -except MOWH90 MOWH90_all MOWH45 MOWH45_all...
    MOW4hrV MOW4hrV_all MOW4hr45 MOW4hr45_all MOW8hrV MOW8hrV_all

cd 'C:\Users\Jay\Desktop\AFIT\AERO799\Yu Data\Mo-30W\8hr Heat\45'
B = dir('**/*.txt');

for i = 1:length(B)
    file = [B(i).folder,'\',B(i).name];
    temp = importdata(file);

    A{i} = -temp.data;

    first_loc = find(A{i}(:,2)>2e-3,1);
    A{i}(:,1) = A{i}(:,1)-A{i}(first_loc,1);

    last_loc = find(A{i}(:,1)>0.5,1);
    if isempty(last_loc) == true
        last_loc = length(A{i}(:,1));
    end

    C{i} = A{i}(first_loc:last_loc-3,:);

     [val(i,1),loc] = max(C{i}(:,2));
    max_disp(i,1) = C{i}(loc,1);
end

speeds = [100;100;100;200;200;200;300;300;400;400;400];
```

```
unique_speeds = unique(speeds);

dims = importdata('MoMeasurement_8hr45.xlsx');
widths = dims(:,1);
thicks = dims(:,2);

real_stress = 3*val*1000*14./(2*widths.*thicks.^2);
real_strain = 6*max_disp.*thicks/14^2;

MOW8hr45_all = [speeds real_strain real_stress];

for i = 1:length(unique_speeds)
    o = (i-1)*3+1;
    p = i*3;
    locs = find(speeds==unique_speeds(i));
    average_stress(i) = mean(real_stress(locs));
    average_strain(i,1) =100*mean(real_strain(locs));

end

EV = 200./(0.020*0.050*unique_speeds);


MOW8hr45 = [unique_speeds EV average_stress' average_strain];
hold on
plot(real_strain*100,real_stress,'o','LineWidth',2)

%% 12hr Heat Vertical
clearvars -except MOWH90 MOWH90_all MOWH45 MOWH45_all...
    MOW4hrV MOW4hrV_all MOW4hr45 MOW4hr45_all ...
    MOW8hrV MOW8hrV_all MOW8hr45 MOW8hr45_all
cd 'C:\Users\Jay\Desktop\AFIT\AERO799\Yu Data\Mo-30W\12hr
Heat\Vertical'
B = dir('**/*.txt');

for i = 1:length(B);
    file = [B(i).folder,'\',B(i).name];
    temp = importdata(file);

    A{i} = -temp.data;

    first_loc = find(A{i}(:,2)>2e-3,1);
    A{i}(:,1) = A{i}(:,1)-A{i}(first_loc,1);

    last_loc = find(A{i}(:,1)>0.5,1);
    if isempty(last_loc) == true
        last_loc = length(A{i}(:,1));
    end

    C{i} = A{i}(first_loc:last_loc-3,:);
```

```
     [val(i,1),loc] = max(C{i}(:,2));
    max_disp(i,1) = C{i}(loc,1);
end

speeds = [100;100;100;200;200;200;300;300;300;400;400;400];
unique_speeds = unique(speeds);
dims = importdata('MoMeasurement_12hrV.xlsx');
widths = dims(:,1);
thicks = dims(:,2);

real_stress = 3*val*1000*14./(2*widths.*thicks.^2);
real_strain = 6*max_disp.*thicks/14^2;

MOW12hrV_all = [speeds real_strain real_stress];

for i = 1:length(unique_speeds)
    o = (i-1)*3+1;
    p = i*3;
    locs = find(speeds==unique_speeds(i));
    average_stress(i) = mean(real_stress(locs));
    average_strain(i,1) =100*mean(real_strain(locs));

end

EV = 200./(0.020*0.050*unique_speeds);

MOW12hrV = [unique_speeds EV average_stress' average_strain];
hold on
plot(real_strain*100,real_stress,'s','LineWidth',2)


%% 12hr Heat 45 deg
clearvars -except MOWH90 MOWH90_all MOWH45 MOWH45_all...
    MOW4hrV MOW4hrV_all MOW4hr45 MOW4hr45_all MOW8hrV MOW8hrV_all ...
    MOW8hr45 MOW8hr45_all MOW12hrV MOW12hrV_all

cd 'C:\Users\Jay\Desktop\AFIT\AERO799\Yu Data\Mo-30W\12hr Heat\45'
B = dir('**/*.txt');

for i = 1:length(B)
    file = [B(i).folder,'\',B(i).name];
    temp = importdata(file);

    A{i} = -temp.data;

    first_loc = find(A{i}(:,2)>2e-3,1);
    A{i}(:,1) = A{i}(:,1)-A{i}(first_loc,1);

    last_loc = find(A{i}(:,1)>0.5,1);
```

```
    if isempty(last_loc) == true
        last_loc = length(A{i}(:,1));
    end

    C{i} = A{i}(first_loc:last_loc-3,:);

     [val(i,1),loc] = max(C{i}(:,2));
    max_disp(i,1) = C{i}(loc,1);
end

speeds = [100;100;100;200;200;200;300;300;300;400;400;400];
unique_speeds = unique(speeds);

dims = importdata('MoMeasurement_12hr45.xlsx');
widths = dims(:,1);
thicks = dims(:,2);

real_stress = 3*val*1000*14./(2*widths.*thicks.^2);
real_strain = 6*max_disp.*thicks/14^2;

MOW12hr45_all = [speeds real_strain real_stress];

for i = 1:length(unique_speeds)
    o = (i-1)*3+1;
    p = i*3;
    locs = find(speeds==unique_speeds(i));
    average_stress(i) = mean(real_stress(locs));
    average_strain(i,1) =100*mean(real_strain(locs));

end

EV = 200./(0.020*0.050*unique_speeds);


MOW12hr45 = [unique_speeds EV average_stress' average_strain];
hold on
plot(real_strain*100,real_stress,'o','LineWidth',2)

%% 24hr Heat Vertical
clearvars -except MOWH90 MOWH90_all MOWH45 MOWH45_all...
    MOW4hrV MOW4hrV_all MOW4hr45 MOW4hr45_all ...
    MOW8hrV MOW8hrV_all MOW8hr45 MOW8hr45_all...
    MOW12hrV MOW12hrV_all MOW12hr45 MOW12hr45_all
cd 'C:\Users\Jay\Desktop\AFIT\AERO799\Yu Data\Mo-30W\24hr
Heat\Vertical'
B = dir('**/*.txt');

for i = 1:length(B);
    file = [B(i).folder,'\',B(i).name];
    temp = importdata(file);
```

```
    A{i} = -temp.data;

    first_loc = find(A{i}(:,2)>2e-3,1);
    A{i}(:,1) = A{i}(:,1)-A{i}(first_loc,1);

    last_loc = find(A{i}(:,1)>0.5,1);
    if isempty(last_loc) == true
        last_loc = length(A{i}(:,1));
    end

    C{i} = A{i}(first_loc:last_loc-3,:);
     [val(i,1),loc] = max(C{i}(:,2));
    max_disp(i,1) = C{i}(loc,1);
end

speeds = [100;100;200;200;200;300;300;300;400;400];
unique_speeds = unique(speeds);
dims = importdata('MoMeasurement_24hrV.xlsx');
widths = dims(:,1);
thicks = dims(:,2);

real_stress = 3*val*1000*14./(2*widths.*thicks.^2);
real_strain = 6*max_disp.*thicks/14^2;

MOW24hrV_all = [speeds real_strain real_stress];

for i = 1:length(unique_speeds)
    o = (i-1)*3+1;
    p = i*3;
    locs = find(speeds==unique_speeds(i));
    average_stress(i) = mean(real_stress(locs));
    average_strain(i,1) =100*mean(real_strain(locs));

end
EV = 200./(0.020*0.050*unique_speeds);

MOW24hrV = [unique_speeds EV average_stress' average_strain];
hold on
plot(real_strain*100,real_stress,'s','LineWidth',2)


%% 24hr Heat 45 deg
clearvars -except MOWH90 MOWH90_all MOWH45 MOWH45_all ...
    MOW4hrV MOW4hrV_all MOW4hr45 MOW4hr45_all MOW8hrV MOW8hrV_all ...
    MOW8hr45 MOW8hr45_all MOW12hrV MOW12hrV_all MOW12hr45
MOW12hr45_all...
    MOW24hrV MOW24hrV_all

cd 'C:\Users\Jay\Desktop\AFIT\AERO799\Yu Data\Mo-30W\24hr Heat\45'
B = dir('**/*.txt');
```

```
for i = 1:length(B);
    file = [B(i).folder,'\',B(i).name];
    temp = importdata(file);

    A{i} = -temp.data;

    first_loc = find(A{i}(:,2)>2e-3,1);
    A{i}(:,1) = A{i}(:,1)-A{i}(first_loc,1);

    last_loc = find(A{i}(:,1)>0.5,1);
    if isempty(last_loc) == true
        last_loc = length(A{i}(:,1));
    end

    C{i} = A{i}(first_loc:last_loc-3,:);

     [val(i,1),loc] = max(C{i}(:,2));
    max_disp(i,1) = C{i}(loc,1);
end

speeds = [100;100;100;200;200;200;300;300;300;400;400;400];
unique_speeds = unique(speeds);

dims = importdata('MoMeasurement_24hr45.xlsx');
widths = dims(:,1);
thicks = dims(:,2);

real_stress = 3*val*1000*14./(2*widths.*thicks.^2);
real_strain = 6*max_disp.*thicks/14^2;

MOW24hr45_all = [speeds real_strain real_stress];

for i = 1:length(unique_speeds)
    o = (i-1)*3+1;
    p = i*3;
    locs = find(speeds==unique_speeds(i));
    average_stress(i) = mean(real_stress(locs));
    average_strain(i,1) =100*mean(real_strain(locs));

end

EV = 200./(0.020*0.050*unique_speeds);


MOW24hr45 = [unique_speeds EV average_stress' average_strain];
hold on
plot(real_strain*100,real_stress,'o','LineWidth',2)

%% 2000 C 12hr Heat Vertical
clearvars -except MOWH90 MOWH90_all MOWH45 MOWH45_all ...
```

```
    MOW4hrV MOW4hrV_all MOW4hr45 MOW4hr45_all MOW8hrV MOW8hrV_all ...
    MOW8hr45 MOW8hr45_all MOW12hrV MOW12hrV_all MOW12hr45
MOW12hr45_all...
    MOW24hrV MOW24hrV_all MOW24hr45 MOW24hr45_all

cd 'C:\Users\Jay\Desktop\AFIT\AERO799\Yu Data\Mo-30W\2000deg 12hr
heat\Vertical'
B = dir('**/*.txt');

for i = 1:length(B)
    file = [B(i).folder,'\',B(i).name];
    temp = importdata(file);

    A{i} = -temp.data;

    first_loc = find(A{i}(:,2)>2e-3,1);
    A{i}(:,1) = A{i}(:,1)-A{i}(first_loc,1);

    last_loc = find(A{i}(:,1)>0.5,1);
    if isempty(last_loc) == true
        last_loc = length(A{i}(:,1));
    end

    C{i} = A{i}(first_loc:last_loc-3,:);

     [val(i,1),loc] = max(C{i}(:,2));
    max_disp(i,1) = C{i}(loc,1);
end

speeds = [100;100;100;100;100;100;400;400;400;400];
unique_speeds = unique(speeds);
dims = importdata('MoMeasurement_2000_12hrV.xlsx');
widths = dims(:,1);
thicks = dims(:,2);

real_stress = 3*val*1000*14./(2*widths.*thicks.^2);
real_strain = 6*max_disp.*thicks/14^2;

MOW2000C_V_all = [speeds real_strain real_stress];
for i = 1:length(unique_speeds)
    o = (i-1)*3+1;
    p = i*3;
    locs = find(speeds==unique_speeds(i));
    average_stress(i) = mean(real_stress(locs));
    average_strain(i,1) =100*mean(real_strain(locs));

end

EV = 200./(0.020*0.050*unique_speeds);
```

```
MOW2000C_V = [unique_speeds EV average_stress' average_strain];
hold on
plot(real_strain*100,real_stress,'s','LineWidth',2); grid on

%% 2000C 12hr Heat 45
clearvars -except MOWH90 MOWH90_all MOWH45 MOWH45_all ...
    MOW4hrV MOW4hrV_all MOW4hr45 MOW4hr45_all MOW8hrV MOW8hrV_all ...
    MOW8hr45 MOW8hr45_all MOW12hrV MOW12hrV_all MOW12hr45
MOW12hr45_all...
    MOW24hrV MOW24hrV_all MOW24hr45 MOW24hr45_all...
    MOW2000C_V MOW2000C_V_all

cd 'C:\Users\Jay\Desktop\AFIT\AERO799\Yu Data\Mo-30W\2000deg 12hr
heat\45'
B = dir('**/*.txt');

for i = 1:length(B)
    file = [B(i).folder,'\',B(i).name];
    temp = importdata(file);

    A{i} = -temp.data;

    first_loc = find(A{i}(:,2)>2e-3,1);
    A{i}(:,1) = A{i}(:,1)-A{i}(first_loc,1);

    last_loc = find(A{i}(:,1)>0.5,1);
    if isempty(last_loc) == true
        last_loc = length(A{i}(:,1));
    end

    C{i} = A{i}(first_loc:last_loc-3,:);

     [val(i,1),loc] = max(C{i}(:,2));
    max_disp(i,1) = C{i}(loc,1);
end

speeds = [100;100;400;400];
unique_speeds = unique(speeds);
dims = importdata('MoMeasurement_2000_12hr45.xlsx');
widths = dims(:,1);
thicks = dims(:,2);

real_stress = 3*val*1000*14./(2*widths.*thicks.^2);
real_strain = 6*max_disp.*thicks/14^2;

MOW2000C_45_all = [speeds real_strain real_stress];
for i = 1:length(unique_speeds)
    o = (i-1)*3+1;
    p = i*3;
    locs = find(speeds==unique_speeds(i));
    average_stress(i) = mean(real_stress(locs));
```

```
    average_strain(i,1) =100*mean(real_strain(locs));

end

EV = 200./(0.020*0.050*unique_speeds);


MOW2000C_45 = [unique_speeds EV average_stress' average_strain];
hold on
plot(real_strain*100,real_stress,'o','LineWidth',2); grid on

%% 2200C 6hr Heat Vertical
clearvars -except MOWH90 MOWH90_all MOWH45 MOWH45_all ...
    MOW4hrV MOW4hrV_all MOW4hr45 MOW4hr45_all MOW8hrV MOW8hrV_all ...
    MOW8hr45 MOW8hr45_all MOW12hrV MOW12hrV_all MOW12hr45
MOW12hr45_all...
    MOW24hrV MOW24hrV_all MOW24hr45 MOW24hr45_all...
    MOW2000C_V MOW2000C_V_all MOW2000C_45 MOW2000C_45_all

cd 'C:\Users\Jay\Desktop\AFIT\AERO799\Yu Data\Mo-30W\2200deg 6hr
heat\Vertical'
B = dir('**/*.txt');

for i = 1:length(B)
    file = [B(i).folder,'\',B(i).name];
    temp = importdata(file);

    A{i} = -temp.data;

    first_loc = find(A{i}(:,2)>2e-3,1);
    A{i}(:,1) = A{i}(:,1)-A{i}(first_loc,1);

    last_loc = find(A{i}(:,1)>0.5,1);
    if isempty(last_loc) == true
        last_loc = length(A{i}(:,1));
    end

    C{i} = A{i}(first_loc:last_loc-3,:);

     [val(i,1),loc] = max(C{i}(:,2));
    max_disp(i,1) = C{i}(loc,1);
end

speeds = [100;100;100;100;100;100;400;400;400;400;400;400];
unique_speeds = unique(speeds);
dims = importdata('MoMeasurement_2200_6hrV.xlsx');
widths = dims(:,1);
thicks = dims(:,2);

real_stress = 3*val*1000*14./(2*widths.*thicks.^2);
real_strain = 6*max_disp.*thicks/14^2;
```

```
MOW2200C_V_all = [speeds real_strain real_stress];
for i = 1:length(unique_speeds)
    o = (i-1)*3+1;
    p = i*3;
    locs = find(speeds==unique_speeds(i));
    average_stress(i) = mean(real_stress(locs));
    average_strain(i,1) =100*mean(real_strain(locs));

end

EV = 200./(0.020*0.050*unique_speeds);


MOW2200C_V = [unique_speeds EV average_stress' average_strain];
hold on
plot(real_strain*100,real_stress,'d','LineWidth',2); grid on


%title('All Samples of 70% Molybdenum 30% Tungsten Strain vs Stress')
xlabel('Strain (dimensionless)')
ylabel('Stress (Newton/milimeter^2)')
legend('MoW 0hr V','MoW 0hr 45','MoW 4hr V','MoW 4hr 45','MoW 8hr
V','MoW 8hr 45',...
    'MoW 12hr V','MoW 12hr 45','MoW 24hr V','MoW 24hr 45',...
    'MoW 6hr-2000C V','MoW 6hr-2000C 45','MoW 12hr-2200C V')
%%
% 8hrV 100-2 400-1 possible outliers
% 12hrV 400-2 possible outlier - strain .0248
% 24hrV 100-1 possible outlier - strain .0102
% fixed outliers by removing offset data - likely due to not clicking
% offset/reset the bend machine
%%
figure
plot(MOWH90(:,4),MOWH90(:,3),'d','LineWidth',2)
hold on
plot(MOWH45(:,4),MOWH45(:,3),'s','LineWidth',2)
plot(MOW4hrV(:,4),MOW4hrV(:,3),'s','LineWidth',2)
plot(MOW4hr45(:,4),MOW4hr45(:,3),'o','LineWidth',2)
plot(MOW8hrV(:,4),MOW8hrV(:,3),'s','LineWidth',2)
plot(MOW8hr45(:,4),MOW8hr45(:,3),'o','LineWidth',2)
plot(MOW12hrV(:,4),MOW12hrV(:,3),'s','LineWidth',2)
plot(MOW12hr45(:,4),MOW12hr45(:,3),'o','LineWidth',2)
plot(MOW24hrV(:,4),MOW24hrV(:,3),'s','LineWidth',2)
plot(MOW24hr45(:,4),MOW24hr45(:,3),'o','LineWidth',2)
grid on
%title('Averaged 70% Molybdenum 30% Tungsten Strain vs Stress')
xlabel('Flexural Strain (dimensionless)')
ylabel('Flexural Stress (Newton/milimeter^2)')

legend('MoW 0hr V','MoW 0hr 45','MoW 4hr V','MoW 4hr 45','MoW 8hr
V','MoW 8hr 45',...
```

```
    'MoW 12hr V','MoW 12hr 45','MoW 24hr V','MoW 24hr 45')
axis([0.3 0.8 100 700])

figure
plot(MOWH90(:,4),MOWH90(:,3),'d','LineWidth',2)
hold on
%plot(MOWH45(:,4),MOWH45(:,3),'s','LineWidth',2)
plot(MOW4hrV(:,4),MOW4hrV(:,3),'s','LineWidth',2)
%plot(MOW4hr45(:,4),MOW4hr45(:,3),'o','LineWidth',2)
plot(MOW8hrV(:,4),MOW8hrV(:,3),'o','LineWidth',2)
%plot(MOW8hr45(:,4),MOW8hr45(:,3),'o','LineWidth',2)
plot(MOW12hrV(:,4),MOW12hrV(:,3),'x','LineWidth',2)
%plot(MOW12hr45(:,4),MOW12hr45(:,3),'o','LineWidth',2)
plot(MOW24hrV(:,4),MOW24hrV(:,3),'+','LineWidth',2)
%plot(MOW24hr45(:,4),MOW24hr45(:,3),'o','LineWidth',2)
plot(MOW2000C_V(:,4),MOW2000C_V(:,3),'*','LineWidth',2)
plot(MOW2200C_V(:,4),MOW2200C_V(:,3),'h','LineWidth',2)
grid on
%title('Averaged 70% Molybdenum 30% Tungsten Strain vs Stress')
xlabel('Flexural Strain (dimensionless)')
ylabel('Flexural Stress (MPa)')

legend('Mo-30W no HT, V','Mo-30W 4hr-1600^{o}C','Mo-30W 8hr-
1600^{o}C',...
    'Mo-30W 12hr-1600^{o}C','Mo-30W 24hr-1600^{o}C','Mo-30W 6hr-
2000^{o}C','Mo-30W 12hr-2200^{o}C')
axis([0.3 0.8 100 700])
%%
figure
%plot(MOWH90(:,4),MOWH90(:,3),'d','LineWidth',2)
plot(MOWH45(:,4),MOWH45(:,3),'d','LineWidth',2)
hold on
%plot(MOW4hrV(:,4),MOW4hrV(:,3),'s','LineWidth',2)
plot(MOW4hr45(:,4),MOW4hr45(:,3),'s','LineWidth',2)
%plot(MOW8hrV(:,4),MOW8hrV(:,3),'o','LineWidth',2)
plot(MOW8hr45(:,4),MOW8hr45(:,3),'o','LineWidth',2)
%plot(MOW12hrV(:,4),MOW12hrV(:,3),'x','LineWidth',2)
plot(MOW12hr45(:,4),MOW12hr45(:,3),'x','LineWidth',2)
%plot(MOW24hrV(:,4),MOW24hrV(:,3),'+','LineWidth',2)
plot(MOW24hr45(:,4),MOW24hr45(:,3),'+','LineWidth',2)
plot(MOW2000C_45(:,4),MOW2000C_45(:,3),'*','LineWidth',2)
grid on
%title('Averaged 70% Molybdenum 30% Tungsten Strain vs Stress')
xlabel('Flexural Strain (dimensionless)')
ylabel('Flexural Stress (MPa)')

legend('Mo-30W no HT, 45^{o}','Mo-30W 4hr-1600^{o}C','Mo-30W 8hr-
1600^{o}C',...
    'Mo-30W 12hr-1600^{o}C','Mo-30W 24hr-1600^{o}C','Mo-30W 12hr-
2000^{o}C')
axis([0.3 1.3 100 700])
```

```
%%%%%%%%%%%%%%%
%
% 70% Molybdenum 30% Tungsten manufactured by selective laser melting
% 4-8-12-24hr Vacuumed Heated at 1600C and 12-6hr at 2000C 2200C
% 100-200-300-400 Print Speeds
% Vertical Orientation
% Box plot of Bend Test Data
%
% Capt Jae Yu - 13 October 2021
% Revised - 24 Feb 2022
%
%%%%%%%%%%%%%%%
%%
import iosr.*
close all; clear all; clc;
set(0,'defaulttextinterpreter','latex')
% clear all displays
%delete(findall(0));
format shortE

% N-way Analysis of Variance

% Read data parameters
cd 'C:\Users\Jay\Desktop\AFIT\AERO799\Yu Data'
data=readtable('Mo-30W_V_Boxplot.xlsx');

% Convert table to matrix format
data=data{:,:};
% Categorize into speed,strain,stress,hour
speed=data(1,:);
% Convert doubles to strings if needed
speed_str=arrayfun(@num2str,speed,'un',0);
strain=data(2,:);
stress=data(3,:);
hour=data(4,:);
hour_str=arrayfun(@num2str,hour,'un',0);

%% Stress [data,hours,speed]
stress=[258.7560161 381.5069586 344.2067533 378.7222402 443.2129113
401.9678088 292.9185914;...
272.115907  420.6962497 372.6547661 432.1057113 420.2222173 374.0712623
318.2858184;...
367.8559 369.3440307    399.2479447 400.8141317 NaN 358.0170181
223.8540692;...
NaN NaN NaN NaN NaN 320.3553208 332.1887195;...
NaN NaN NaN NaN NaN 364.5903635 278.8182411;...
NaN NaN NaN NaN NaN 429.6709238 222.1333178];
stress(:,:,2)=[133.9879928  325.125469  266.8624239 245.4409307
265.387758 NaN NaN;...
86.87922319 279.0536541 261.6126605 330.4940281 221.9826205 NaN NaN;...
114.5800472 286.8578569 370.1206862 257.1782127 276.478671 NaN NaN;...
NaN NaN NaN NaN NaN NaN NaN;...
NaN NaN NaN NaN NaN NaN NaN;...
```

```
NaN NaN NaN NaN NaN NaN NaN];
stress(:,:,3)=[152.0226553  208.3960241 222.8460743 243.2494137
242.7569975 NaN NaN;...
142.6967394 243.9064759 264.1352092 191.7636592 225.0482402 NaN NaN;...
NaN 233.6985538 278.5620309 248.6348827 236.5609068 NaN NaN;...
NaN NaN NaN NaN NaN NaN NaN;...
NaN NaN NaN NaN NaN NaN NaN;...
NaN NaN NaN NaN NaN NaN NaN];
stress(:,:,4)=[79.4352125   238.7156252 217.3568215 204.3700696
180.4001314 500.8933565 280.9936201;...
85.89511593 238.9088251 180.0045142 175.8591417 227.8332364 305.4022887
302.041223;...
79.48614188 NaN NaN 215.2637831 NaN 427.4466935 368.9120834;...
NaN NaN NaN NaN NaN 399.9738025 332.0610292;...
NaN NaN NaN NaN NaN NaN 344.7845705;...
NaN NaN NaN NaN NaN NaN 249.8224321];
%% Strain [data,hours,speed]
strain=[0.008043291 0.006130174 0.005175211 0.008065346 0.006585613
0.006491194 0.004768474;...
0.007428187 0.007400663 0.005559178 0.006974498 0.006283427 0.006240477
0.005555191;...
0.009462704 0.006133111 0.005660461 0.00658862 NaN 0.005713396
0.004056686;...
NaN NaN NaN NaN NaN 0.006017112 0.005976029;...
NaN NaN NaN NaN NaN 0.006717217 0.005239223;...
NaN NaN NaN NaN NaN 0.005952803 0.004392245];
strain(:,:,2)=[0.005793012  0.0047025   0.004082114 0.004725
0.007326624 NaN NaN;...
0.004324203 0.004380866 0.004106939 0.006904186 0.00574854 NaN NaN;...
0.005520321 0.004150314 0.006365162 0.004537699 0.005078572 NaN NaN;...
NaN NaN NaN NaN NaN NaN NaN;...
NaN NaN NaN NaN NaN NaN NaN;...
NaN NaN NaN NaN NaN NaN NaN];
strain(:,:,3)=[0.006870758  0.003792857 0.003489796 0.006108802
0.008206072 NaN NaN;...
0.008150453 0.004179294 0.004545    0.003934495 0.003921428 NaN NaN;...
NaN 0.003711066 0.003977602 0.004070114 0.004730022 NaN NaN;...
NaN NaN NaN NaN NaN NaN NaN;...
NaN NaN NaN NaN NaN NaN NaN;...
NaN NaN NaN NaN NaN NaN NaN];
strain(:,:,4)=[0.004195371  0.003934745 0.003611939 0.003374446
0.003681735 0.00738946  0.004489413;...
0.005429109 0.003802041 0.003711066 0.003055828 0.003880755 0.005491072
0.005287072;...
0.005742427 NaN NaN 0.003528779 NaN 0.006330032 0.00495476;...
NaN NaN NaN NaN NaN 0.006887144 0.005295918;...
NaN NaN NaN NaN NaN NaN 0.004870187;...
NaN NaN NaN NaN NaN NaN 0.00402];

%%
x = {'No HT','4hr-1600$^{o}$C','8hr-1600$^{o}$C','12hr-
1600$^{o}$C','24hr-1600$^{o}$C','12hr-2000$^{o}$C','6hr-2200$^{o}$C'};
% first matrix is the data, second is the hours, third is speed
```

```
y = randn(50,5,4);
figure;
% x is the very outside
% grouplabel is subbox label
h=iosr.statistics.boxPlot(x,strain,...
'symbolMarker',{'x','x','x','x'},...
'style','hierarchy',...
'xSeparator',true,...
'percentile', [0,0],...
'showMean',true,...
'medianColor', 'none',...
'groupLabels',{{'100','200','300','400'}});
box on
set(h,'boxColor',@gray) %@parula
xlabel('Laser Speed (mm/s) Heat Treatment Method')
ylabel('Flexural Strain (dimensionless)')
%title('All Vertical Mo-30W Flexural Strains Obtained by Three Point
Bending Tests')


figure
j=iosr.statistics.boxPlot(x,stress,...
'medianColor','k',...
'symbolMarker',{'+','+','+','+'},...
'boxcolor','auto',...
'style','hierarchy',...
'xSeparator',true,...
'percentile', [0,0],...
'showMean',true,...
'medianColor', 'none',...
'groupLabels',{{'100','200','300','400'}});
box on
set(j,'boxColor',@gray) %@parula
xlabel('Laser Speed (mm/s) Heat Treatment Method')
ylabel('Flexural Stress (MPa)')
%ylabel('Flexural Stress (N/mm$^{2}$)')
%title('All Vertical Mo-30W Flexural Stresses Obtained by Three Point
Bending Test')
```

```
%%%%%%%%%%%%%%%
%
% 70% Molybdenum 30% Tungsten manufactured by selective laser melting
% No Heat treatment, in Argon or H2
% 100-200-300-400 Print Speed
% Vertical-45deg Orientation
% ANOVA
%
% Capt Jae Yu - 13 October 2021
% Revised: 25 Feb 2022
%
%%%%%%%%%%%%%%%
%%
close all; clear all; clc;
format longE

% N-way Analysis of Variance

% Read data parameters
cd 'C:\Users\Jay\Desktop\AFIT\AERO799\Yu Data\'
data=readtable('Mo-30W_ANOVA_v5.xlsx');

% Convert table to matrix format
data=data{:,:};
% Categorize into speed,strain,stress,hour
speed=data(:,1);
% Convert doubles to strings if needed
%speed_str=arrayfun(@num2str,speed,'un',0);
strain=data(:,2);
stress=data(:,3);
heat=data(:,4);
orientation=data(:,5);
gas=data(:,6);
%heat_str=arrayfun(@num2str,hour,'un',0);

% ANOVA analysis
[p,tbl,stats]=anovan(strain,{speed heat orientation gas},...

'display','on','model','full','sstype',1,'varnames',{'speed','heat','or
ientation','gas'},'continuous',1:4);
h=figure;
% Remove 4th Singularity? column
tbl(:,4) = [];
% Position table into figure and resize automatically
u=uitable('Position',[20 20 500 70],'Data', tbl);
table_extent = get(u,'Extent');
set(u,'Position',[1 1 table_extent(3) table_extent(4)])
figure_size = get(h,'outerposition');
desired_fig_size = [figure_size(1) figure_size(2) table_extent(3)+15
table_extent(4)+65];
set(h,'outerposition', desired_fig_size);
```

Appendix B

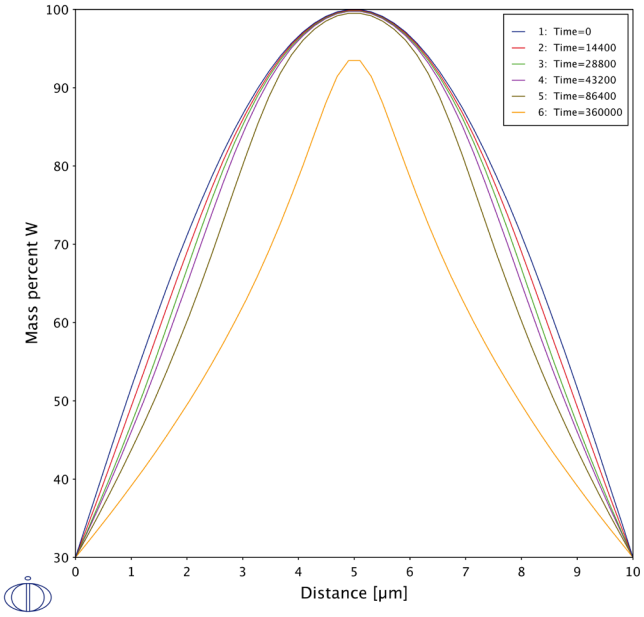

Figure B. 1. Thermo-Calc diffusion software – Mo-30W heat treatment simulation for 1800 °C.

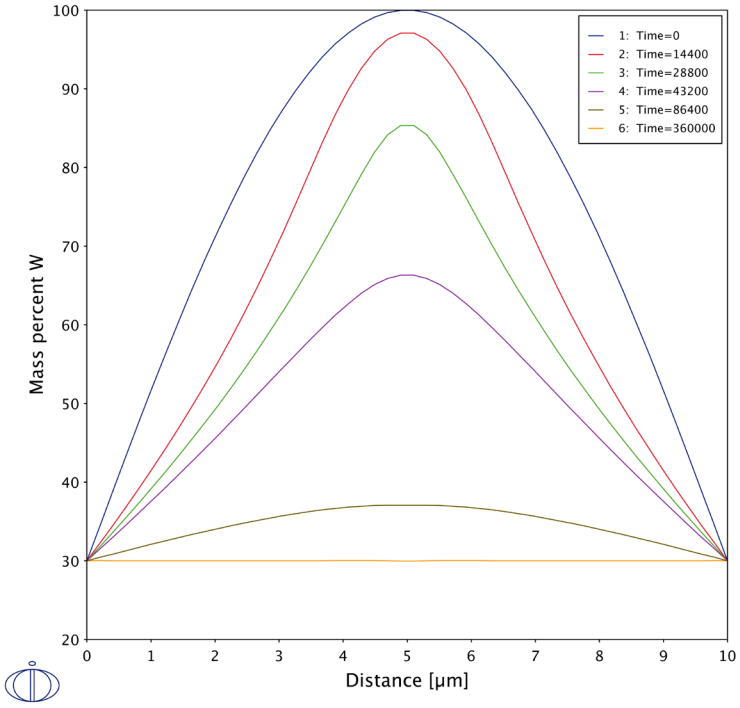

Figure B. 2. Thermo-Calc diffusion software – Mo-30W heat treatment simulation for 2000 °C above, 2200 °C below.

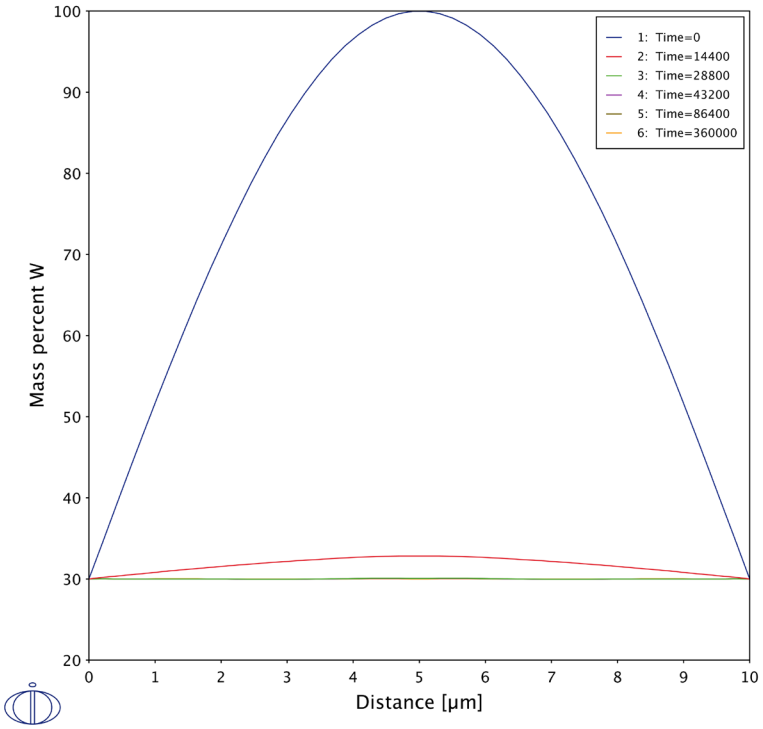

Appendix C

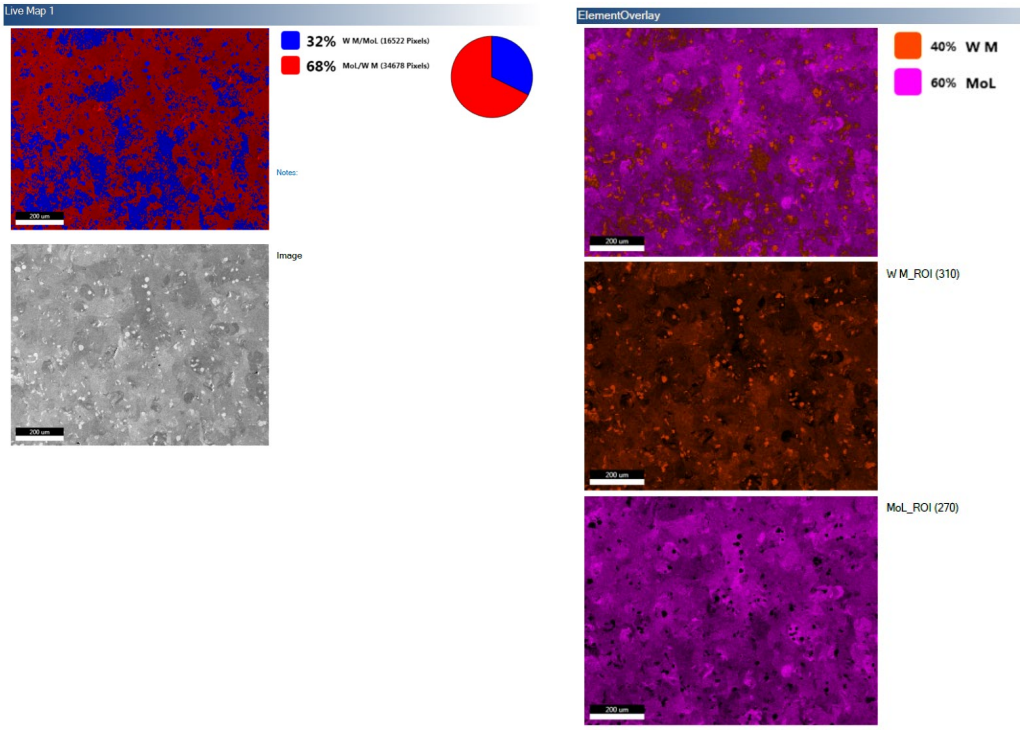

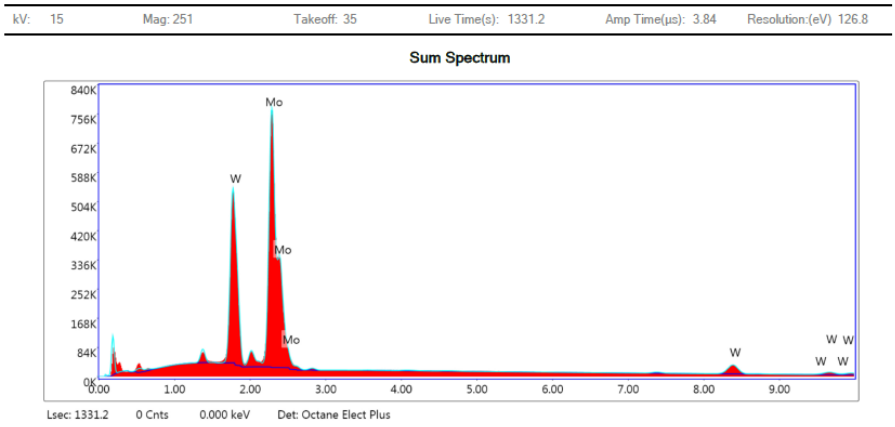

eZAF Smart Quant Results

Element	Weight %	Atomic %	Net Int.	Error %	Kratio	Z	A	F
W M	32.80	20.30	2868.20	2.11	0.3165	0.8967	1.0685	1.0071
MoL	67.20	79.70	4967.60	3.60	0.5547	1.0516	0.7851	0.9997

Figure C. 1. EDS snapshot of Mo-30W sample 1 out 3, print speed of 100 mm/s, vertical orientation, no HT, and printed in pure Ar build chamber gas.

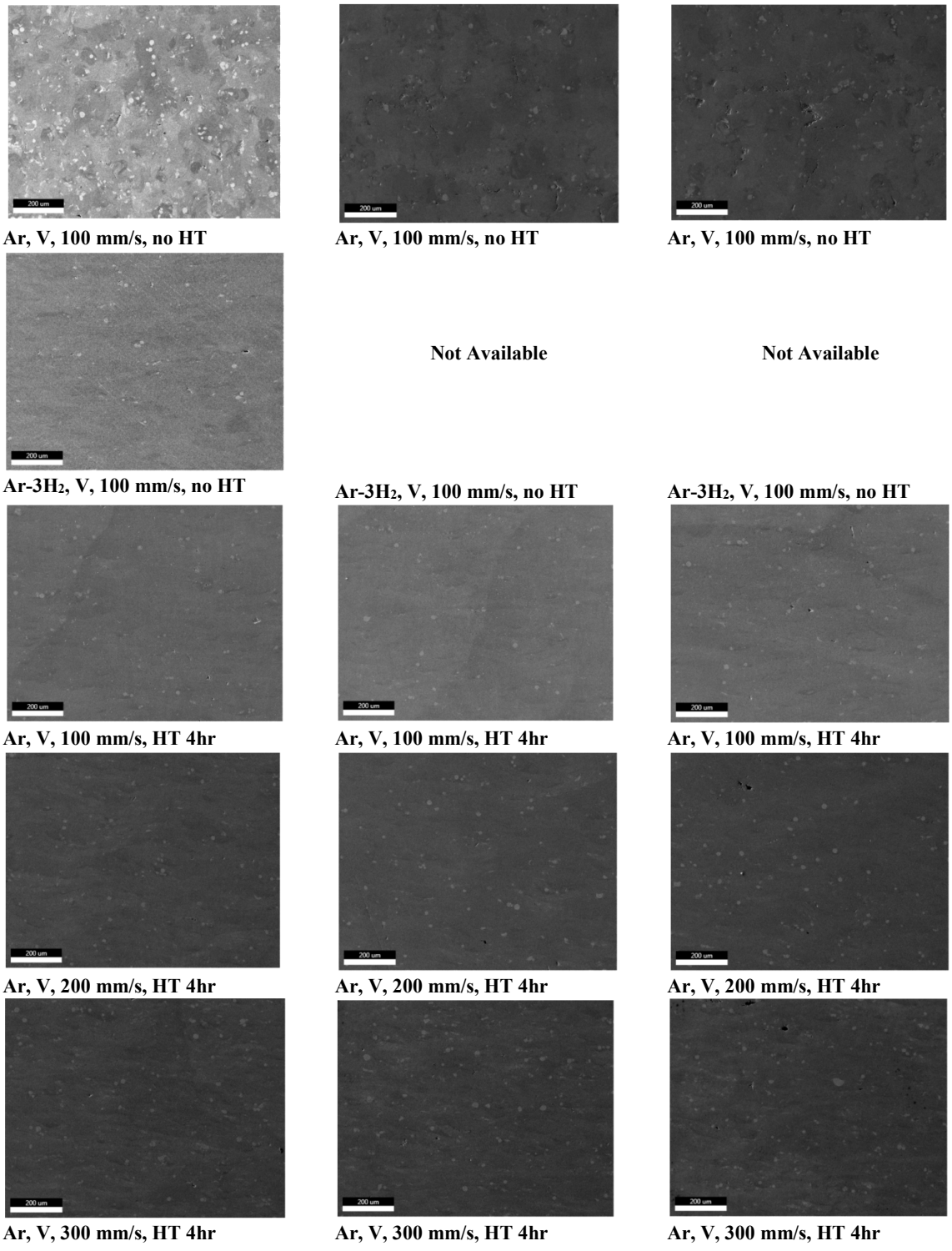

Figure C. 2. SEM images of various Mo-30W surfaces (HT temperature at 1600°C).

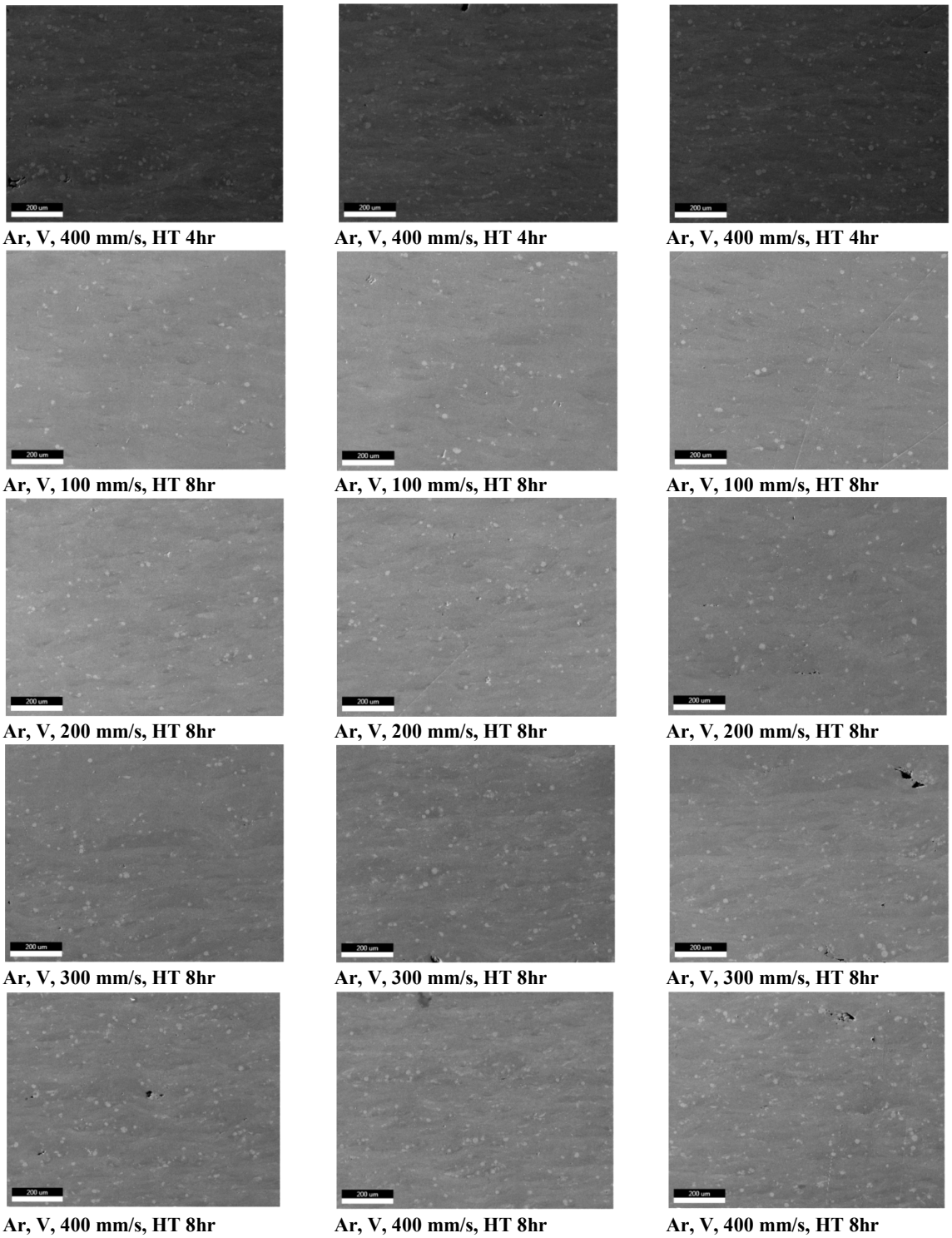

Figure C. 3. SEM images of various Mo-30W surfaces (HT temperature at 1600°C).

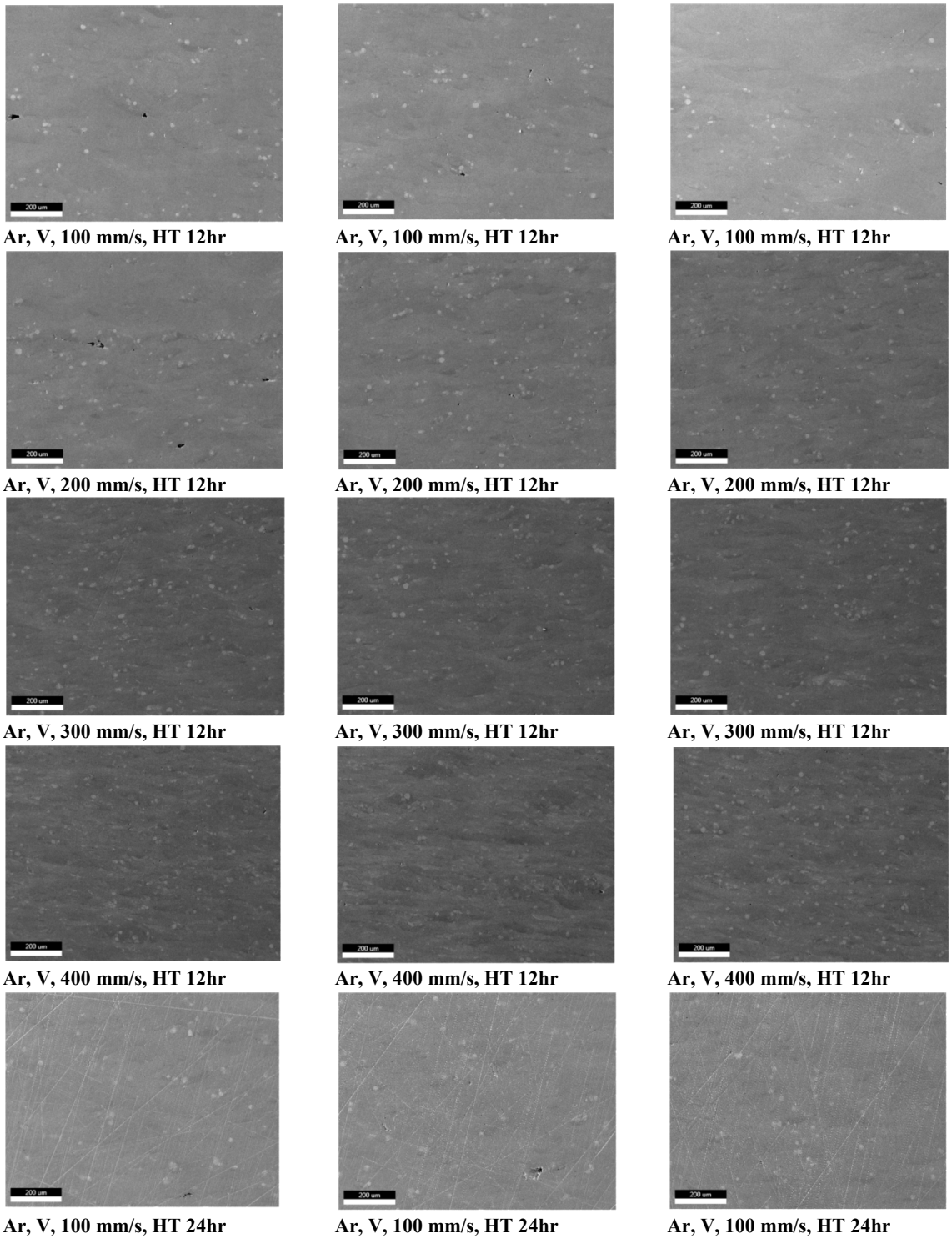

Figure C. 4. SEM images of various Mo-30W surfaces (HT temperature at 1600°C).

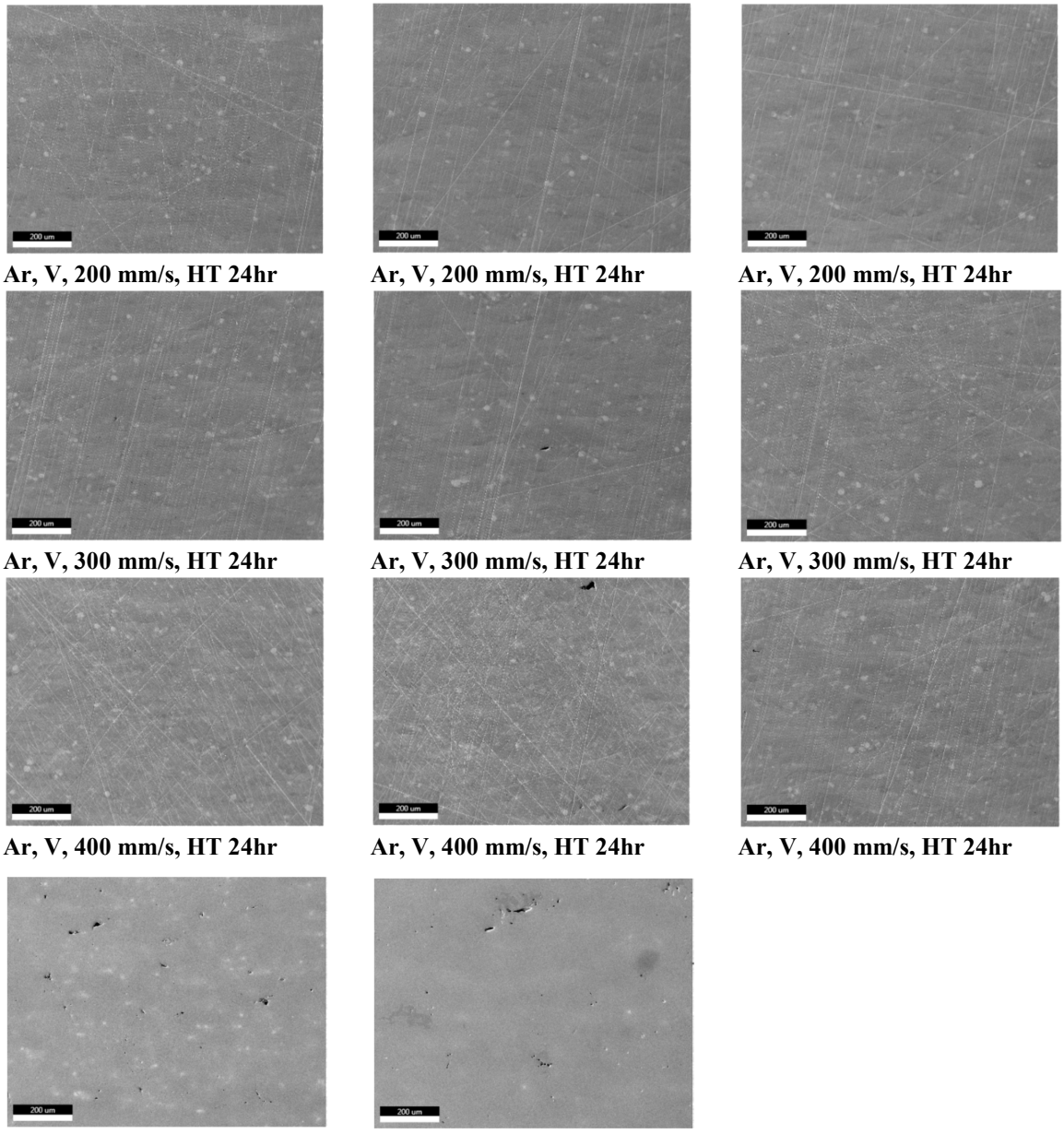

Ar, V, 200 mm/s, HT 24hr **Ar, V, 200 mm/s, HT 24hr** **Ar, V, 200 mm/s, HT 24hr**

Ar, V, 300 mm/s, HT 24hr **Ar, V, 300 mm/s, HT 24hr** **Ar, V, 300 mm/s, HT 24hr**

Ar, V, 400 mm/s, HT 24hr **Ar, V, 400 mm/s, HT 24hr** **Ar, V, 400 mm/s, HT 24hr**

Ar, V, 100 mm/s, HT 12hr-2000°C **Ar2, V, 400 mm/s, HT 12hr-2000°C**

Figure C. 5. SEM images of various Mo-30W surfaces (HT temperature at 1600°C unless otherwise noted).

Appendix D

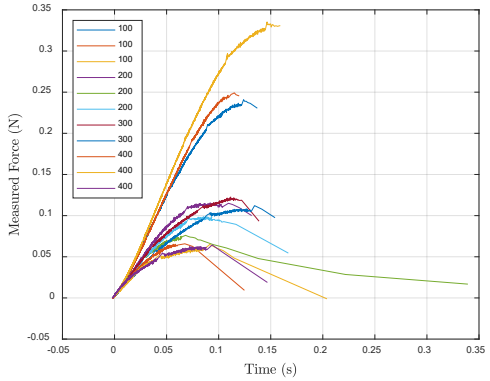

Ar, V, 100 – 400 mm/s, no HT

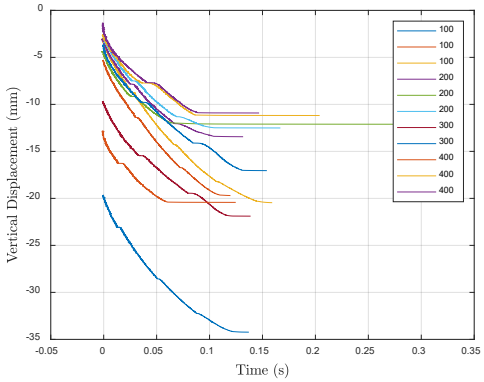

Ar, V, 100 – 400 mm/s, no HT

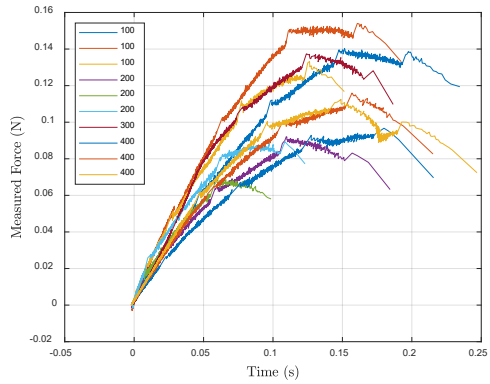

Ar, 45, 100 – 400 mm/s, no HT

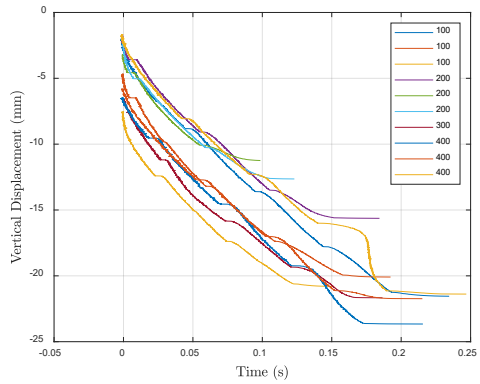

Ar, 45, 100 – 400 mm/s, no HT

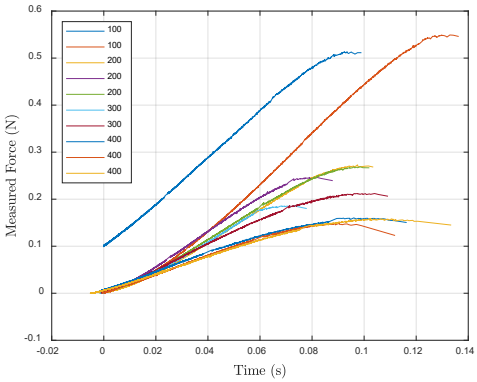

Ar-3H$_2$, V, 100 – 400 mm/s, no HT

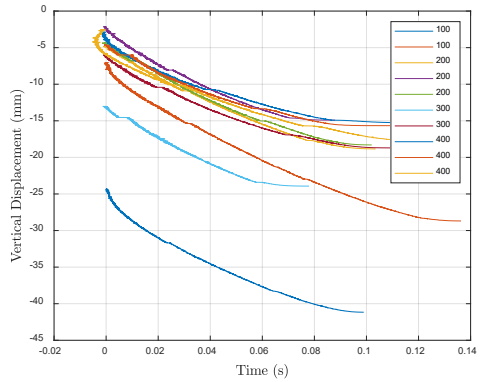

Ar-3H$_2$, V, 100 – 400 mm/s, no HT

Figure D. 1. Full measured load (N/mm) and vertical displacement (mm) vs time of Mo-30W specimen obtained from three-point bend test (left column – measured load vs time, right column – vertical displacement vs time).

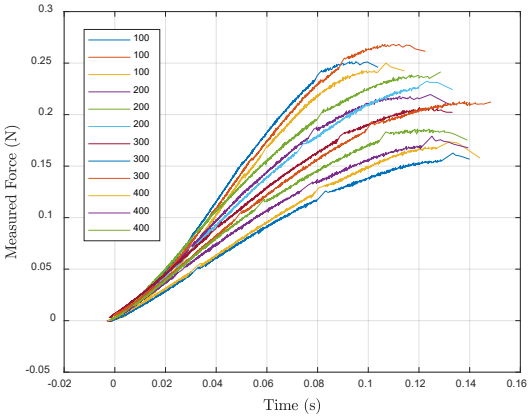

Ar-3H$_2$, 45, 100 – 400 mm/s, no HT

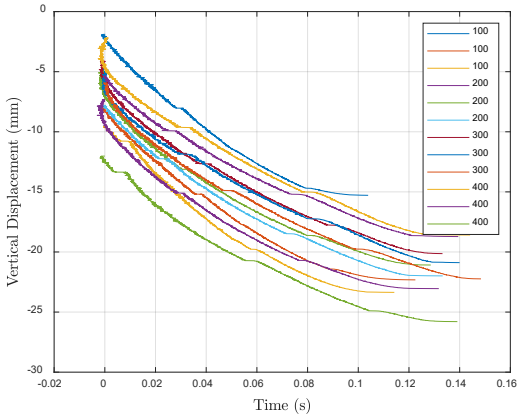

Ar-3H$_2$, 45, 100 – 400 mm/s, no HT

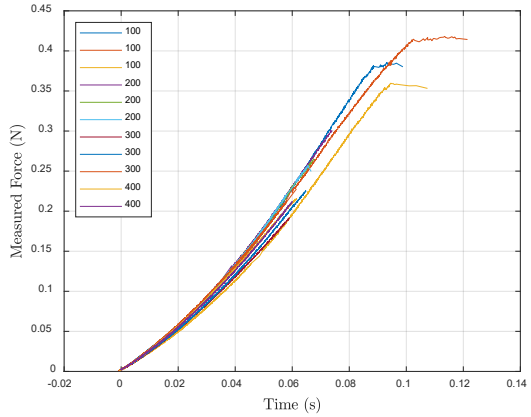

Ar, V, 100 – 400 mm/s, HT 4hr 1600°C

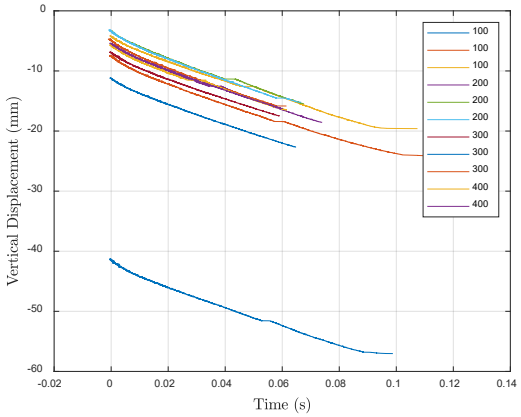

Ar, V, 100 – 400 mm/s, HT 4hr 1600°C

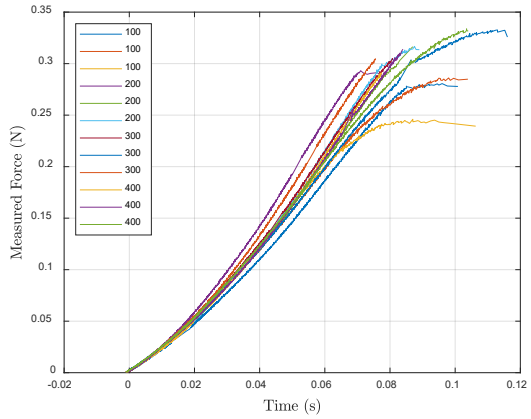

Ar, 45, 100 – 400 mm/s, HT 4hr 1600°C

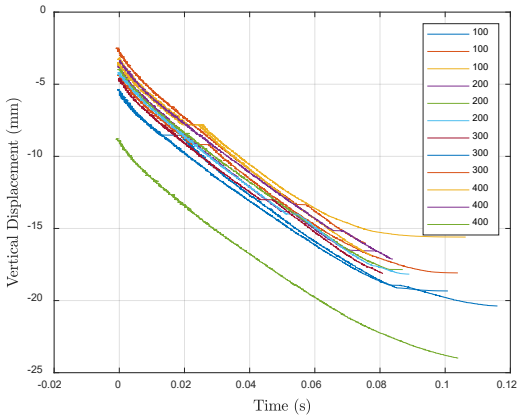

Ar, 45, 100 – 400 mm/s, HT 4hr 1600°C

Figure D. 2. Full measured load (N/mm) and vertical displacement (mm) vs time of Mo-30W specimen obtained from three-point bend test (left column – measured load vs time, right column – vertical displacement vs time).

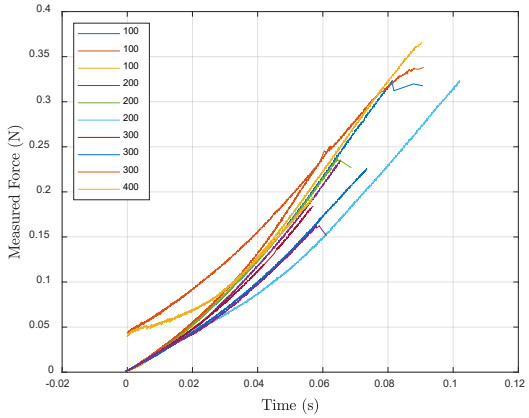

Ar, V, 100 – 400 mm/s, HT 8hr 1600°C

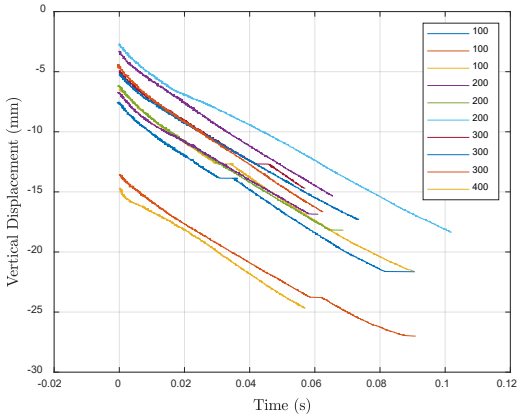

Ar, V, 100 – 400 mm/s, HT 8hr 1600°C

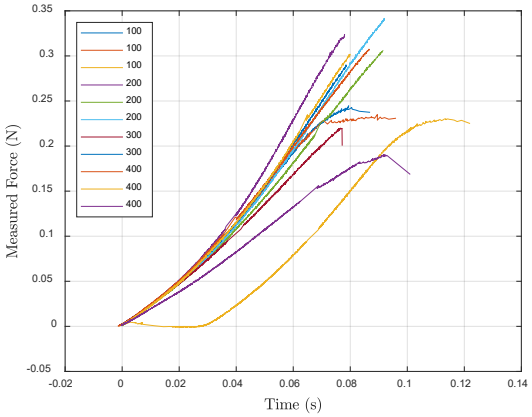

Ar, 45, 100 – 400 mm/s, HT 8hr 1600°C

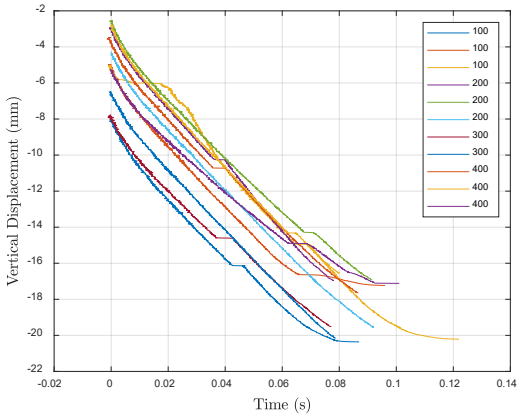

Ar, 45, 100 – 400 mm/s, HT 8hr 1600°C

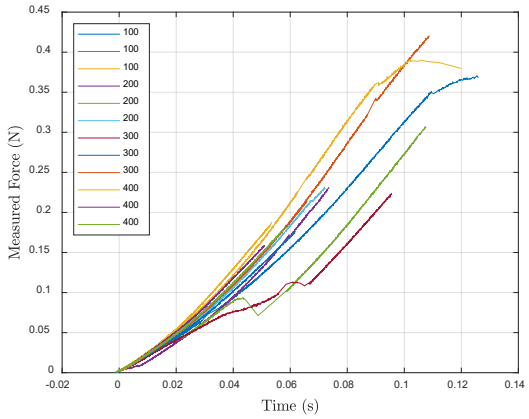

Ar, V, 100 – 400 mm/s, HT 12hr 1600°C

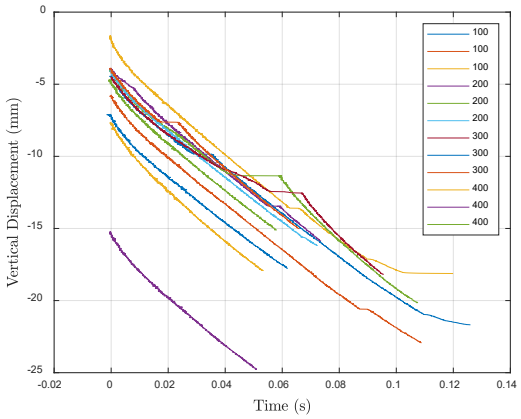

Ar, V, 100 – 400 mm/s, HT 12hr 1600°C

Figure D. 3. Full measured load (N/mm) and vertical displacement (mm) vs time of Mo-30W specimen obtained from three-point bend test (left column – measured load vs time, right column – vertical displacement vs time).

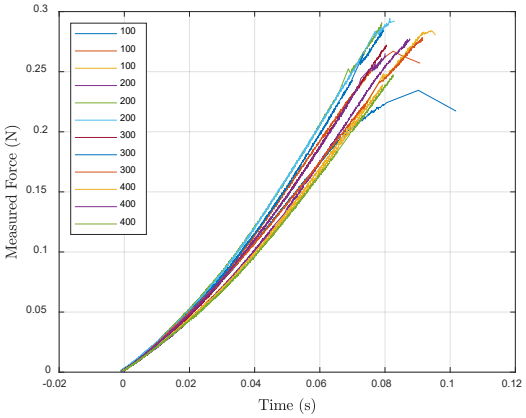

Ar, 45, 100 – 400 mm/s, HT 12hr 1600°C

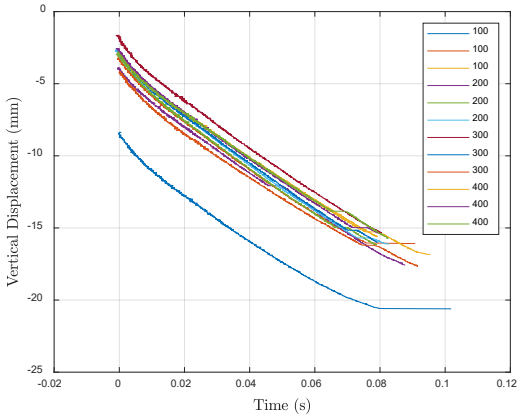

Ar, 45, 100 – 400 mm/s, HT 12hr 1600°C

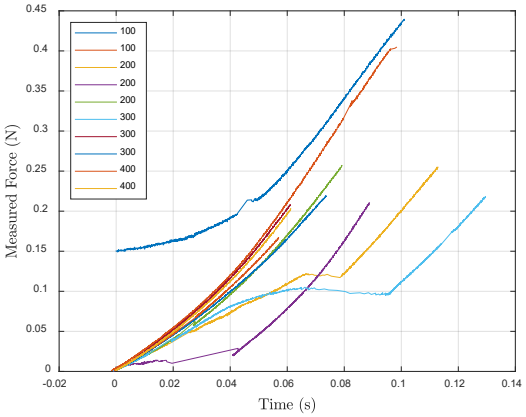

Ar, V, 100 – 400 mm/s, HT 24hr 1600°C

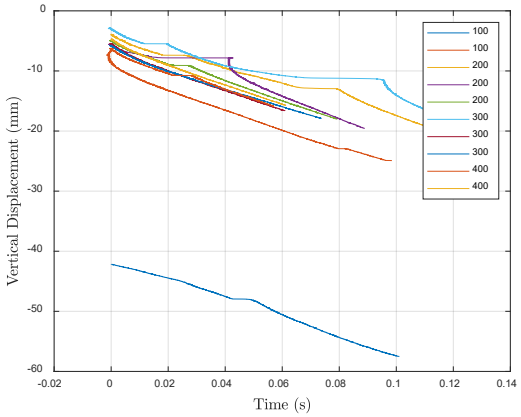

Ar, V, 100 – 400 mm/s, HT 24hr 1600°C

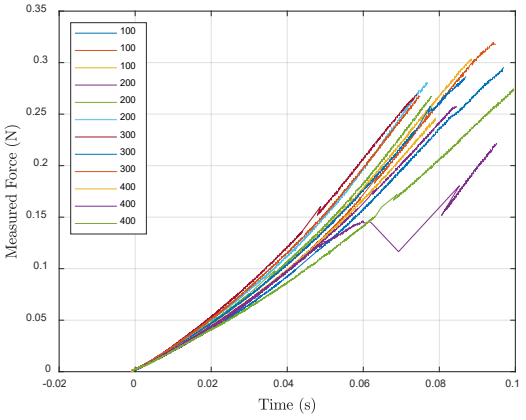

Ar, 45, 100 – 400 mm/s, HT 24hr 1600°C

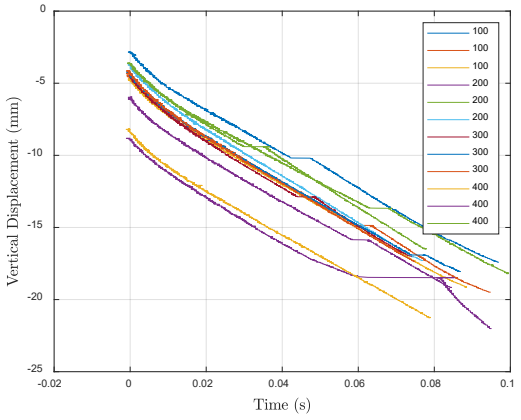

Ar, 45, 100 – 400 mm/s, HT 24hr 1600°C

Figure D. 4. Full measured load (N/mm) and vertical displacement (mm) vs time of Mo-30W specimen obtained from three-point bend test (left column – measured load vs time, right column – vertical displacement vs time).

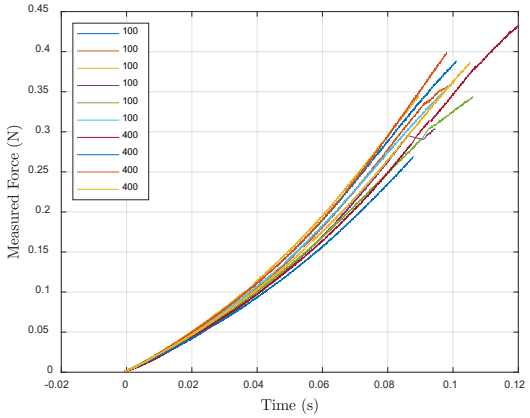

Ar, V, 100,400 mm/s, HT 12hr 2000°C

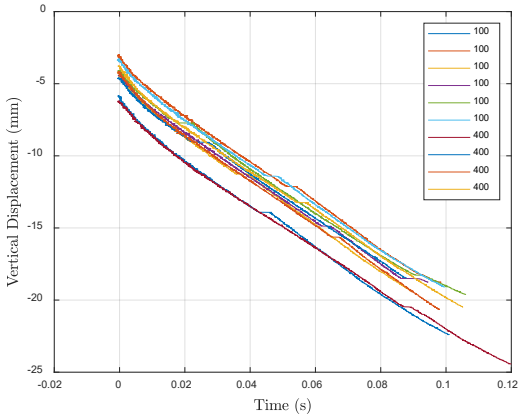

Ar, V, 100,400 mm/s, HT 12hr 2000°C

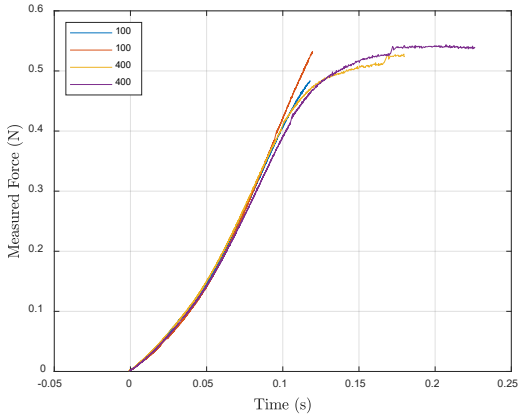

Ar, 45, 100,400 mm/s, HT 12hr 2000°C

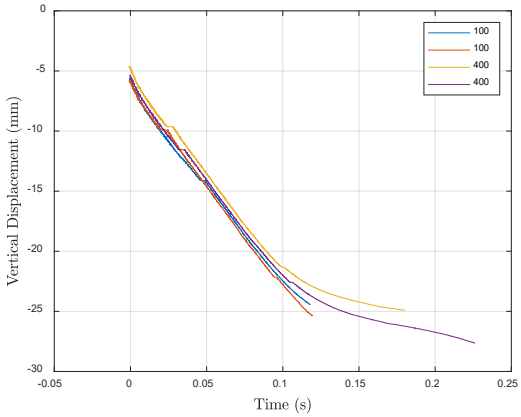

Ar, 45, 100,400 mm/s, HT 12hr 2000°C

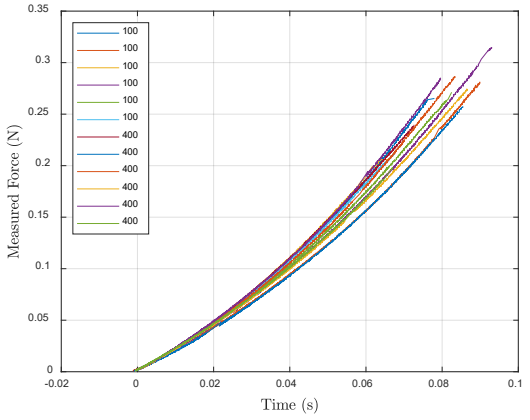

Ar, 45, 100,400 mm/s, HT 6hr 2200°C

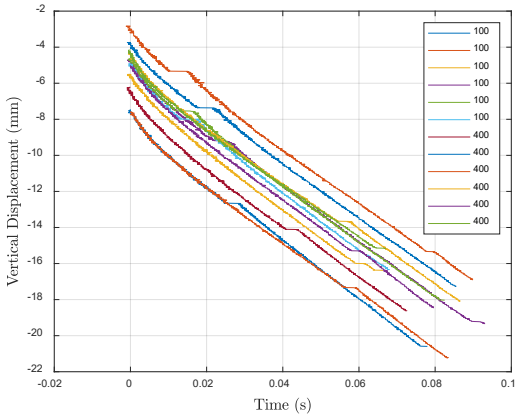

Ar, 45, 100,400 mm/s, HT 6hr 2200°C

Figure D. 5. Full measured load (N/mm) and vertical displacement (mm) vs time of Mo-30W specimen obtained from three-point bend test (left column – measured load vs time, right column – vertical displacement vs time).

Appendix E

Table E. 1. Vertically printed Mo-30W dimensions.

Vertical Mo-30W in Ar				Vertical Mo-30W in Ar-3H_2			
Print speed (mm/s)	Length (mm)	Width (mm)	Thickness (mm)	Print speed (mm/s)	Length (mm)	Width (mm)	Thickness (mm)
100	18.5	4.35	2.12	100	18.32	4.31	2.06
100	18.53	4.32	2.11	100	18.31	4.24	2.06
100	18.53	4.3	2.11	200	18.34	4.04	2.01
200	18.48	4.27	2.06	200	18.38	4.03	2.07
200	18.48	4.29	2.07	200	18.36	4.03	2.05
200	18.49	4.3	2.06	300	18.31	3.98	1.98
300	16.74	4.19	2.01	300	18.37	3.99	1.99
300	17.17	4.21	1.98	400	18.37	4.13	2.02
400	18.55	4.22	2.03	400	18.34	4.13	1.99
400	17.14	4.22	1.94	400	18.37	4.15	1.92
400	17.43	4.25	2				

Table E. 2. Diagonally printed Mo-30W dimensions.

Diagonal Mo-30W in Ar				Diagonal Mo-30W in Ar-3H_2			
Print speed (mm/s)	Length (mm)	Width (mm)	Thickness (mm)	Print speed (mm/s)	Length (mm)	Width (mm)	Thickness (mm)
100	19.96	3.14	2.03	100	19.29	3.04	2.01
100	20.025	3.13	2.11	100	19.31	3.06	2.07
100	19.98	3.15	2.07	100	19.23	3.11	2.04
200	20.015	3.07	2.01	200	19.86	2.97	2.03
200	20.03	3.09	2.04	200	19.72	2.98	2.04
200	19.945	3.07	2.05	200	19.19	2.99	2.03
300	19.985	3.08	2.02	300	20.05	2.74	1.97
400	19.315	3.17	1.82	300	19.32	2.7	1.94
400	19.005	3.13	1.89	300	19.55	2.71	1.99
400	18.785	3.12	1.97	400	19.46	2.73	1.97
				400	19.27	2.75	1.99
				400	19.21	2.72	1.99

Table E. 3. Vertically printed Mo-30W in pure Ar with 1600°C heat treatment dimensions.

Vertical Mo-30W in 4-hour Heat Treatment				Vertical Mo-30W in 8-hour Heat Treatment			
Print speed (mm/s)	Length (mm)	Width (mm)	Thickness (mm)	Print speed (mm/s)	Length (mm)	Width (mm)	Thickness (mm)
100	18.6	4.59	2.15	100	18.57	4.56	2.08
100	18.58	4.6	2.13	100	18.62	4.57	2.04
100	18.55	4.55	2.12	100	18.58	4.58	2.05
200	18.51	4.45	2.09	200	18.61	4.45	2.04
200	18.55	4.44	2.12	200	18.56	4.43	2.08
200	18.57	4.39	2.07	200	18.55	4.41	2.04
300	18.56	4.38	2.1	300	18.68	4.34	2
300	18.58	4.36	2.11	300	18.61	4.4	2.02
300	1858	4.38	2.09	300	18.57	4.37	2.08
400	18.57	4.35	2.09	400	18.62	4.37	2.07
400	18.64	4.35	2.07	400	18.64	4.36	2.09
Vertical Mo-30W in 12-hour Heat Treatment				Vertical Mo-30W in 24-hour Heat Treatment			
Print speed (mm/s)	Length (mm)	Width (mm)	Thickness (mm)	Print speed (mm/s)	Length (mm)	Width (mm)	Thickness (mm)
100	18.65	4.66	2.1	100	18.62	4.59	2.13
100	18.59	4.63	2.1	100	18.61	4.57	2.1
100	18.62	4.6	2.11	200	18.58	4.49	2.12
200	18.63	4.48	2.1	200	18.65	4.42	2.12
200	18.58	4.42	2.1	200	18.61	4.42	2.1
200	18.59	4.44	2.06	300	18.62	4.4	2.07
300	18.63	4.42	2.09	300	18.7	4.41	2.1
300	18.61	4.4	2.09	300	18.64	4.41	2.1
300	18.65	4.38	2.03	400	18.77	4.37	2.11
400	18.66	4.38	2.08	400	18.66	4.37	2.07
400	18.64	4.38	2.08				
400	18.63	4.37	2				

Table E. 4. Diagonally printed Mo-30W in pure Ar with 1600°C heat treatment dimensions.

Diagonal Mo-30W in 4-hour Heat Treatment				Diagonal Mo-30W in 8-hour Heat Treatment			
Print speed (mm/s)	Length (mm)	Width (mm)	Thickness (mm)	Print speed (mm/s)	Length (mm)	Width (mm)	Thickness (mm)
100	25.3	4.34	2.11	100	25.02	4.4	2.08
100	25.2	4.39	2.14	100	25.03	4.38	2.09
100	25.3	4.38	2.13	100	25.06	4.42	2.05
200	25.23	4.38	2.09	200	25.17	4.31	2.08
200	25.08	4.31	2.1	200	25.06	4.36	2.08
200	25.12	4.34	2.13	200	25.08	4.35	2.07
300	25.08	4.31	2.05	300	25.05	4.32	1.91
300	25.28	4.33	2.05	300	19.55	4.31	2.07
300	24.9	4.31	2.1	400	25	4.31	2.05
400	25.27	4.32	2.09	400	24.9	4.29	2.03
400	25.26	4.33	2.09	400	25.3	4.31	1.82
400	25.18	4.34	2.05				
Diagonal Mo-30W in 12-hour Heat Treatment				Diagonal Mo-30W in 24-hour Heat Treatment			
Print speed (mm/s)	Length (mm)	Width (mm)	Thickness (mm)	Print speed (mm/s)	Length (mm)	Width (mm)	Thickness (mm)
100	25.08	4.46	2.03	100	25.02	4.41	2.07
100	24.78	4.42	2.09	100	25.08	4.43	2.11
100	25.03	4.42	2.1	100	25.08	4.39	2.03
200	25	4.33	2.09	200	25.08	4.38	2.06
200	24.93	4.32	2.09	200	25.1	4.31	2.03
200	25.11	4.32	2.1	200	25	4.29	2.05
300	25.04	4.29	2.08	300	25.02	4.29	2.02
300	25.06	4.33	2.1	300	25.1	4.3	2.04
300	25	4.3	2.08	300	25.08	4.32	2.07
400	25.05	4.31	2.05	400	24.07	4.4	1.99
400	25.13	4.35	2.08	400	25.11	4.29	2.02
400	23.98	4.34	2.07	400	25.14	4.34	2.04

Table E. 5. Mo-30W in pure Ar with 2000°C heat treatment dimensions.

Vertical Mo-30W in 12-hour Heat Treatment				Diagonal Mo-30W in 12-hour Heat Treatment			
Print speed (mm/s)	Length (mm)	Width (mm)	Thickness (mm)	Print speed (mm/s)	Length (mm)	Width (mm)	Thickness (mm)
100	17.53	4.6	2.1	100	25.2	4.37	2.13
100	17.59	4.68	2.07	100	23.96	4.38	2.23
100	17.67	4.63	2.09	400	24.59	4.38	2.02
100	17.53	4.6	2.08	400	23.61	4.42	2.06
100	17.52	4.62	2.07				
100	17.54	4.57	1.96				
400	17.26	4.43	2.02				
400	17.4	4.38	2.05				
400	17.22	4.4	2.11				
400	17.56	4.43	2.14				

Table E. 6. Mo-30W in pure Ar with 2200°C heat treatment dimensions.

Vertical Mo-30W in 6-hour Heat Treatment			
Print speed (mm/s)	Length (mm)	Width (mm)	Thickness (mm)
100	17.33	4.55	2.04
100	17.28	4.54	2.02
100	17.33	4.54	2.07
100	17.3	4.51	2.1
100	17.24	4.51	2.1
100	17.38	4.56	2.11
400	17.26	4.37	2.02
400	17.14	4.38	2.02
400	17.24	4.33	1.94
400	16.59	4.34	2
400	16.91	4.34	2
400	17.22	4.34	1.96

Appendix F

Test series

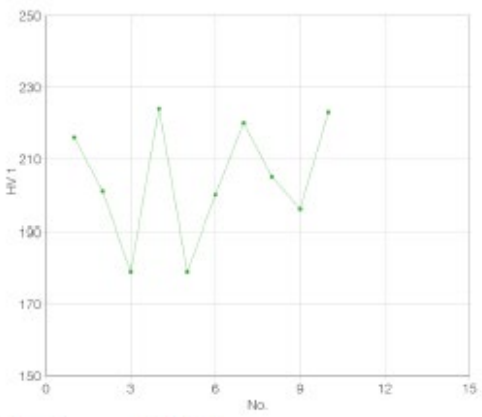

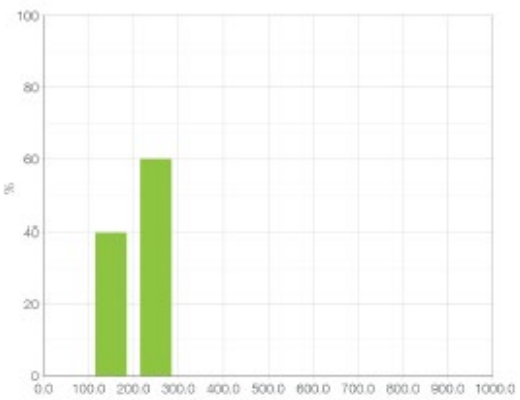

Result: 204 HV 1

Test points:

No.	Value	Method	X pos. [mm]	Y pos. [mm]	d1 [mm]	d2 [mm]	Description
1	216	HV 1	0.50	0.00	0.09	0.09	
2	201	HV 1	1.23	0.00	0.10	0.10	
3	179	HV 1	1.95	0.00	0.10	0.10	
4	224	HV 1	2.68	0.00	0.09	0.09	
5	179	HV 1	3.41	0.00	0.10	0.10	
6	200	HV 1	4.14	0.00	0.10	0.10	
7	220	HV 1	4.86	0.00	0.09	0.09	
8	205	HV 1	5.59	0.00	0.10	0.09	
9	196	HV 1	6.32	0.00	0.10	0.10	
10	223	HV 1	7.04	0.00	0.09	0.09	

ATM Qness GmbH
A-5440 Golling, Reitbauernweg 26

Date: 1/27/2022 1:14 PM
Test according to DIN EN ISO 6507-1

1 / 3

Testing report

Statistics:

Mean value	Range	Hardness min.	Hardness max.	Standard dev.	Results OK
204.30	45	179	224	16.67	10

Figure F. 1. Vicker micro harness test results for Mo-30W – vertical print orientation, 100 mm/s print speed, no heat treatment, and printed in in Ar.

Test series (1)

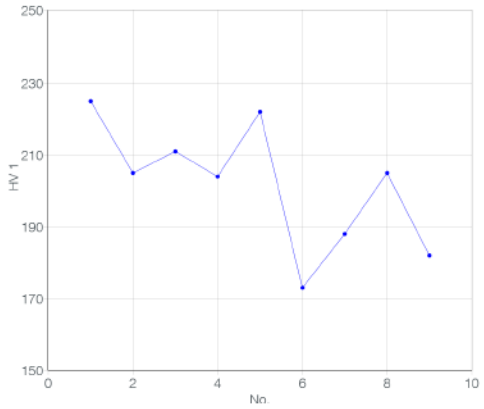

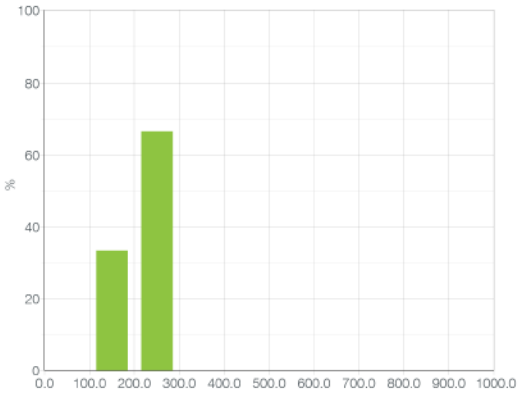

Result: 202 HV 1

Test points:

No.	Value	Method	X pos. [mm]	Y pos. [mm]	d1 [mm]	d2 [mm]	Description
1	225	HV 1	0.50	0.00	0.09	0.09	
2	205	HV 1	1.41	0.00	0.09	0.10	
3	211	HV 1	2.31	0.00	0.09	0.09	
4	204	HV 1	3.22	0.00	0.10	0.10	
5	222	HV 1	4.13	0.00	0.09	0.09	
6	173	HV 1	5.03	0.00	0.10	0.10	
7	188	HV 1	5.94	0.00	0.10	0.10	
8	205	HV 1	6.84	0.00	0.10	0.09	
9	182	HV 1	7.75	0.00	0.10	0.10	
10	162	HV 1	8.66	0.00	0.11	0.10	

Testing report

Statistics:

Mean value	Range	Hardness min.	Hardness max.	Standard dev.	Results OK
201.67	52	173	225	17.56	9

Figure F. 2. Vicker micro harness test results for Mo-30W – vertical print orientation, 400 mm/s print speed, no heat treatment, and printed in in Ar.

20 Point Hardness

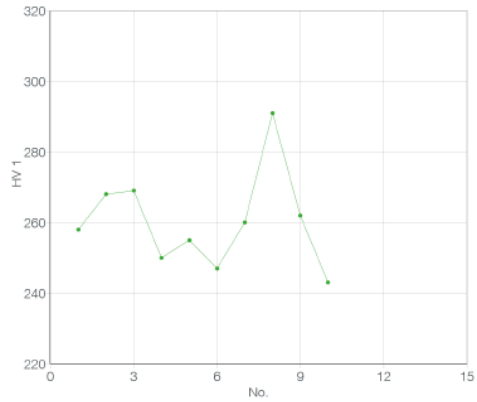

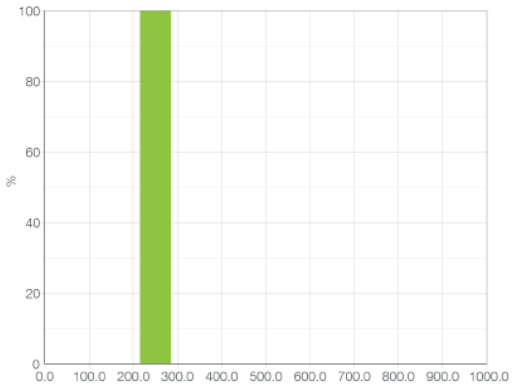

Result: 260 HV 1

Test points:

No.	Value	Method	X pos. [mm]	Y pos. [mm]	d1 [mm]	d2 [mm]	Description
1	258	HV 1	0.50	0.00	0.09	0.08	
2	268	HV 1	1.35	0.00	0.08	0.08	
3	269	HV 1	2.20	0.00	0.08	0.08	
4	250	HV 1	3.06	0.00	0.09	0.09	
5	255	HV 1	3.91	0.00	0.09	0.09	
6	247	HV 1	4.76	0.00	0.09	0.09	
7	260	HV 1	5.61	0.00	0.08	0.08	
8	291	HV 1	6.46	0.00	0.08	0.08	
9	262	HV 1	7.32	0.00	0.08	0.08	
10	243	HV 1	8.17	0.00	0.09	0.09	

ATM Qness GmbH
A-5440 Golling, Reitbauernweg 26

Date: 10/22/2021 10:17 AM
Testing report

1 / 2

Testing report

Statistics:

Mean value	Range	Hardness min.	Hardness max.	Standard dev.	Results OK
260.30	48	243	291	13.73	10

Figure F. 3. Vicker micro harness test results for Mo-30W – vertical print orientation, 100 mm/s print speed, no heat treatment, and printed in in Ar-3H_2.

20 Point Hardness

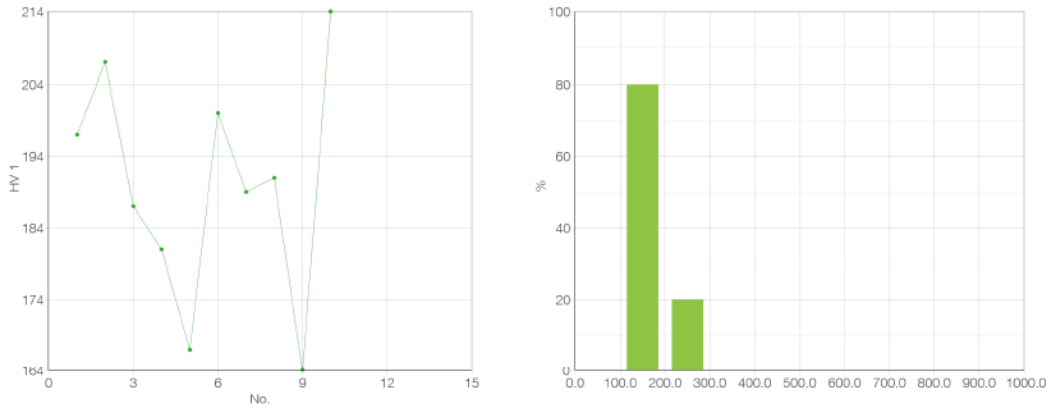

Result: 190 HV 1

Test points:

No.	Value	Method	X pos. [mm]	Y pos. [mm]	d1 [mm]	d2 [mm]	Description
1	197	HV 1	0.50	0.00	0.10	0.10	
2	207	HV 1	1.32	0.00	0.09	0.09	
3	187	HV 1	2.14	0.00	0.10	0.10	
4	181	HV 1	2.96	0.00	0.10	0.10	
5	167	HV 1	3.78	0.00	0.11	0.10	
6	200	HV 1	4.60	0.00	0.10	0.10	
7	189	HV 1	5.41	0.00	0.10	0.10	
8	191	HV 1	6.23	0.00	0.10	0.10	
9	164	HV 1	7.05	0.00	0.11	0.11	
10	214	HV 1	7.87	0.00	0.09	0.09	

ATM Qness GmbH
A-5440 Golling, Reitbauernweg 26

Date: 10/22/2021 10:17 AM
Testing report

1 / 2

Testing report

Statistics:

Mean value	Range	Hardness min.	Hardness max.	Standard dev.	Results OK
189.70	50	164	214	16.02	10

Figure F. 4. Vicker micro harness test results for Mo-30W – vertical print orientation, 100 mm/s print speed, 4-hour 1600°C heat treatment, and printed in Ar.

20 Point Hardness

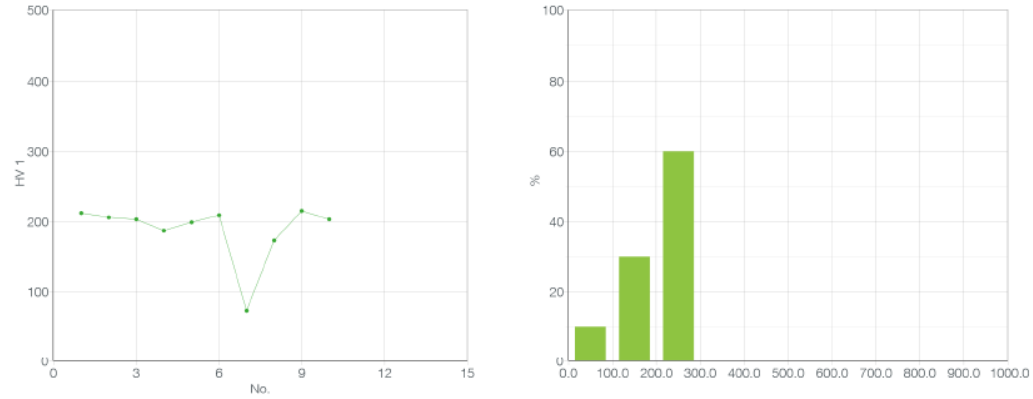

Result: 188 HV 1

Test points:

No.	Value	Method	X pos. [mm]	Y pos. [mm]	d1 [mm]	d2 [mm]	Description
1	212	HV 1	0.50	0.00	0.09	0.09	
2	206	HV 1	1.25	0.00	0.10	0.09	
3	203	HV 1	2.00	0.00	0.10	0.10	
4	187	HV 1	2.75	0.00	0.10	0.10	
5	199	HV 1	3.50	0.00	0.10	0.10	
6	209	HV 1	4.25	0.00	0.09	0.09	
7	72.8	HV 1	5.00	0.00	0.16	0.16	
8	173	HV 1	5.75	0.00	0.10	0.10	
9	215	HV 1	6.50	0.00	0.09	0.09	
10	203	HV 1	7.25	0.00	0.09	0.10	

ATM Qness GmbH
A-5440 Golling, Reitbauernweg 26

Date: 10/22/2021 10:17 AM
Testing report

1 / 2

Testing report

Statistics:

Mean value	Range	Hardness min.	Hardness max.	Standard dev.	Results OK
187.98	142.20	72.80	215	42.35	10

Figure F. 5. Vicker micro harness test results for Mo-30W – vertical print orientation, 100 mm/s print speed, 8-hour 1600°C heat treatment, and printed in Ar.

20 Point Hardness

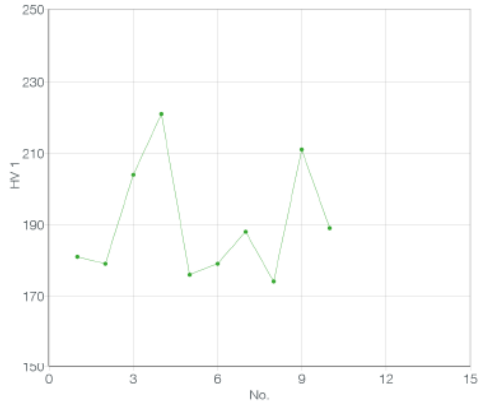

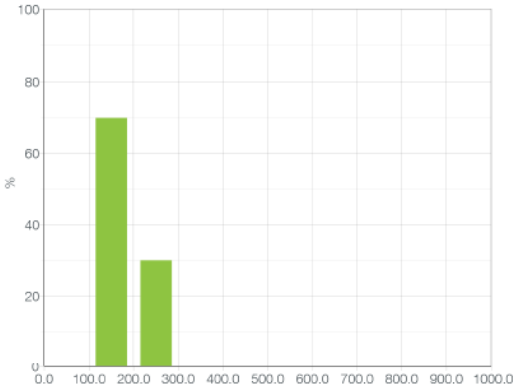

Result: 190 HV 1

Test points:

No.	Value	Method	X pos. [mm]	Y pos. [mm]	d1 [mm]	d2 [mm]	Description
1	181	HV 1	0.50	0.00	0.10	0.10	
2	179	HV 1	1.36	0.00	0.10	0.10	
3	204	HV 1	2.23	0.00	0.10	0.10	
4	221	HV 1	3.09	0.00	0.09	0.09	
5	176	HV 1	3.95	0.00	0.10	0.10	
6	179	HV 1	4.82	0.00	0.10	0.10	
7	188	HV 1	5.68	0.00	0.10	0.10	
8	174	HV 1	6.54	0.00	0.10	0.10	
9	211	HV 1	7.40	0.00	0.09	0.09	
10	189	HV 1	8.27	0.00	0.10	0.10	

ATM Qness GmbH
A-5440 Golling, Reitbauernweg 26

Date: 10/22/2021 10:16 AM
Testing report

1 / 2

Testing report

Statistics:

Mean value	Range	Hardness min.	Hardness max.	Standard dev.	Results OK
190.20	47	174	221	16.25	10

Figure F. 6. Vicker micro harness test results for Mo-30W – vertical print orientation, 100 mm/s print speed, 12-hour 1600°C heat treatment, and printed in Ar.

20 Point Hardness

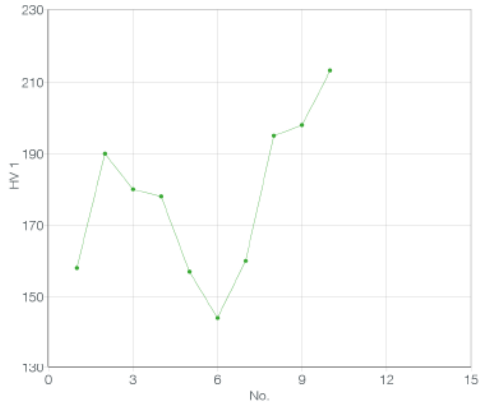

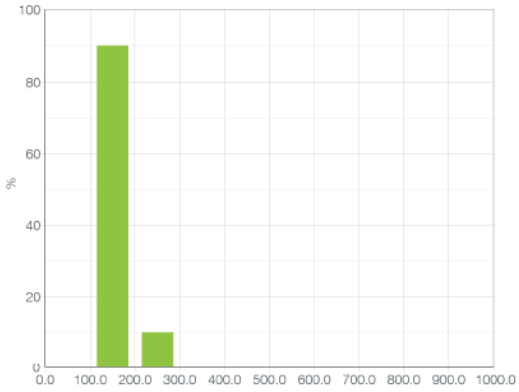

Result: 177 HV 1

Test points:

No.	Value	Method	X pos. [mm]	Y pos. [mm]	d1 [mm]	d2 [mm]	Description
1	158	HV 1	0.50	0.00	0.11	0.11	
2	190	HV 1	1.27	0.00	0.10	0.10	
3	180	HV 1	2.04	0.00	0.10	0.10	
4	178	HV 1	2.81	0.00	0.10	0.10	
5	157	HV 1	3.58	0.00	0.11	0.11	
6	144	HV 1	4.35	0.00	0.11	0.11	
7	160	HV 1	5.12	0.00	0.11	0.11	
8	195	HV 1	5.89	0.00	0.10	0.10	
9	198	HV 1	6.66	0.00	0.10	0.10	
10	213	HV 1	7.43	0.00	0.09	0.10	

ATM Qness GmbH
A-5440 Golling, Reitbauernweg 26

Date: 10/22/2021 10:14 AM
Testing report

1 / 2

Testing report

Statistics:

Mean value	Range	Hardness min.	Hardness max.	Standard dev.	Results OK
177.30	69	144	213	22.06	10

Figure F. 7. Vicker micro harness test results for Mo-30W – vertical print orientation, 100 mm/s print speed, 24-hour 1600°C heat treatment, and printed in Ar.

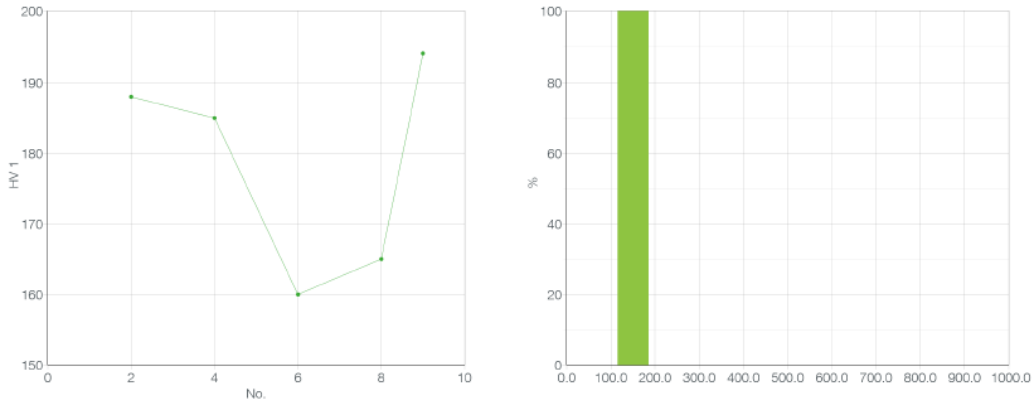

Result: 178 HV 1

Test points:

No.	Value	Method	X pos. [mm]	Y pos. [mm]	d1 [mm]	d2 [mm]	Description
1	147	HV 1	0.50	0.00	0.12	0.11	
2	188	HV 1	1.37	0.00	0.10	0.10	
3	155	HV 1	2.24	0.00	0.11	0.11	
4	185	HV 1	3.11	0.00	0.10	0.10	
5	148	HV 1	3.98	0.00	0.12	0.11	
6	160	HV 1	4.86	0.00	0.11	0.11	
7	170	HV 1	5.73	0.00	0.11	0.10	
8	165	HV 1	6.60	0.00	0.11	0.11	
9	194	HV 1	7.47	0.00	0.10	0.10	
10	132	HV 1	8.34	0.00	0.13	0.11	

ATM Qness GmbH
A-5440 Golling, Reitbauernweg 26

Date: 1/27/2022 1:38 PM
Test according to DIN EN ISO 6507-1

1 / 3

Testing report

Statistics:

Mean value	Range	Hardness min.	Hardness max.	Standard dev.	Results OK
178.40	34	160	194	14.98	5

Figure F. 8. Vicker micro harness test results for Mo-30W – vertical print orientation, 100 mm/s print speed, 12-hour 2000°C heat treatment, and printed in Ar.

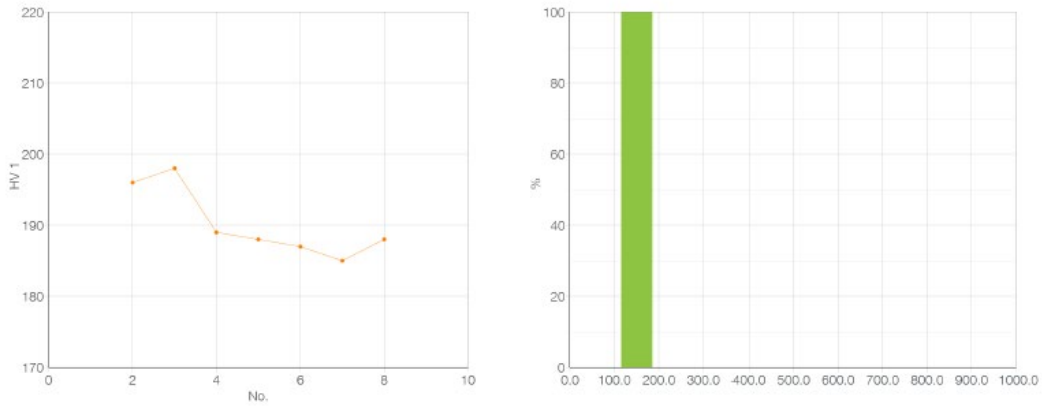

Result: 190 HV 1

Test points:

No.	Value	Method	X pos. [mm]	Y pos. [mm]	d1 [mm]	d2 [mm]	Description
1	405	HV 1	0.50	0.00	0.07	0.07	
2	196	HV 1	1.52	0.00	0.10	0.10	
3	198	HV 1	2.54	0.00	0.10	0.10	
4	189	HV 1	3.56	0.00	0.10	0.10	
5	188	HV 1	4.58	0.00	0.10	0.10	
6	187	HV 1	5.60	0.00	0.10	0.10	
7	185	HV 1	6.62	0.00	0.10	0.10	
8	188	HV 1	7.64	0.00	0.10	0.10	
9	155	HV 1	8.66	0.00	0.11	0.10	
10	264	HV 1	9.68	0.00	0.08	0.09	

ATM Qness GmbH
A-5440 Golling, Reitbauernweg 26

Date: 1/27/2022 2:10 PM
Test according to DIN EN ISO 6507-1

1 / 3

Testing report

Statistics:

Mean value	Range	Hardness min.	Hardness max.	Standard dev.	Results OK
190.14	13	185	198	4.88	7

Figure F. 9. Vicker micro harness test results for Mo-30W – diagonal print orientation, 400 mm/s print speed, 12-hour 2000°C heat treatment, and printed in Ar.

Appendix G

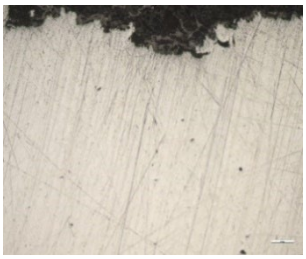

Ar-3H_2, V, 100 mm/s, no HT

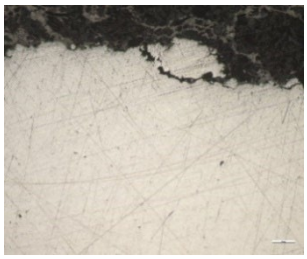

Ar-3H_2, V, 400 mm/s, no HT

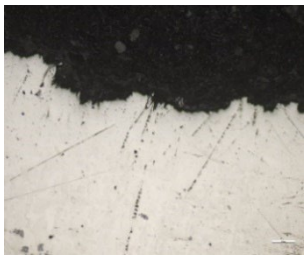

Ar, V, 100 mm/s, HT 4hr

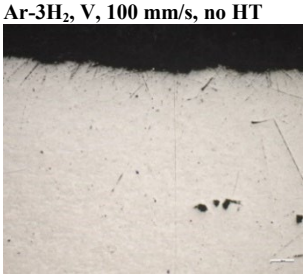

Ar, V, 400 mm/s, HT 4hr

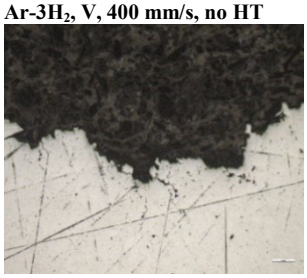

Ar-3H2, V, 100 mm/s, HT 8hr

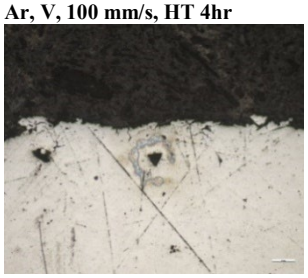

Ar-3H2, V, 400 mm/s, HT 8hr

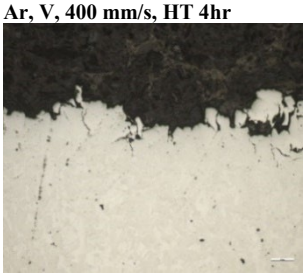

Ar, V, 100 mm/s, HT 12hr

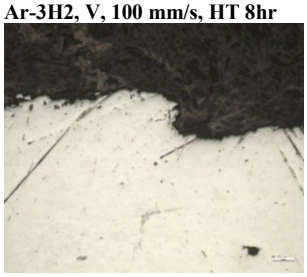

Ar, V, 400 mm/s, HT 12hr

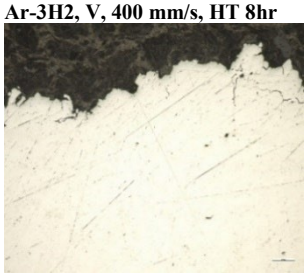

Ar, V, 100 mm/s, HT 24hr

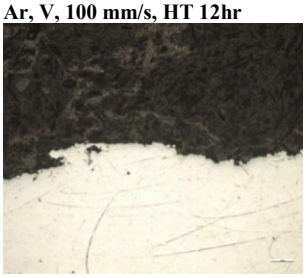

Ar, V, 400 mm/s, HT 24hr

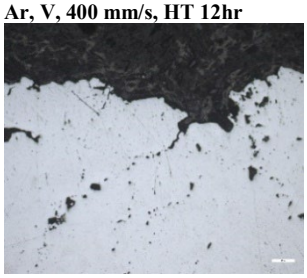

Ar, V, 100 mm/s, HT 12hr 2000°C

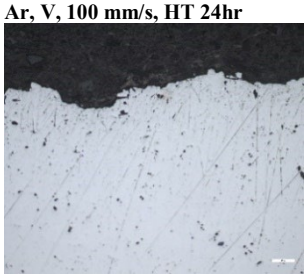

Ar, V, 400 mm/s, HT 12hr 2000°C

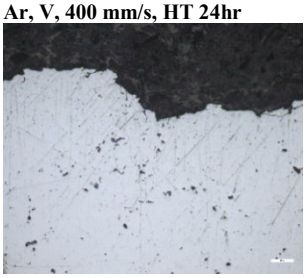

Ar, 45°, 100 mm/s, HT 12hr 2000°C

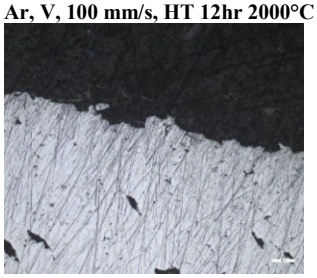

Ar2, 45°, 400 mm/s, HT 12hr 2000°C

Figure G. 1. Optical cross-sectional images of various Mo-30W fracture surfaces.

Bibliography

[1] H. L. Moody, D. H. Smith, R. L. Haddock and S. S. Dunn, "Tungsten and Molybdenum Ablation Modeling for Reentry Applications," *Journal of Spacecraft and Rockets,* vol. 13, no. 12, 1976.

[2] E. Lassner and W.-D. Schubert, Tungsten: Properties, Chemistry, Technology of the Element, Alloys, and Chemical Compounds, New York: Kluwer Academic & Plenum Publishers, 1999.

[3] I. Gibson, D. Rosen and B. Stucker, Additive Manufacturing Technologies, New York: Springer, 2015.

[4] B. Dutta and F. H. Froes, "Additive Manufacturing of Titanium Alloys: State of the Art, Challenges, and Opportunities," Oxford, Elsevier, 2016.

[5] C. G. Vayenas, R. E. White and M. E. Gamboa-Aldeco, Modern Aspect of Electrochemistry, New York: Springer, 2008.

[6] R. K. Enneti, R. Morgan and S. V. Atre, "Effect of process parameters on the Selective Laser Melting (SLM) of tungsten," *International Journal of Refractory Metals & Hard Materials,* pp. 315-319, 2018.

[7] D. Faidel, D. Jonas, G. Natour and W. Behr, "Investigation of the Selective Laser Melting Process with Molybdenum powder," *Additive Manufacturing,* pp. 88-94, 2015.

[8] J. Braun, L. Kaserer, J. Stajkovic, K.-H. Leitz, B. Tabernig, P. Singer, I. Letofsky-Papst, H. Kestler and G. Leichtfried, "Molybdenum and tungsten manufactured by selective laser melting: Analysis of defect structure and solidification mechanisms," *International Journal of Refractory Metals & Hard Materials,* vol. 84, 2019.

[9] D. Burns and S. Johnson, Nuclear Thermal Propulsion Reactor Materials, Idaho Falls, Idaho: IntechOpen, 2020.

[10] D. Wang, C. Yu, J. Ma, W. Liu and Z. Shen, "Densification and crack suppression in selective laser melting of," *Materials & Design,* 2017.

[11] A. Ivekovic, N. Omidvari, B. Vrancken, K. Lietaert, L. Thijs, K. Vanmeensel, J. Vleugels and J.-P. Kruth, "Selective laser melting of tungsten and tungsten alloys," *International Journal of Refractory Metals and Hard Materials,* 2017.

[12] A. T. Sidambe, Y. Tian, P. B. Prangnell and P. Fox, "Effect of processing parameters on the densification, microstructure and crystallographic texture during the laser powder bed fusion of pure tungsten," *International Journal of Refractory Metals & Hard Materials,* 2018.

[13] J. Zhang, D. Gu, Y. Yang, H. Zhang, H. Chen, D. Dai and K. Lin, "Influence of Particle Size on Laser Absorption and Scanning Track Formation Mechanisms of Pure Tungsten Powder During Selective Laser Melting," *Engineering,* pp. 736-745, 2019.

[14] L. Kaserer, J. Braun, J. Stajkovic, K. H. Leitz, B. Tabernig, P. Singer, I. Letofsky-Papst, H. Kestler and G. Leichfried, "Fully dense and crack free molybdenum manufactured by Selective Laser," *International Journal of Refractory Metals & Hard Materials,* 2019.

[15] M. Higashi and T. Ozaki, "Selective laser melting of pure molybdenum: Evolution of defect and crystallographic texture with process parameters," *Materials & Design,* p. 2018, 2020.

[16] C. C. Eckley, R. A. Kemnitz, C. P. Fassio, C. R. Hartsfield and T. A. Leonhardt, "Selective Laser Melting of Tungsten-Rhenium Alloys," *JOM,* pp. 1-12, 2021.

[17] R. A. Kemnitz, C. C. Eckley, B. M. Sexton and A. R. LeSieur, "Strengthening of additively manufactured tungsten by use of hydrogen in argon shielding gas," *Additive Manufacturing,* 2021.

[18] E. M. Savitskii and G. S. Burkhanov, Physical Metallurgy of Refractory Metals and Alloys, New York and London: Consultants Bureau, 1970.

[19] I. Machlin, R. T. Begley and E. D. Weisert, Refractory Metal Alloys Metallurgy and Technology, New York: Plenum Press, 1968.

[20] W. T. Elwell and D. F. Wood, Analytical Chemistry of Molybdenum and Tungsten, New York: Pergamon Press Inc., 1971.

[21] *Molybdenum Data Sheet - Mineral Commodity Summaries,* U.S. Geological Survey, Mineral Commodity Summaries, 2020.

[22] A. Brenner, "Electrodeposition of Alloys Principles and Practice," Academic Press, New York and London, 1963.

[23] *Tungsten Data Sheet,* U.S. Geological Survey, Mineral Commodity Summaries, 2020.

[24] C. Agte and J. Vacek, Tungsten and Molybdenum, Prague, State Publishing House of Techinical Literature, 1954.

[25] S. Singh, S. Ramakrishna and R. Singh, "Material issues in additive manufacturing: A review," *Journal of Manufacturing Processes,* vol. 25, 2016.

[26] "ISO 10303-242:2020 Industrial automation systems and integration — Product data representation and exchange — Part 242: Application protocol: Managed model-based 3D engineering," 2020.

[27] D. Herzog, V. Seyda, E. Wycisk and C. Emmelmann, "Additive Manufacturing of Metals," *Acta Materialia,* pp. 1-22, 2016.

[28] P. M., "NASA 3D-prints a rocket engine," The Economist, 3rd September 2013. [Online]. Available: https://bright-am.com/tracking-production/. [Accessed 15th November 2021].

[29] H. Proff and S. Andreas, *Challenges of Additive Manufacturing,* Deloitte, 2019.

[30] A. Bandyopadhyay and K. D. Traxel, "Invited Review Article: Metal-additive manufacturing — Modeling strategies for application-optimized designs," *PMC,* 2019.

[31] J. Dawes, R. Bowerman and R. Trepleton, "Introduction to the Additive Manufacturing Powder Metallurgy Supply Chain," *TECHNOLOGY REVIEW,* vol. 59, no. 3, pp. 243-256, 2015.

[32] S. Vock, B. Klöden, A. Kirchner, T. Weißgärber and B. Kieback, "Powders for powder bed fusion: a review," *Progress in Additive Manufacturing,* vol. 4, pp. 383-397, 2019.

[33] L. Mugwagwa, D. Dimitrov, S. Matope and R. Muvunzi, "Residual Stresses and Distortions in Selective Laser Melting," ResearchGate, 2019.

[34] A. B. Spierings, M. Schneider and R. Eggenberger, "Comparison of density measurement techniques for additive manufactured metallic parts," *Rapid Prototyping Journal,* vol. 17, no. 5, pp. 380-386, 2011.

[35] Q. Wu, J. Lu, C. Liu, H. Fan, X. Shi, J. Fu and S. Ma, "Effect of Molten Pool Size on Microstructure and Tensile Properties of Wire Arc Additive Manufacturing of Ti-6Al-4V Alloy," *Materials,* vol. 10, no. 7, p. 749, 2017.

[36] A. Y. Al-Maharma, S. P. Patil and B. Markert, "Effects of porosity on the mechanical properties of additively manufactured components: a critical review," *Materials Research Express,* pp. 1-27, 2020.

[37] T. DebRoy, H. L. Wei, J. S. Zuback, T. Mukherjee, J. W. Elmer, J. O. Milewski, A. M. Beese, A. Wilson-Heid, A. De and W. Zhang, "Additive manufacturing of metallic components – Process, structure, and properties," *Progress in Materials Science,* vol. 92, 2017.

[38] W. D. Klopp, P. L. Raffo and W. R. Witzke, "Strengthening of Molybdenum and Tungsten Alloys with HfC," *Journal of Metals,* pp. 27-38, 1971.

[39] M. E. Pink and I. K. Sedlatschek, "The Brittle-Ductile Transition of Body-Centered Cubic Metals with Special Considerations of Tungsten and Molybdenum," *Metall.,* vol. 23, no. 12, 1969.

[40] C. L. Rollinson, The Chemistry of Chromium, Molybdenum, and Tungsten, New York: Robert Maxwell, M.C., 1975.

[41] V. T. Ababkov and N. N. Morgunova, "Mechanical Properties of Mo-W Alloys," in *Refractory Metals and Alloys*, New York, Consultants Bureau, 1973, pp. 376-378.

[42] V. T. Ababkov, N. N. Morgunova and T. V. Gulyaeva, "Alloys of the Mo-W System," *Refractory Metals and Alloys,* pp. 907-911.

[43] F. F. Schmidt and H. R. Ogden, "The Engineering Properties of Molybdenum and Molybdenum Alloys," Defense Metals Information Center, Columbus, Ohio, 1963.

[44] R. V. Batienkov, A. N. Bol'shakova and I. Y. Efimochkin, "Materials based on Refractory Metals for Manufacturing High-Temperature Engineering Components," *Metallurgist,* vol. 62, no. 7-8, pp. 801-808, 2018.

[45] "Helping Our World," ASTM International, May 2018. [Online]. Available: https://www.astm.org/media/files/about-overview/Helping-Our-World-EN-2018.pdf. [Accessed 4th November 2021].

[46] *ASTM E1409-08: Standard Test Method for Determination of Oxygen and Nitrogen in Titanium and Titanium Alloys by the Inert Gas Fusion Technique,* ASTM International, 2013.

[47] "Mlab cusing 200R Metal laser melting system," [Online]. Available: https://pdf.directindustry.com/pdf/concept-laser/mlab-cusing-200r/15662-683546.html. [Accessed 10 October 2012].

[48] C.-S. Han, A. Hartmaier, H. Gao and Y. Huang, "Discrete dislocation dynamics simulations of surface," *Materials Science and Engineering A,* pp. 225-233, 2006.

[49] R. Morrell, Measurement Good Practice Guide No. 7: Flexural Strength Testing of Ceramics and Hardmetals, Teddington, Middlesex, UK: National Physical Laboratory, 1997.

[50] C. C. Chamis, "Analysis of the Three-Point Bend Test for Materials with Unequal Tension and Compression Properties," National Aeronautics and Space Administration, Washington D.C., 1974.

[51] ASTM E92-17: Standard Test Methods for Vickers Hardness and Knoop Hardness of Metallic Material, ASTM International, 2017.

[52] "MAIA3 model 2016 brochure," [Online]. Available: https://atomikateknik.com/uploads/belgeler/maia-3-brosur-10624.pdf. [Accessed 15th October 2012].

[53] C. Zeiss, "SteREO DiscoveryStereomicroscopeOperating Manual," Zeiss, 5 2012. [Online]. Available: https://p.widencdn.net/megzlc/EN_operating-manual_SteREO-Discovery. [Accessed 4th November 2021].

[54] *MATLAB and Statistics Toolbox Release 2021a,* Natick, Massachusetts: The MathWorks, Inc, 2021.

[55] D. C. Montgomery, E. A. Peck and G. G. Vining, Introduction to Linear Regression Analysis, Hoboken, New Jersey: John Wiley & Sons, Inc., 2012.

[56] *Eutectic Chart of Maximum Temperatures,* Cherry Valley: Ipsen USA.

[57] B. Vrancken, V. Cain, R. Knutsen and J. V. Humbeeck, "Residual stress via the contour method in compact tension specimens produced via selective laser melting," *Scripta Materialia,* vol. 87, no. 15, pp. 29-32, 2014.

[58] M. A. Abdou et al., "On the exploration of innovative concepts for fusion," *Fusion Engineering and Design,* vol. 54, pp. 181-247, 2001.

[59] G. Leichtfried and B. Tabernig, "Additively manufactured component and production method for the same, WO 2019/068117 (A1)," [Online]. Available: https://worldwide.espacenet.com/publicationDetails/originalDocument?CC=WO&NR=2019068117A1&KC=A1&FT=D&ND=4&date=20190411&DB=EPODOC&locale=en_EP. [Accessed 9 12 2021].

[60] T. Leonhardt, "Properties of Tungsten-Rhenium and Tungsten-Rhenium with Hafnium Carbide," *Refractory Metals Research,* vol. 61, no. 7, pp. 68-71, 2009.

[61] A. Srivastava, S. Osovski and A. Needlema, "Engineering the crack path by controlling the," *Journal of the Mechanics and Physics of Solids,* 2016.

REPORT DOCUMENTATION PAGE

Form Approved
OMB No. 074-0188

1. REPORT DATE *(DD-MM-YYYY)*	2. REPORT TYPE	3. DATES COVERED *(From – To)*
07-03-2022	Master's Thesis	March 2021 – March 2022

TITLE AND SUBTITLE
Potential Solution to Meet Growing Demands of Refractory Metal: Selective Laser Melting of Molybdenum-Tungsten Alloy.

5a. CONTRACT NUMBER

5b. GRANT NUMBER

5c. PROGRAM ELEMENT NUMBER

6. AUTHOR(S)

Yu, Jae H., Captain, USAF

5d. PROJECT NUMBER

5e. TASK NUMBER

5f. WORK UNIT NUMBER

7. PERFORMING ORGANIZATION NAMES(S) AND ADDRESS(S)
Air Force Institute of Technology
Graduate School of Engineering and Management (AFIT/EN)
2950 Hobson Way, Building 640
WPAFB OH 45433-7765

8. PERFORMING ORGANIZATION REPORT NUMBER
AFIT-ENY-MS-22-M-319

9. SPONSORING/MONITORING AGENCY NAME(S) AND ADDRESS(ES)
Air Force Research Laboratory

10. SPONSOR/MONITOR'S ACRONYM(S)
AFRL/RXMS

11. SPONSOR/MONITOR'S REPORT NUMBER(S)

12. DISTRIBUTION/AVAILABILITY STATEMENT
DISTRUBTION STATEMENT A. APPROVED FOR PUBLIC RELEASE; DISTRIBUTION UNLIMITED.

13. SUPPLEMENTARY NOTES

14. ABSTRACT

Selective laser melting (SLM) of refractory metals has been of high interest in research due to the metals' potential desirable characteristics in aeronautical and space applications. In particular, molybdenum and tungsten have been the focus of several studies in the search for high temperature and high strength purposes. However, there is still a significant knowledge gap to process defect-free alloys and make use of them in practical engineering functions. The aim of this study is to characterize the relationship between the microstructure and mechanical properties of the additive manufacturing (AM) of molybdenum and 30% tungsten system (Mo-30W) specimens and interpret how unique microstructural characteristics and defects relating to AM of Mo-30W alloy influence the fracture behavior. This study provides qualitative and quantitative approaches to characterize microstructure and mechanical properties of the various AM Mo-30W specimen by evaluating the effects of print build chamber gas, print speeds, build orientations, and post processing heat treatments through means of mechanical tests, chemical composition analysis, porosity identification, and fracture surface assessments.

15. SUBJECT TERMS
Additive Manufacturing, Selective Laser Melting, Laser Powder Bed Fusion, Molybdenum, Tungsten, Print Speed, Build Orientation, Post Processing Heat Treatment,

16. SECURITY CLASSIFICATION OF:			17. LIMITATION OF ABSTRACT	18. NUMBER OF PAGES	19a. NAME OF RESPONSIBLE PERSON
a. REPORT	b. ABSTRACT	c. THIS PAGE			Ryan Kemnitz, AFIT/ENY
U	U	U	UU	148	19b. TELEPHONE NUMBER *(Include area code)* (937) 255-3636, ext 4775; ryan.kemnitz@afit.edu